A Study on High Performance Control for Industrial Robot Manipulators

LinFeng Lan

Kyushu Institute of Technology
Ph.D. Thesis
March 2014

Acknowledgements

It would not have been possible to write this doctoral thesis without the help and support of the kind people around me, to only some of whom it is possible to give particular mention here.

First and foremost, I want to express my heartfelt thanks and sincere gratitude to my advisor Prof. Eitaku Nobuyama for the continuous support of my Ph.D. study and research, for his patience, enthusiasm and immense knowledge. Prof. Eitaku Nobuyama is one of the smartest and kindest people I have ever known. As an excellent scientist, he encouraged me to enlarge my vision and improve research skills. His perpetual enthusiasm for science and research, and thoughtful insights have kept inspiring me to discover and develop continuously. It was really a great honor for me to be his student. This thesis would have not been possible without or with less support and guidance from him. At the same time, he was always there for me to consult and discuss with, especially when I was in trouble to look for a job. His enthusiastic advice made me stand in proud array in the face of difficulties of job hunting.

I would like to express the deepest appreciation to my second advisor and mentor Prof. Hideki Honda, who has supported me throughout my Ph.D. study and research with his patience, unsurpassed knowledge and consistent encouragement. Prof. Hideki Honda is one of the most excellent scientists, who has many years of useful practical experiences. He has not only complemented my academic knowledge, but also given me very helpful and effective advice in theoretical examination through experiments. “independent thought” and “freedom in research” are what he always encourages me to perform, without any constrain in idea. This thesis and many research papers would have not been possible without the help and support of him.

I am most grateful to my first teacher Mr. R. Oguro, who initiated me into the “control world” and helped me to get on the right track of academic research. He continually and convincingly conveyed a spirit of freedom and independent thought in regard to research. This spirit have constantly inspired me to be a good researcher, who has deep and independent thinking, original ideas, persistent enthusiasm and efforts in regard to research. The thesis would not have come to a completion without the enlightenment and encouragement of my first teacher.

Special thanks are due to Prof. Koga, Prof. Sebe, Assoc. and Prof. Ito, for serving on the examination committee. Their valuable comments and insightful suggestions have greatly improved my work.

I have been blessed with a friendly and cheerful group of laboratory members. I would like to offer thanks to every people in my lovely laboratory, who always supported me not only in my Ph.D. research work, but also in my daily life. Special thanks to Mr. Y. Sameshima, who was my tutor and also one of my best Japanese friends, for his constant and enthusiastic help. Special thanks to Mr. D. Shiotsuka, who was my best fellow student, for his excellent advice to my research.

Acknowledgements

I wish to extend my sincere gratitude to the JASSO Scholarship, the 100th Anniversary Memorial Scholarship of KIT and the Fukuoka International Exchange Foundation Scholarship for their financial support during my study in Japan. Without these important resources, I would not have totally focused on completion of my research.

I want to thank Doctor Nawata for giving the free medical check-ups to me during my life in Japan. I also want to express my deepest appreciation to all my Japanese teachers. They have not only taught me Japanese, but also let me know how to adapt to life in Japan, how to communicate and make friends with Japanese.

I owe a lot to my parents, who encouraged and helped me at every stage of my personal and academic life, and longed to see this achievement come true. I express my greatest gratitude for their too much dedication.

I am very much indebted to my wife Yang Mu. In order to make me be successful in academic, she has sacrificed too much self-time to do part-time job for a living. But even though she relentlessly encouraged me. I am grateful to her as she believed in me, helped me, and supported me.

At last, I would like to thank all people I met at Kyushu Institute of Technology and those who have made a comfortable environment for me during my graduate time.

THANK YOU, THANK JAPAN.

LinFeng Lan
Kyushu Institute of Technology
March 2014

Contents

List of Tables

List of Figures

List of Figures

Chapter 1

Introduction

1.1 Short history and definitions of industrial robots

A definition of an industrial robot is essential for understanding control of industrial robots. Therefore, nowadays, some formal definitions are given for consideration. But before that, it is necessary to trace back to the beginning that why robots were invented, and recall the development history of industrial robots.

The word “robot” was introduced by a Czech novelist Karel Capek in a 1920 play *Rossum's Universal Robots*. He used the Czech word “robota” to mean simply “work”. In the course of centuries, human beings have constantly attempted to find out substitutes that would be able to mimic their behavior in the various instances of interaction with the surrounding environment. They hope the substitute to do jobs that are dangerous, repetitive jobs that are boring, stressful and laborintensive, and menial tasks that human don’t want to do. Especially when humans are intolerable or impossible to survive in some very special circumstances, they hope robots can complete the desired operations instead of them.

It may be precisely because of these motivations, in 1941, the Russian science fiction writer Isaac Asimov first used the word "robotics" to describe a robot as an automaton of human appearance but devoid of feelings. Its behavior was dictated by a “positronic” brain programmed by a human being in such way as to satisfy tertian rules of ethical conduct. In the short story "Runaround" of Isaac Asimov, which was presented in 1942, a set of rules was introduced. The set of rules, as a symbol of the science devoted to the study of robots, was called The Three Laws.

The Three Laws with a later added zeroth (forth) law are:

1. A robot may not injure humanity, or, through inaction, allow humanity to come to harm.
2. A robot may not injure a human being or, through inaction, allow a human being to come to harm.
3. A robot must obey the orders given to it by human beings, except where such orders would conflict with the First Law.
4. A robot must protect its own existence as long as such protection does not conflict with the First or Second Law.

From science fiction into reality, in 1954, George Devol and Joe Engleberger invented the first programmable material handling arm, see Fig.1.1. With Joseph F. Engelberger, George Devol founded the first company Unimation in 1956 to produce a robot that its main use at first was to transfer objects from one point to another. Then, this later became the first industrial robot, completing spot welding

and extracted die castings on an assembly line at General Motors in 1962 [1]. In the 1960s, the original imagination and expectation of "robot" ultimately came true and since then, the world robotics revolution began quickly along with the computer revolution.

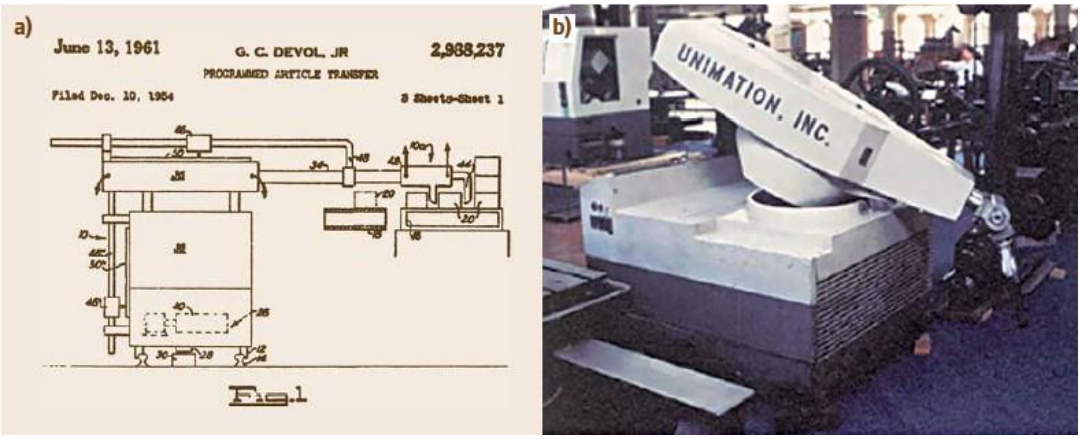

Fig. 1.1 The invention of industrial robot (an extract from [1])

Between the 1960s and 1980s, several representative events in the development history of industrial robots shall be remembered [2].

In 1963, the first artificial robotic arm to be controlled by a computer is designed at Rancho Los Amigos Hospital in Downey, California.

In 1969, a six-degree-of-freedom Stanford arm, which is the first successful electrically powered, computer-controlled robot arm was created by Victor Scheinman, who was a mechanical engineering student working in the Stanford Artificial Intelligence Lab. Scheinman's concepts have strongly influenced the subsequent designs of robots.

In 1973, the first industrial robot with six electric motor-driven axes known as FAMULUS, was born in German robotics company KUKA. In the same year, the world's first microcomputer controlled electric industrial robot, IRB-6 was introduced by company ASEA (now ABB).

In 1974, Pf. Victor Scheinman, a developer of the Stanford Arm, invented the Silver Arm which was a robotic arm that small part assembly using touch and pressure sensors to feedback information to a microcomputer.

In 1977, a five axis vertically jointed, articulated type industrial robot MOTOMAN-L10 with a capability of a maximum workload of 10 kg was introduced by Japanese company Yaskawa Elec. Corp. A control system of the robot was equipped with a separate programming pendant used to record the robot's position one by one and had a magnetic memory which did not require a backup.

In 1978, a selective compliance assembly robot arm (SCARA) was invented by Hiroshi Makino of

Yamanashi University, Japan. A ground-breaking four-axis low-cost design was perfectly suited for small parts assembly as the kinematic configuration allows fast and compliant arm motions.

In 1981, Takeo Kanade built a direct drive arm. It is first to have motors installed directly into the joints of the arm. This development makes joints faster and much more accurate than previous robotic arms.

From 1980s, the industrial robot industry started to grow rapidly. With growing requirements for industrial robots, many companies focused on industrial robots to evolve them to be used for more extensive and complicated applications.

Then, what exactly is an industrial robot?

One of interesting definitions of manipulator which was adopted by JIRA (Japan Industrial Robot Association) in 1986 is given as follows.

- A machine, the mechanism of which usually consisting of a series of segments jointed or sliding relative to on another, for the purpose of grasping and moving objects usually in several degrees of freedom. It may be controlled by an operator, a programmable electronic controller, or any logic system (e.g. cam device, wired, etc.)

This definition is representative and includes general characteristics of other definitions in use. It states a basic "structure" of a manipulator, "purpose" of use of manipulators and the most important characteristic of a manipulator that is "programmable".

Several other definitions such as the definition adopted by RIA (USA Robotic Industries Association):

- A robot is a reprogrammable multifunctional manipulator designed to move material, parts, tools, and specialized devices through variable programmed motions for the performance of a variety of tasks,

and the definition adopted by BRA (British Robot Association):

- An industrial robot is a reprogrammable device designed to both manipulate and transport parts, tools, or specialized manufacturing implements through variable programmed motions for the performance of specific manufacturing tasks,

state more precisely that robots are reprogrammable manipulators.

Most of the organizations nowadays agree more or less to the definition of industrial robots, formulated by the ISO (International Standardization Organization).

- An automatically controlled, reprogrammable, multipurpose manipulator programmable in three or more axes, which may be either fixed in place or mobile for use in industrial automation applications.

In this definition, several key words: automatically controlled, reprogrammable, multipurpose, axes, fixed or mobile shall be emphasized. These key words precisely and integrally interpret the essential characteristics of the modern robots used for industrial applications. In details, it also can be

understood that a robot shall be reprogrammable for automation without physical alteration of mechanical structure and control system, shall be capable of being adapted to a different application with physical alternations. It can be used in a fixed place or either in the form of mobile.

1.2 Current main applications and requirements for industrial robots

Up to now, after nearly sixty years of development of industrial robot manipulators, it is not a rare thing to see that industrial robot manipulators are working instead of human beings. In six decades, the industrial robot manipulators were mainly used in automotive industry. They served for welding, car body painting, automobile parts cutting and so on; see Fig.1.2, [3]. At the same time, in general industry, industrial robot manipulators are also extensively used for instance, conveyor line assembly, silicon wafer transfer and so on; see Fig. 1.3, [3]. For different industrial applications, requirements for industrial robot manipulators are of course different. Brief descriptions about several main applications of industrial robot manipulators and their requirements are presented as follows.

(a) Welding

(b) Car body painting

(c) Auto parts cutting

Fig. 1.2 Typical applications of industrial robots

(a) Conveyor line packaging

(b) Silicon wafer transfer

Fig. 1.3 Applications of industrial robots for general industry

Welding is one of the major uses of industrial robot manipulators. Generally, industrial robot manipulators that are used for welding are called welding robots and welding robots are mainly employed to complete two distinct types of welding operations, spot and arc welding. The former spot welding is a process to join two contacting metal parts by the heat obtained from resistance to electric current. The process uses two shaped copper alloy electrodes to concentrate welding current into a small "spot" and to simultaneously clamp two contacting metal parts together. A welding robot used for spot welding is required to have higher mobility and dexterity to permit the welding tool to be aligned properly at the desired weld point without the gun coming into contact with other portions of the metal parts. Meantime, in order to carry the reasonably heavy welding tools, large point-to-point servo-controlled robot manipulators are normally used. The second arc welding is to create an electric arc between an electrode and the base material by welding power supply, then, to melt the metals at the welding point. In this case, a welding robot is required to have better weld consistency and decrease cycle times of welding, in other words, high quality and high efficiency of welding. A continuous-path servo-controller robot that is specially designed for this single application is most usually the choice.

Industrial robot manipulators are also the best choice for spray-painting operation of car bodies, which is a task that human beings should not perform due to the potential health risks. The major benefit of using industrial robot manipulators for spray-painting is that the resultant coating will be far more uniform than a human being could ever produce. This results in a higher-quality product, less reworking of parts, and considerably less paint being used [4]. Almost for the same reason, industrial robot manipulators are often used for parts cutting. The uses of parts cutting robots in a great extent avoid potential fire hazard, and more importantly, higher quality of cutting can be expected.

Without considering potential dangerous factors of above shown operations, industrial robot manipulators are also employed for completing repetitive jobs such as typical assembly and parts transfer because human beings feel extremely tedious for these long time and repetitive jobs. In these applications, industrial robot manipulators are taught the desired points and the sequence of operations. Then, industrial robot manipulators are strictly required to work according to the taught sequence and to complete entire operations of assembly or transfer. In these applications, certainly, human beings hope industrial robot manipulators can assemble diverse parts or transfer some certain parts like veteran workers, who have very good work efficiencies.

The various applications of industrial robot manipulators both in automotive industry and general industry truly reflect initial hopes of human beings for industrial robots. As the substitute of human labor, industrial robot manipulators are strongly expected to work at higher accuracy and with higher efficiency. According to a study of the International Federation of Robotics (IFR) titled “Positive Impact of Industrial Robots on employment”, the adoption rate of robots measured in number of robots per 10,000 employees in manufacturing between 2008 and 2011 is on the rise. With more and more adoption of industrial robot manipulators, the requirements of high accuracy and high efficiency for industrial robot manipulators increasingly become more and more severe. Therefore, the achievement of high productivity of industrial robot manipulators becomes an extremely important research topic.

In addition, in modern world, an industrial robot manipulator is also required to be able to cope with a variety of operations. In other words, an industrial robot manipulator is not only able be used for certain kind of operations, it must be capable of producing a variety of products, rather than a large number of the same product models [5] [6].

1.3 Research topics and outline of the thesis

The field of robotics draws on a multitude of engineering disciplines. As a branch of robotics, the industrial robot manipulator also covers very large technical areas such as mechanical, electrical, software and control. To meet growing requirements for industrial robot manipulators, studies in control area are conducted in this paper. From control perspective, there is no doubt that high performance control of industrial robot manipulators is important and especially necessary for productivity improvement and a variety of productions. High performance control is in fact a basic

but broad concept. What exactly is high performance control? In this paper, high performance control of industrial robots indicates high speed and high accuracy positioning control of industrial robot manipulators.

To achieve high performance control of industrial robot manipulators, researchers have tried their best to study some new control strategies for several decades. As a result, many effective control strategies such as computed-torque control, trajectory tracking control and so on have been extensively used nowadays, and the applications of these strategies have made the high performance control of industrial robot manipulators to a new level. However, for the studies of control strategies, it can be said to some extent that these studies have only concerned with control strategies. Some other factors such as command and mechanical characteristics that are closely related to high performance control have not been paid too much attention. In this paper, in addition to presentation of a new control strategy, research topics that are related to command processing and mechanical characteristics are also described. But before explaining the corresponding details, basic components of an industrial robot system are given as follows for better understanding the research topics.

An industrial robot manipulator system is given in Fig. 1.4. The basic components of an industrial robot manipulator system are:

- Command generation system
- Controller system
- Industrial manipulator

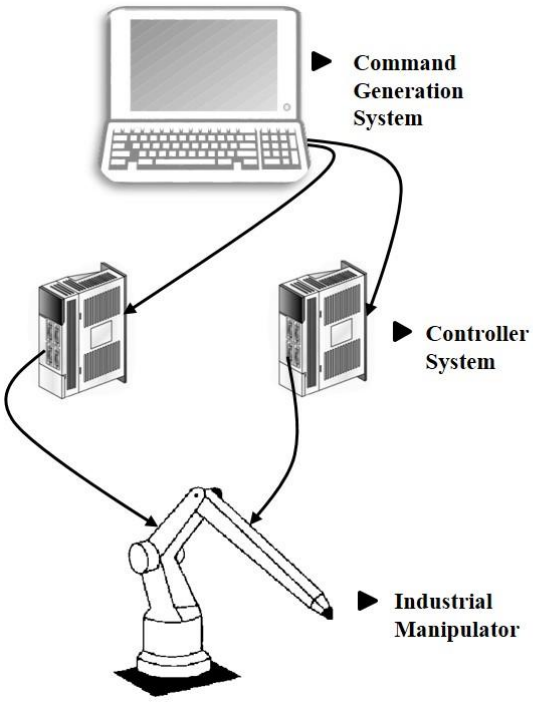

Fig. 1.4 Industrial robot manipulator system

Strictly speaking, sensory devices should be also included in an industrial robot manipulator system. In this paper, the most usual welding applications of industrial robot manipulators are mainly taken into account. The high performance control study objects are assumed to be welding robots. Generally, welding robots are not equipped with sensory devices that are used for observing spatial positions due to two reasons. One is high cost of sensory devices. The other is that the very poor working conditions of welding robots are not suitable for using sensory devices. Hence, sensory devices are not taken into account in this paper.

High accuracy is one of important parameters for high performance control of industrial robot manipulators. The factors of accuracy improvement are improvement of the actuators, speed reduces and encoders, progress of the calibration and control methods, and application of external sensors [7]. In other words, the improvement of control performance of industrial robot manipulators should not rely on study of single aspect. From this perspective, this paper differs from traditional literature of high performance control. The achievement of high performance control is considered in three aspects; command processing, control strategy and identification of mechanical characteristics.

Generally, command is firstly essential for no matter what kind of completion of operation. The application of command processing technique contributes to high quality of completion of operation because in some cases the processed command becomes smooth and easy for tracking of industrial robot manipulators. In addition, mechanical characteristics fundamentally dominate performance of industrial robot manipulators. Meantime, they are also closely related to control performance. Clearly understanding some special mechanical characteristics probably advances control performance. So, good results are expected in which command processing and mechanical characteristics are studied together with study of control strategy.

Specifically, first, in some cases industrial robot manipulators must be moved along the desired trajectory (e.g. arc welding robots, painting robots). However, due to some hardware limitations such as low computing performance of command generation system, a series of digital commands output from command generation system may be not the most suitable form for the follow-up performance of arc welding or painting robots. The unsuitable digital commands perform longer sampling cycle due to lower computing speed of command generation system. As a result, a multi-rate sampling problem occurs between command generation system and controller system and it mostly leads to appear of control delay and deterioration of tracking performance. Therefore, to reduce the control delay and improve the tracking performance of industrial robot manipulators, the original digital command is usually processed by using a technique called interpolation. The interpolated command becomes smooth and easy for tracking. Especially, it becomes possible to be used for achieving perfect tracking control [8], which is a digital feed-forward control algorithm to track desired time varying signals. In many interpolation techniques, Spline interpolation is considered to be the best and it has been extensively used in usual cases. But, Spline interpolation technique has some shortcomings in

the case of interpolation of position command, which may be very critical for positioning control of industrial robot manipulators. To resolve the problems, a simple and successive command processing technique titled "A new interpolation methodology for position" is studied for high-speed and high-accuracy control of industrial robot manipulators in this paper.

The second topic is related to control strategy, which is decoupling control of industrial robot manipulators. For the control problem of spot welding robots, it is different from arc welding or painting robots. The control problem is concerned with moving the control object from one point to another. This type of robots are usually called Point to Point (PTP) robots. From the perspective of accuracy, the transient path to the final point is not important in control of PTP robots. Therefore, the coupling effect that normally results in small vibration of end effector of a spot welding robot during the transient path is not taken seriously. Especially, in traditional high-speed control applications, control input may be large enough that coupling torque between two links of an industrial robot manipulator will be small in comparison and may not significantly affect control results. Conversely, if a small control input is used to obtain precise movement, in some instances, the coupling torques reduce the control input to a point where no motion results. According to [7], the accuracy has been improved from 1mm to 0.5mm~0.3mm in the case of large robots, and from 0.1mm to 0.005mm in the case of small robots. In the case, decoupling control becomes especially important, no matter for accuracy or efficiency. The goal of the decoupling control is to give a spot welding robot an ability to perform fast, precise movements and links of the spot welding robot can perform independently without influence of coupling effect. In this paper, a new decoupling control strategy by using Model Following Control is proposed.

The last topic is an identification problem of friction. Friction is a very important mechanical characteristic for control. For industrial robot manipulators, friction is an old but new subject. Researcher have studied friction for a long time since the industrial robot manipulators was produced. Friction research is also new for industrial robot manipulators because new and effective friction models have been proposed continually with development of understanding of friction. Therefore, the corresponding identification of friction with new friction model is important for the high performance control of industrial robot manipulators. In this paper, a new identification strategy for friction is proposed in order to effectively and accurately identify the friction of gear transmissions, which has not been studied so far.

This paper is arranged in five chapters

In chapter 2, a new interpolation methodology of position command is proposed and described in details. The description begins with in comparison with spline interpolation, which is considered to be the most effective interpolation technique and frequently used for command interpolation. With the proposed interpolation algorithm, simulations are employed to show that the new interpolation methodology is a successive interpolation technique and better than Spline interpolation, and it is

characterized by the high interpolation accuracy.

In chapter 3, the proposed decoupling control of 2-link manipulator by using Model Following Control will be presented. The derivation of Lagrange's equation is reviewed firstly to contribute to the derivation of the coupling model of a 2-link manipulator. Then, designs of feed-forward loop and feedback loop of Model Following Control are shown respectively in details. At last, several simulations are conducted to verify the effectiveness of the proposed decoupling control strategy.

The content of identification of gear transmissions' friction will be shown in chapter 4. As the applied friction model of this paper, LuGre friction model is presented firstly. Then, the problems of identification of industrial robot manipulators are listed and the respective resolutions are given. With the identified LuGre model, simulation results are employed to compare with the experimental results, to verify the effectiveness of the proposed new identification methodology.

The conclusions of this paper are shown in chapter 5. The successful points and problems of whole research, and future study will be described.

Chapter 2

A new interpolation methodology for position command

2.1 Interpolation technique

Interpolation is used to estimate a value of a function between two discrete known position commands. With interpolation technique, the function that passes through all the original discrete data points will be found. One of typical applications of the interpolation technique is curve fitting and a well-known Spline interpolation [9] [10] is mostly used for curve fitting.

Due to the superior characteristic of Spline interpolation that is much fit for original data points, Spline interpolation is conventionally used in the optimum trajectory planning of industrial robot manipulators [11] [12]. Moreover, Spline interpolation technique has also been extensively studied and used in high-speed and high-accuracy control for industrial robot manipulators. It has been demonstrated very good effect of improving control speed and accuracy [13]-[16].

However, there are several shortcomings in the case of position command interpolation using Spline interpolation.

(1) Spline interpolation is not an efficient interpolation manner in the case of digital position command interpolation. In high performance control of industrial robot manipulators, interpolation can be seen as a medium, which connects command output and command execution and plays the role of command processing. An efficient interpolation technique shall be able to realize successive (means one by one) interpolation when the digital data point of command is output one by one from command generation system. Controller system of industrial robot manipulators is thereby able to instantly obtain the processed digital data point of command and begins to execute command. However, Spline interpolation is inapplicable to successive position command interpolation because Spline function that is a function to connect all digital data points of command will not be found if all digital data points of position command are not known. As a result, control process of controller system is delayed and finally Spline interpolation results in deterioration in whole control performance.

(2) Position command interpolation using Spline interpolation has an overshoot problem, which is the most unacceptable problem in high-speed and high accuracy positioning control for industrial robot manipulators. An interpolation example of the position command using Spline interpolation is shown in Fig. 2.1. Notice that the interpolated position command vibrates around the goal position (0.05m). The vibration around goal position is most likely to lead to the overshoot of a position response when the interpolated command is originally used. Hence, Spline interpolation is not a proper interpolation technique for the interpolation of position command.

(3) Enormous computation complexity of algorithm of Spline interpolation makes Spline interpolation difficult to be put into practice. Especially, it is nearly impossible when the digital position command of industrial robot manipulators is too long. In fact, general industrial robot manipulators are not and also not able to be equipped with high performance computing systems (controller system) due to an issue of cost. Therefore, taking computation complexity of Spline interpolation and capacity of computing systems into account, Spline interpolation is too complex for general industrial robot manipulators.

With above considerations, there is no doubt that it is necessary to study a new interpolation methodology which is capable of interpolating position command in successive manner. The new methodology should be able to avoid the overshoot problem and be simple for practical application. In this paper, the new interpolation methodology for position command is proposed.

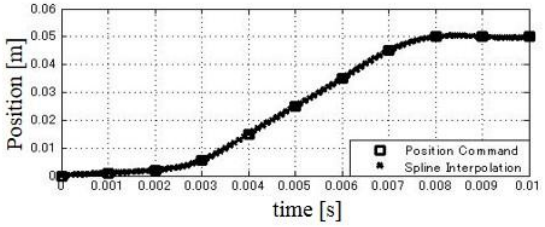

(a) Whole view

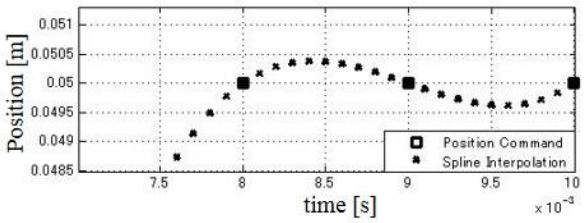

(b) Enlarged view of steady part

Fig. 2.1 Overshoot problem in Spline interpolation

2.2 Basic function used for a new interpolation methodology

A function is introduced in the new interpolation methodology. The function is called basic function in this paper and it is given by

$$f = t^{2N}(t - T_{su})^{2N}, \quad \text{..... (2.1)}$$

where t is a time variable, T_{su} is a sampling time of position command generation system (i.e. a high-order controller), N is the natural number. Three essential properties of the basic function are given as follows in order to better understand details of the new interpolation methodology presented later.

Property 1: The basic function f is a function of t and is continuous and symmetric over interval of $[0 \quad T_{su}]$.

Property 2: The basic function f is integrable over interval of $[0 \quad T_{su}]$.

Property 3: The basic function f is continuously differentiable over interval of $[0 \quad T_{su}]$.

The basic function f with its integral and differential are shown in Fig. 2.2. Notice that integral and differential of the basic function are also functions of time variable t and both are continuous over interval of $[0 \quad T_{su}]$. The new interpolation methodology is based on above three properties, which will be presented in detail in next section.

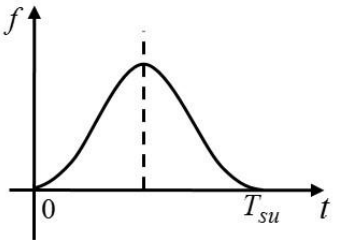

(a) Basic function

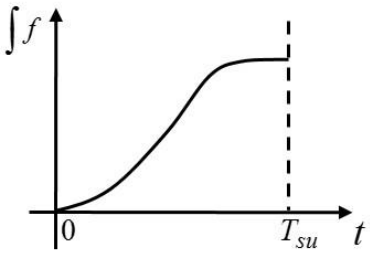

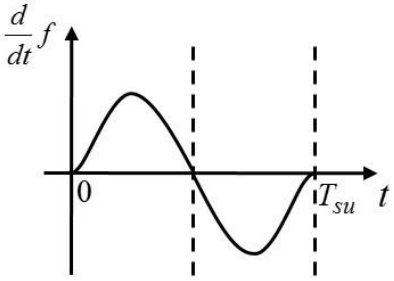

(b) Integral **(c) Differential**

Fig. 2.2 Basic function, integral and differential

2.3 Policies and algorithm of a new interpolation methodology

In this section, policies and algorithm of the proposed new interpolation methodology will be illustrated. But first of all, for simplicity, the process of interpolation will be illustrated with Fig. 2.3.

Digital data point of position command $X_{ref}(1)$, $X_{ref}(2)$, $X_{ref}(3)$ and so on are generated in a high-order controller of an industrial robot manipulator. The sampling time of the high-order controller is usually longer than the sampling time of a low-order controller (i.e. servo controller). The sampling time of a low-order controller is shown as T_s in Fig. 2.3. Each digital data point is output to low-order controller (i.e. servo controller) in chronological order. Interpolation between two digital data points will be implemented in low-order controller (i.e. servo controller) with sampling time of T_s during time interval from 0 to T_{su}. The same process continues till the interpolation between the last two digital data points is completed.

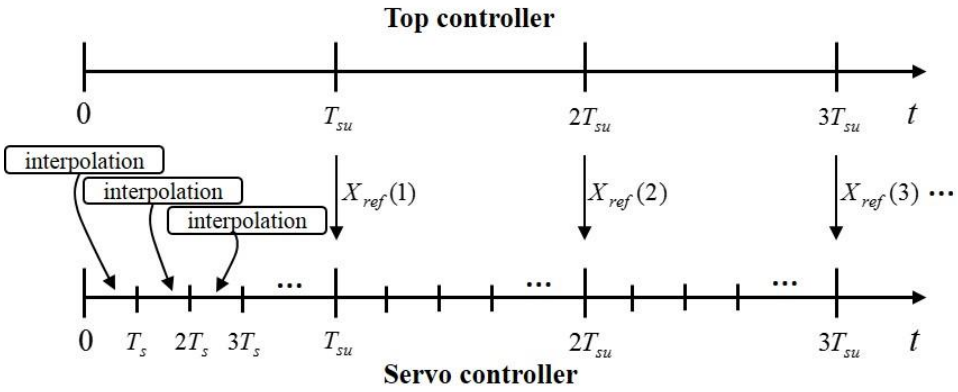

Fig. 2.3 Process of interpolation

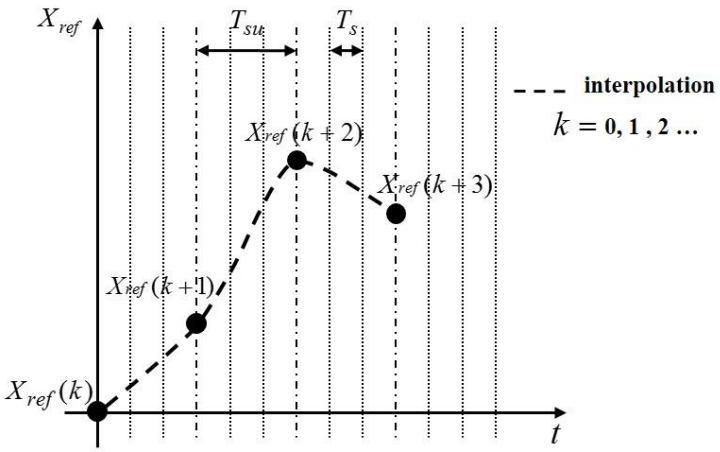

Fig. 2.4 Position command and interpolation

An ideal successive interpolation manner is supposed to be like that to conduct the interpolation between two digital data points in the servo controller instantly when the second of two digital data points is output from the high-order controller. In contrast, the new interpolation methodology have achieved the successive interpolation manner by using information of three digital data points. An idea of the new successive interpolation is illustrated as follows with Fig. 2.4.

The new interpolation methodology also attempts to achieve high-accuracy interpolation of position command in addition to achievement of a successive interpolation manner. Thus, interpolation of acceleration and velocity are also carried out. To complete acceleration and velocity interpolation, acceleration and velocity of each data point of position command must be known in advance. In new interpolation methodology, acceleration and velocity of each digital data point is defined and is considered to be acceleration and velocity command of interpolation. The definitions are based on position information of three digital data points, hence, the achievement of the new successive interpolation manner is based on three digital data points.

Specifically, assuming that three digital data points of position command $X_{ref}(k)$, $X_{ref}(k+1)$ and $X_{ref}(k+2)$ are output from the high-order controller to the servo controller, the new idea for successive interpolation is to conduct the interpolation between two digital data points ($X_{ref}(k)$, $X_{ref}(k+1)$) when the third digital data point ($X_{ref}(k+2)$) is output. Acceleration and velocity command become possible to be defined when the third position command point ($X_{ref}(k+2)$) is output. Therefore, the interpolation between two digital data points $X_{ref}(k)$ and $X_{ref}(k+1)$ is able to be completed until the high-order controller outputs the third digital data point $X_{ref}(k+2)$. With position information of $X_{ref}(k+2)$, a successive interpolation is ultimately able to be implemented. The relevant details are presented subsection 2.3.1

2.3.1 Policies

Three policies of the new interpolation methodology are summarized as follows. For simplicity, the basic function and its integral and differential are called function A, function B and function C.

Policy 1: Specify acceleration and velocity command of digital data point $X_{ref}(k+1)$.
Policy 2: Do acceleration interpolation between $X_{ref}(k)$ and $X_{ref}(k+1)$ by using function B.
Policy 3: Calibrate velocity and position errors by using function B.

The definitions of acceleration and velocity command of $X_{ref}(k+1)$ are the beginning of the new interpolation methodology. Acceleration command of $X_{ref}(k+1)$ is specified for acceleration interpolation and velocity command is specified for calibrating velocity errors. With specified acceleration command, the acceleration interpolation is implemented by using function B. Function B is continuous and smooth over interval of $[0 \quad T_{su}]$, it can be thereby used for obtaining a smooth acceleration interpolation.

After acceleration interpolation, as a matter of fact, there are errors between actual velocity and velocity command, actual position and position command. The errors must be corrected. Function B is employed to correct the velocity and position errors. The reason why function B is employed for correcting velocity and position errors is that to avoid the interaction among three policies.

Acceleration is generated when function B is used to correct velocity error. The generated acceleration is the differential of function B, which is also function A. Referring to Fig. 2.2 (a), notice that value of function A is zero when t is equal to 0 and T_{su}. It indicates that the calibration of the velocity error with function B will not cause any value errors to acceleration interpolation. It can be also said that policy 2 does not interact with policy 1.

Velocity and acceleration are generated when function B is used to correct position error. The generated velocity and acceleration are function A and function C. Values of function A and C are also zero when t is 0 and T_{su}. It also means that calibration of the position error with function B will

not have any influence on previous acceleration interpolation and calibration of velocity error. Consequently, it can be said that three policies do not interact with each other. Acceleration, velocity and position can be accurately interpolated by using these three policies.

2.3.2 Algorithm

In order to realize the three policies, an interpolation algorithm is provided as follows. There are five steps in the algorithm.

(1) Define acceleration and velocity command.

In the new interpolation methodology, velocity and acceleration command are respectively defined as follows.

$$V_{ref}(k+1) = \frac{X_{ref}(k+2) - X_{ref}(k)}{2T_{su}}, \quad \text{..... (2.2)}$$

$$U_{ref}(k+1) = \frac{\dfrac{X_{ref}(k+2) - X_{ref}(k+1)}{T_{su}} - \dfrac{X_{ref}(k+1) - X_{ref}(k)}{T_{su}}}{T_{su}}, \quad \text{..... (2.3)}$$

where $V_{ref}(k+1)$ and $U_{ref}(k+1)$ are specified velocity and acceleration command. Initial velocity and acceleration command is assumed to be zero in the new interpolation methodology.

In definitions, notice that three digital data points $X_{ref}(k)$, $X_{ref}(k+1)$ and $X_{ref}(k+2)$ are used. The definitions of velocity and acceleration command offer an explanation for that why three digital data points of position command are necessary for the new interpolation methodology. In addition, values of velocity and acceleration command are the values of average velocity and acceleration between $X_{ref}(k)$ and $X_{ref}(k+2)$. It means that motion between $X_{ref}(k)$ and $X_{ref}(k+2)$ is assumed to be the uniform motion when velocity command is specified. Motion between $X_{ref}(k)$ and $X_{ref}(k+2)$ is assumed to be the uniformly-accelerated motion when acceleration command is specified. The specified velocity and acceleration command in Eq. 2.2 and Eq. 2.3 also obey the laws of physics; velocity is equal to the acceleration multiplied by the time,

$$V_{ref}(k+1) = U_{ref}(k+1)T_{su}. \quad \text{..... (2.4)}$$

(2) Implementation of acceleration interpolation.

With specified acceleration command, the interpolation of acceleration will be implemented by using function B. An example of the basic function is given by

$$f = t^4(t - T_{su})^4, \quad \text{..... (2.5)}$$

where

$$t = iT_s \quad i = 0,1,2,.... \quad \text{..... (2.6)}$$

An integral of the basic function is

$$630\int f\,dt = 70t^9 - 315T_{su}t^8 + 540T_{su}^2t^7 - 420T_{su}^3t^6 + 126T_{su}^4t^5, \quad \text{..... (2.7)}$$

where the integral is multiplied by 630 for simplicity of calculations and a constant of integration is considered to be zero.

Assuming that the value error between $U_{ref}(k)$ and $U_{ref}(k+1)$ is given by

$$U_\Delta = U_{ref}(k+1) - U_{ref}(k), \quad \text{..... (2.8)}$$

then, according to policy 2, the integral of the basic function is used to calculate U_Δ

$$U_\Delta = C_\alpha 630\int_0^{T_{su}} f\,dt$$

$$= C_\alpha\left[70t^9 - 315T_{su}t^8 + 540T_{su}^2t^7 - 420T_{su}^3t^6 + 126T_{su}^4t^5\right]_0^{T_{su}},$$

..... (2.9)

where C_α is a constant and

$$C_a = \frac{U_{ref}(k+1) - U_{ref}(k)}{T_{su}^9}.$$

Acceleration interpolation shown as a_{REF} can be obtained as

$$a_{REF} = U_{ref}(k) + U_\Delta. \quad \text{..... (2.10)}$$

Velocity and position are generated by U_Δ and the generated velocity V_a and position X_a can be obtained by following calculations.

$$V_a = \int_0^{T_{su}} U_\Delta dt$$

$$= \frac{C_a}{2}\left[14t^{10} - 70T_{su}t^9 + 135T_{su}^2t^8 - 120T_{su}^3t^7 + 42T_{su}^4t^6\right]_0^{T_{su}},$$

..... (2.11)

$$X_a = \int_0^{T_{su}}\left(\int U_\Delta dt\right)dt$$

$$= \frac{C_\alpha}{22}\left[14T_s^{11} - 77T_{su}T_s^{10} + 165T_{su}^2T_s^9 - 165T_{su}^3T_s^8 + 66T_{su}^4T_s^7\right]_0^{T_{su}},$$

..... (2.12)

The real value of velocity and position of interpolation at $X_{ref}(k+1)$ are

$$V_{real}(k+1) = V_{ref}(k) + U_{ref}(k)T_{su} + V_\alpha, \quad \text{..... (2.13)}$$

$$X_{real}(k+1) = X_{ref}(k) + V_{ref}(k)T_{su} + \frac{1}{2}U_{ref}(k)T_{su}^2 + X_{\alpha}. \quad \text{..... (2.14)}$$

(3) Calibration of velocity error.

After acceleration interpolation, velocity error will be calibrated. According policy 4, the integral of the basic function is applied to calibrate the velocity error. Velocity error between $V_{ref}(k+1)$ and $V_{real}(k+1)$ is given by

$$V_{REF} = V_{ref}(k+1) - V_{real}(k+1). \quad \text{..... (2.15)}$$

Then, with integral of the basic function, velocity error is corrected by

$$V_{REF} = C_v 630\int_0^{T_{su}} f\,dt$$

$$= C_v\left[70t^9 - 315T_{su}t^8 + 540T_{su}^2t^7 - 420T_{su}^3t^6 + 126T_{su}^4t^5\right]_0^{T_{su}},$$

..... (2.16)

where

$$C_v = \frac{V_{ref}(k+1) - V_{real}(k+1)}{T_{su}^9}.$$

The generated acceleration and position are given by

$$a_v = \frac{d}{dt}V_{REF} = 630C_v\left[t^4(t-T_{su})^4\right]_0^{T_{su}}, \quad \text{.....(2.17)}$$

$$X_v = \int_0^{T_{su}} V_{REF}\,dt$$

$$= \frac{C_v}{2}\left[14t^{10} - 70T_{su}t^9 + 135T_{su}^2t^8 - 120T_{su}^3t^7 + 42T_{su}^4t^6\right]_0^{T_{su}}.$$

..... (2.18)

In Eq. 2.17, notice that the value of a_v is zero when t is equal to 0 and T_{su}. This demonstrates that the calibration of the velocity error with function B do not cause any value error to acceleration interpolation.

(4) Calibration of position error.

After the calibration of velocity error, position error is corrected by using function B. After the second and third step, position error is obtained as

$$X_{REF} = X_{ref}(k+1) - X_{real}(k+1) - X_v. \quad \text{..... (2.19)}$$

Also with the integral of the basic function, position error is corrected by

$$X_{REF} = C_x 630\int_0^{T_{su}} f\,dt$$

$$= C_x\left[70t^9 - 315T_{su}t^8 + 540T_{su}^2t^7 - 420T_{su}^3t^6 + 126T_{su}^4t^5\right]_0^{T_{su}},$$

……...…… (2.20)

The generated acceleration and velocity are given by

$$a_x = \frac{d^2}{dt^2}X_{REF} = 630C_x\left[4t^3(t-T_{su})^4 + 4t^4(t-T_{su})^3\right]_0^{T_{su}},\ \text{……..…… (2.21)}$$

$$V_x = \frac{d}{dt}X_{REF} = 630C_x\left[t^4(t-T_{su})^4\right]_0^{T_{su}}.\ \text{……..……..… (2.22)}$$

In Eq. 2.21 and Eq. 2.22, the value of the generated acceleration a_x and velocity V_x is zero when t is equal to 0 and T_{su}. This also demonstrates that the generated acceleration and position do not cause any value errors to acceleration interpolation and velocity error calibration.

(5) Derivation of final acceleration, velocity and position.

At last, final acceleration, velocity and position of interpolation are obtained as

$$a_T = a_{REF} + a_v + a_x,\ \text{…… (2.23)}$$

$$V_T = V_a + V_{REF} + V_x,\ \text{……..…… (2.24)}$$

$$X_T = X_a + X_v + X_{REF},\ \text{……..…… (2.25)}$$

where a_T, V_T and X_T are the final acceleration, velocity and position of interpolation.

Up to here, three policies and an algorithm of the new interpolation methodology have been presented. However, the new interpolation methodology for position command is imperfect for practical applications because of two problems.

One is an interpolation problem of initial three digital data points. Initially, digital data point $X_{ref}(2)$ must be provided by the high-order controller, then, servo controller can start the interpolation of the first two digital data points $X_{ref}(0)$ and $X_{ref}(1)$. During the time interval of waiting for $X_{ref}(2)$, control process during time interval from 0 to T_{su} is unable to proceed in servo controller. As a result, industrial robot manipulators perform no motion during time interval of $[0 \quad 2T_{su}]$. Because of this result, control systems of industrial robot manipulators judge that there is a mechanical failure and the whole system of industrial robot manipulators may be urgently shut down. Considering that time delay arises from the interpolation of initial three digital data points may lead to mechanical failure, to avoid this misrecognition, some kind of countermeasure is necessary.

In the new interpolation methodology, initial digital data points are processed to cope with the time delay problem. The process includes two steps and with Fig. 2.5, two steps will be illustrated.

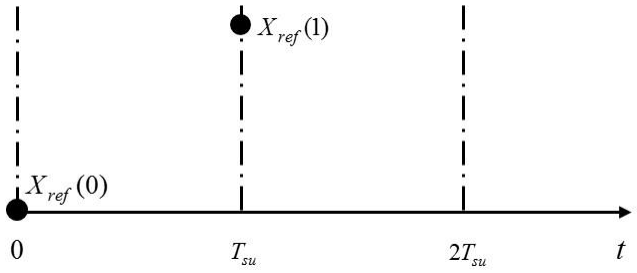

(a) Original position command

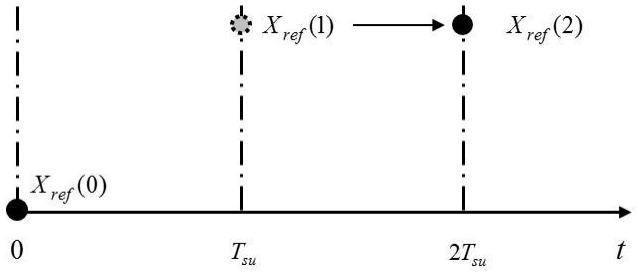

(b) Assumption of position command $X_{ref}(2)$

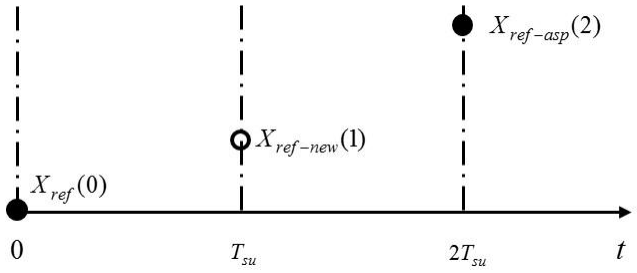

(c) Generation of new position command $X_{ref}(1)$

Fig. 2.5 Initial processes

The first step is to assume a $X_{ref}(2)$, which is shown in Fig. 2.5 (b). Without waiting for output of the actual $X_{ref}(2)$, a virtual $X_{ref}(2)$ shown by $X_{ref-asp}(2)$ is assumed, which is in fact $X_{ref}(1)$. The second step is to generate a new $X_{ref}(1)$, which is shown in Fig. 2.5 (c). The new $X_{ref}(1)$ is shown by $X_{ref-new}(1)$. In the first step, $X_{ref}(1)$ is assumed to be the virtual $X_{ref}(2)$. A new $X_{ref}(1)$ needs to be generated for interpolation. To obtain a smooth interpolation between $X_{ref}(0)$ and $X_{ref-asp}(2)$, which is in fact the interpolation between $X_{ref}(0)$ and $X_{ref}(1)$, the new $X_{ref}(1)$ is generated by

$$X_{ref-new}(1) = X_{ref}(0) + \frac{X_{ref}(0) + X_{ref-asp}(2)}{4} \quad \text{..... (2.26)}$$

With above process, initial time delay problem can be resolved. With the interpolation between $X_{ref}(0)$ and $X_{ref-new}(1)$, control process between 0 and T_{su} can start instantly when $X_{ref}(1)$ is

provided. Ultimately, the misrecognition problem can be avoided.

After interpolation of $X_{ref}(0)$ and $X_{ref-new}(1)$, the real position command $X_{ref}(2)$ is output. With the new generated $X_{ref-new}(1)$, the interpolation between $X_{ref-new}(1)$ and $X_{ref-asp}(2)$ continues and finally, the interpolation between $X_{ref}(0)$ and $X_{ref}(1)$ is completed.

The other problem is an interpolation problem of the last two digital data points of position command. In Fig. 2.6, it is assumed that $X_{ref}(N)$ is the last digital data point. Due to the absence of the next digital data point of position command, the interpolation between $X_{ref}(N-1)$ and $X_{ref}(N)$ is unable to be completed. To complete the interpolation of $X_{ref}(N-1)$ and $X_{ref}(N)$, the presence of one more digital data point is assumed. With the assumed digital data point $X_{ref}(N+1)$, three digital data points of position command that are necessary for interpolation between $X_{ref}(N-1)$ and $X_{ref}(N)$ are collected.

In Fig. 2.6 (b), $X_{ref}(N+1)$ is specified as follows

$$X_{ref}(N+1) = X_{ref}(N) \quad \text{..... (2.27)}$$

As a matter of fact, $X_{ref}(N+1)$ is specified as the same with $X_{ref}(N)$. It is reasonable because industrial robot manipulators perform no motion after the execution of the last digital data point of position command. In other words, industrial robot manipulators terminate all operations and permanently stop at the goal position. So, if the next of the last digital data point exists, it shall be assumed to be the same with the last digital data point of position command.

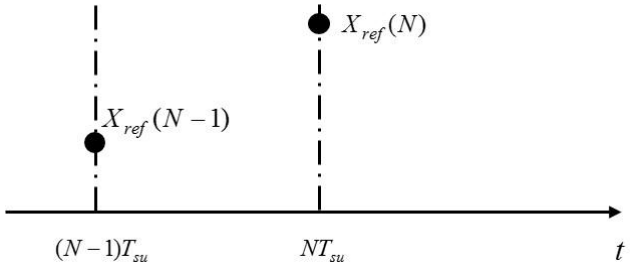

(a) The last two position commands

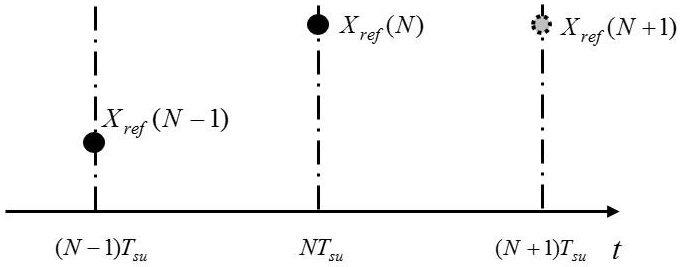

(b) Assumption of position command $X_{ref}(N+1)$

Fig. 2.6 Last processes

With initial and last processes of position command, the entire presentation of the new interpolation methodology is given. To verify the effectiveness of the new interpolation methodology, several simulations are conducted with results reported in section 2.4.

2.4 Simulation verifications

In subsection 2.4.1, some simulation results will be offered to evaluate the effectiveness of the new interpolation methodology with sampling time reported in Table. 2.1. In subsection 2.4.2, an interpolation application for perfect tracking control is given and with the simulation result, advantages of the new interpolation for improvement of control performance will be presented.

Table. 2.1 Sampling time

Parameters	Value	Unit
T_{su}	2	$[m\text{sec}]$
T_s	125	$[\mu\text{sec}]$

2.4.1 Position command interpolation

Without loss of generality, two types of position command are taken as original position command, which will be interpolated by using the new interpolation methodology. The two types of position command are ramp and parabola, which respectively represents typical uniform motion and uniformly-accelerated motion. In addition, a random position command is also employed to represent random motion. Results of simulations are given in Fig. 2.7, where the results of Spline interpolation are also offered to compare with the results of the new interpolation methodology.

Intuitively, the common thing in the simulation results is that interpolated command obtained by both the new interpolation methodology and Spline interpolation accurately pass through original digital data points. It at least indicates that the new interpolation methodology is not worse than Spline interpolation in interpolation accuracy. However, the interpolated command obtained by the new interpolation methodology differs from Spline interpolation in ramp position command. For instance, in the result of ramp position command, the difference is the interpolation between the initial and the last two digital data points. In the case of Spline interpolation, the most suitable interpolation curve that is ramp is finally found only when servo controller obtains the last digital data point of position command. In contrast, in the case of the new interpolation methodology, interpolation proceeds successively. The interpolation curve between the first two digital data points is instantly obtained when the second digital data point is output from the high-order controller. The interpolation curve is not a ramp due to the initial process. The interpolation curve between the last two digital data points is also not a ramp due to the last process. The new interpolation methodology works as the same with Spline interpolation in addition to the interpolation between the first and the last two digital data points because the interpolation curve is a ramp between the second and the sixth digital data point.

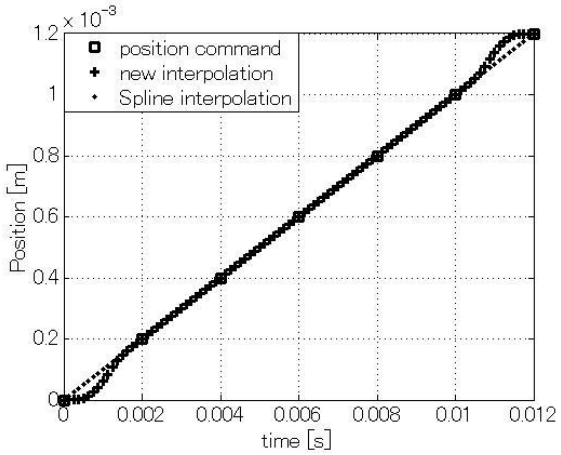

(a) Ramp position command

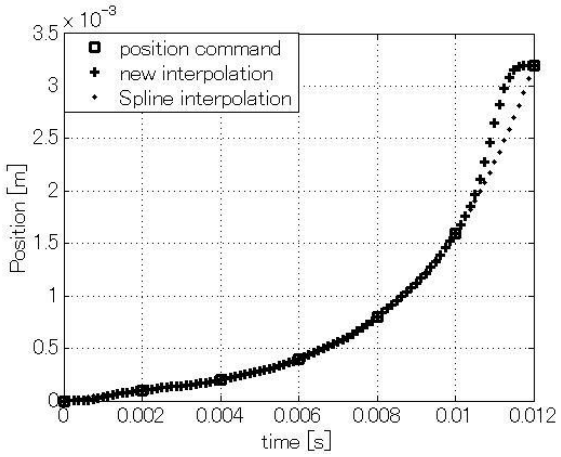

(b) Parabola position command

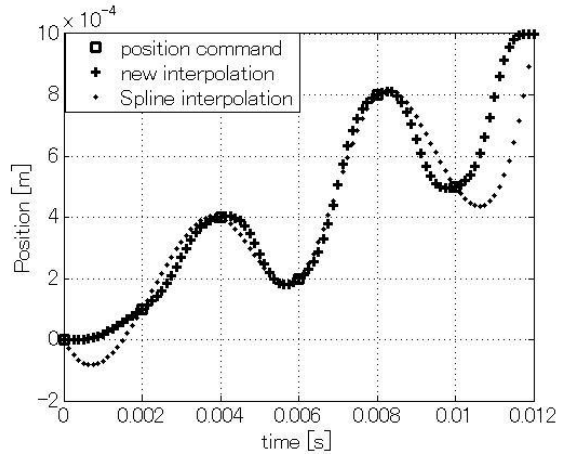

(c) Random position command

Fig. 2.7 Simulation verification for interpolation

Simulation results shown in Fig. 2.8 are employed to confirm the overshoot problem of both Spline interpolation and the new interpolation methodology. In contrast, the improved interpolation results obtained by using the new interpolation methodology are shown in Fig. 2.9.

In Fig. 2.8 (a), rest time is assumed in ramp position command, which is time between 0 and 0.002 second and time between 0.01 and 0.012 second. In practical situations, the rest time means that an industrial robot manipulator holds original point before operations or keeps stationary condition after operations. As the same with Fig. 2.8 (a), an interpolation example of the typical step command with rest time is given in Fig. 2.8 (b). In the simulation results, a conspicuous overshoot problem exists in both the new interpolation methodology and Spline interpolation although the amplitude of overshoot is smaller in the simulation result of using the new interpolation methodology.

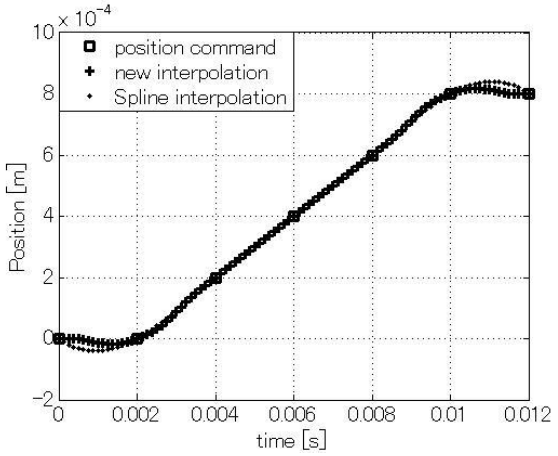

(a) Ramp position command with rest time

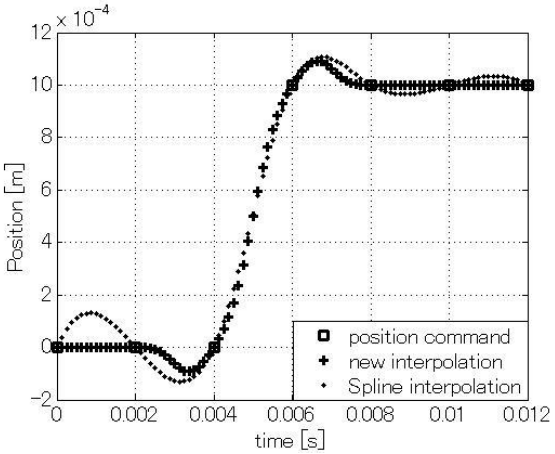

(b) Step command

Fig. 2.8 Simulation verification for overshoot problem

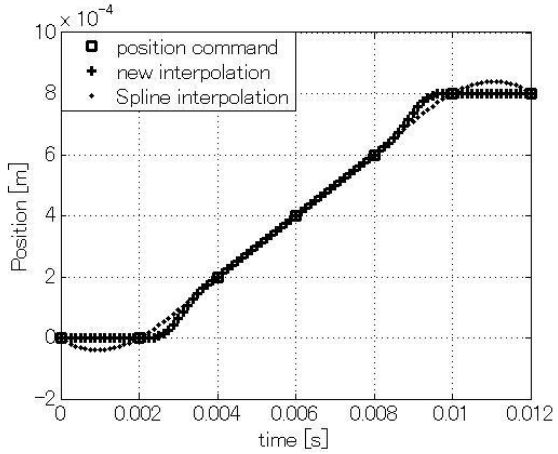

(a) Ramp command with rest time

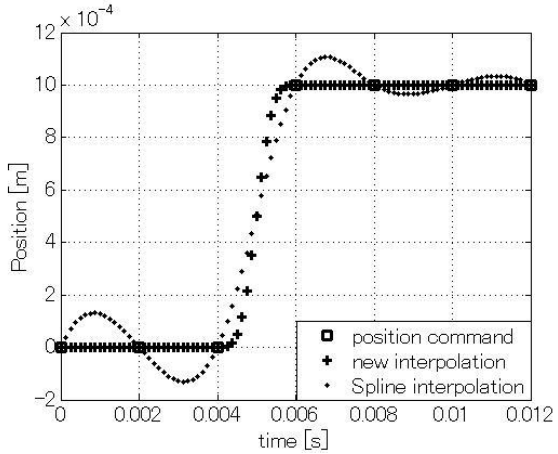

(b) Step command

Fig. 2.9 Simulation verifications for improvement of interpolation

As it is stated in section 2.1, overshoot is absolutely not allowed behavior for interpolation of position command. To resolve the overshoot problem, some improvements have been made in the new interpolation methodology. For the position command points that are in rest time, values of velocity and acceleration command are specified to be zero,

$$V_{ref-0} = V_{ref-goal} = 0 \quad \text{..... (2.28)}$$

$$U_{ref-0} = U_{ref-goal} = 0 \quad \text{..... (2.29)}$$

where V_{ref-0}, $V_{ref-goal}$, U_{ref-0} and $U_{ref-goal}$ are velocity and acceleration command of the digital data points that are positioned in rest time. The specifications are based on consideration that industrial robot manipulators perform no motion during the rest time and therefore, velocity and acceleration are zero. Naturally, a premise of the above specifications is that types of position command are known in advance. In comparison with Fig. 2.8, overshoot phenomenon disappears in the simulation results of using the improved new interpolation methodology.

2.4.2 An application for control

In this section, an application of the interpolated command is presented. The interpolated command is used in a perfect tracking control. For simplicity, a second order system is assumed to be the control object, which is given by

$$\frac{X(s)}{F(s)} = \frac{1}{Ms^2}, \quad \text{……(2.30)}$$

where $X(s)$ represents a displacement output and $F(s)$ represents a force input, M is the mass of the system. Supposing that the feedback controller already exists, the closed-loop transfer function is expressed as

$$\frac{X(s)}{X_{ref}(s)} = \frac{K_1}{s^2 + K_2 s + K_1}, \quad \text{……(2.31)}$$

where $X_{ref}(s)$ represents the position command, K_1 and K_2 are feedback gains.

To realize the perfect tracking control, a feed-forward controller is designed as

$$F_{FF}(s) = \left(\frac{1}{K_1} s^2 + \frac{K_2}{K_1} s + 1 \right) X_{ref}(s), \quad \text{……(2.32)}$$

where $F_{FF}(s)$ represents a feed-forward output. $F_{FF}(s)$ is expressed in the form of discrete time, then,

$$F_{FF}(k) = \frac{1}{K_1} \ddot{X}_{ref}(k) + \frac{K_2}{K_1} X_{ref}(\dot{k}) + X_{ref}(k). \quad \text{……(2.33)}$$

Notice that a differential and a second-order differential of the position command are necessary for completing perfect tracking control of the second order system. The differential and second-order differential of position command can be directly obtained from the interpolated position command because the velocity (differential) and acceleration command (second-order differential) have been specified in the process of interpolation. Hence, one of the merits of the new interpolation methodology is the convenience of implementing the perfect tracking control for the second-order system.

An improvement of control performance by using the perfect tracking control is explicit and the improvement will be not presented in this paper. In addition to the merit of convenience, the new interpolation methodology can be also compared with Spline interpolation in the improvement of control performance. The new interpolation methodology and Spline interpolation are respectively applied to a simulation of perfect tracking control. The simulation results are shown in Fig. 2.10 and Fig. 2.14. The initial, transient and steady state is respectively shown in Fig. 2.11, Fig. 2.12 and Fig. 2.13; Fig. 2.15, Fig. 2.16 and Fig. 2.17. Comparing Fig. 2.11 with Fig. 2.15, notice that vibration occurs in the initial state of position response of using Spline interpolation. In contrast, a smooth position response is obtained in the case of the new interpolation methodology. In Fig. 2.12 and Fig. 2.16, differences of both are not obvious and nearly the same tracking performances can be seen.

Referring to Fig. 2.13 and Fig. 2.17, in steady state, the common problem in both is the overshoot problem, which is also a general problem of applications of the perfect tracking control. In the case of Spline interpolation, bigger amplitude of overshoot occurs in position response. The only reason of this is considered to be that the overshoot in Spline interpolation itself is causes bigger amplitude of overshoot of position response. Therefore, it can be said that the new interpolation methodology is more suitable than Spline interpolation for positioning control of industrial robot manipulators.

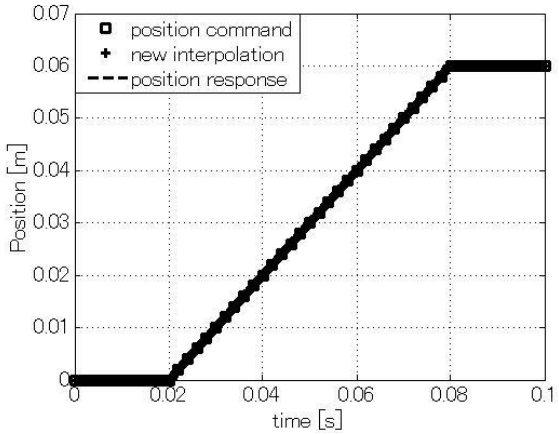

Fig. 2.10 Control results of using the new interpolation methodology

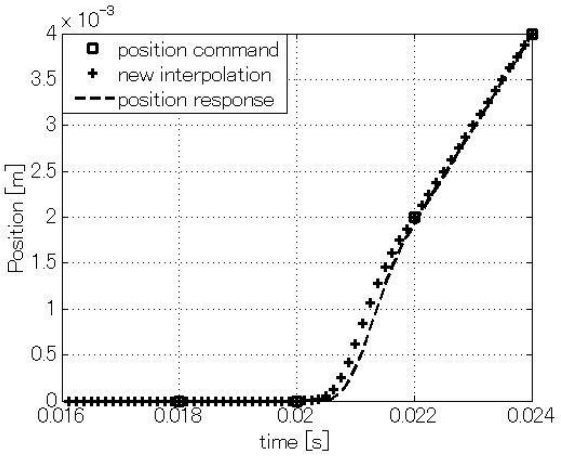

Fig. 2.11 Enlarged view between 0.016 and 0.024 second

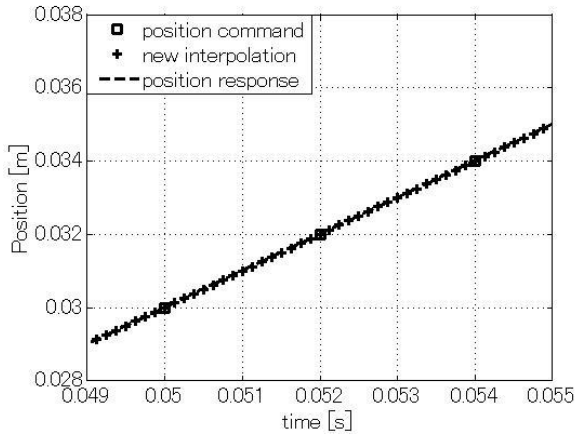

Fig. 2.12 Enlarged view between 0.049 and 0.055 second

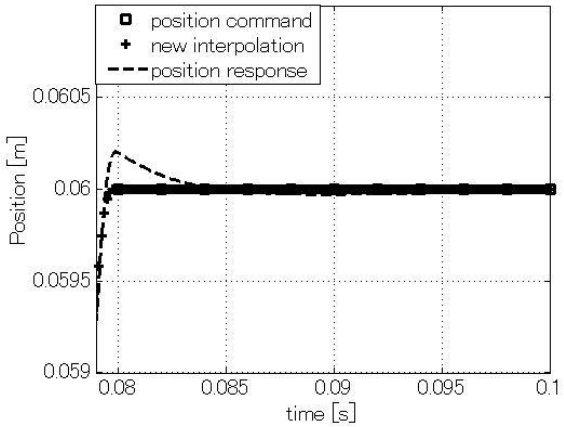

Fig. 2.13 Enlarged view between 0.079 and 0.01 second

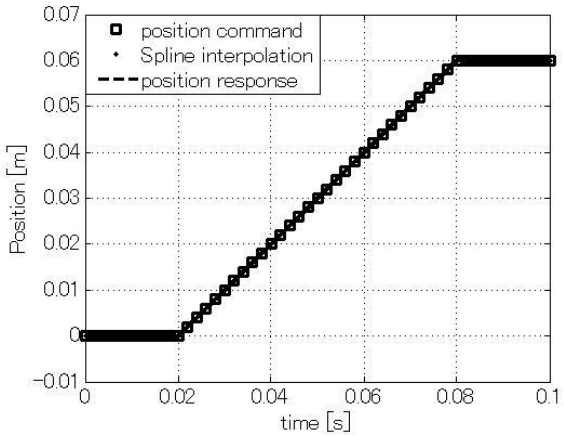

Fig. 2.14 Control results of using Spline interpolation

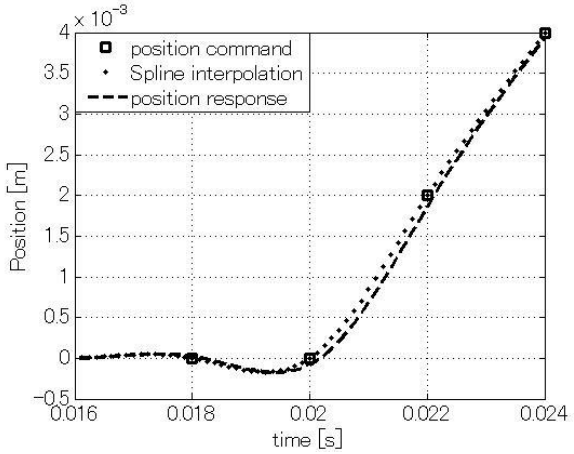

Fig. 2.15 Enlarged view between 0.016 and 0.024 second

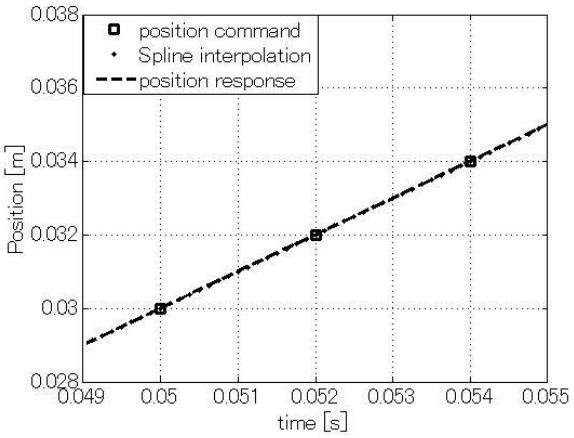

Fig. 2.16 Enlarged view between 0.049 and 0.055 second

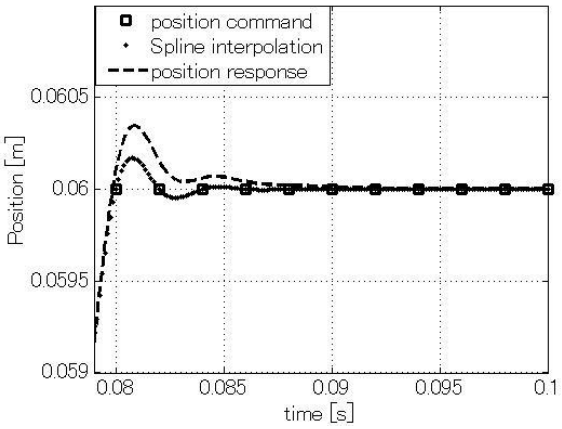

Fig. 2.17 Enlarged view between 0.079 and 0.01 second

2.5 Conclusions

A new interpolation methodology for high-speed and high accuracy control of industrial robot

manipulators has been proposed in this chapter. Several results achieved by using the proposed methodology are

(1) Successive interpolation manner has been achieved by using the new interpolation methodology. Due to this, time delay problem caused by position command interpolation in the case of Spline interpolation has been resolved and the proposed interpolation methodology has made great improvement of efficiency of a whole control process.

(2) The critical overshoot problem of by using Spline interpolation has been also resolved by the proposed interpolation methodology.

(3) In comparison with Spline interpolation, the algorithm of the proposed interpolation methodology is much simpler and less computation is also a very good merit for practical application, especially for general-purposed servo control systems.

Chapter 3

Decoupling control by using Model Following Control

3.1 About decoupling control

In order to make an industrial manipulator track a specified trajectory at a high speed and with higher accuracy, various studies have been made. Decoupling control theory has been established in 1980s which has been considered to be one of effective ways to realize high-speed and high-accuracy control of industrial robot manipulators.

In most cases, some theoretical decoupling controls have been planned and developed for the typical direct drive (DD) robot shown in Fig.3.1. Fround [17], Iwakane and Inoue [18] proposed a decoupling control method that compensates for the coupling forces between two links of a 2-link manipulator according to the dynamic equations. Decoupling control considered in robust control area [19] with disturbance observers has been also reported in [20] - [22]. Moreover, Ito and Shiraishi [23] used a feed-forward (abbreviated as FF) control loop combined with a disturbance observer to accomplish simple robust decoupling control for articulated robots. In these literature, decoupling control strategy are based on a model of rigid system because the control objects are DD robots. For the industrial robot manipulators equipped with flexible joints (usually are gear transmissions), they have not offered a discussion. Nakashima et al. [24] considered that the elasticity of the flexible joints is non-negligible, and firstly presented that the coupling forces do not directly act on actuators due to the elasticity and offered a decoupling control strategy in which each link of the industrial robot manipulator is modeled by a 2-inetia system.

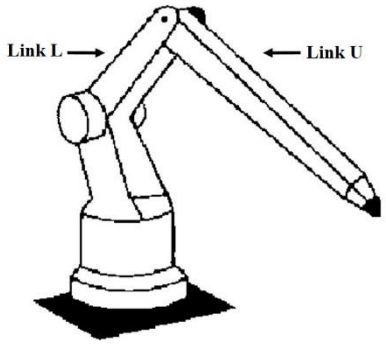

Fig. 3.1 Direct drive robot manipulator

Chapter 3 Decoupling control by using Model Following Control

In all above presented decoupling control literature, the basic control manner is feedback control and decoupling control strategies are conducted in basic feedback control (abbreviated as FB). However, with the growing stringent requirements of high performance for industrial robot manipulators, a sort of advanced control manner that is Model Following Control (MFC) has been gradually adopt. For MFC, its purpose is to force the dynamic response of a plant to follow the response of a reference model by a correction mechanism within itself. The MFC technique has been widely described in the literature [25]-[27]. Under condition of knowing the exact dynamics of industrial robot manipulators, decoupling control strategy that is based on MFC has achieved very good result [28]. However, the decoupling strategy in [28] is complex and difficult to be implemented in practical application. In this paper, an industrial robot manipulator with flexible joints is taken as decoupling control object and a new decoupling control strategy is proposed, which is based on MFC.

In addition, in comparison with conventional decoupling strategies, some favorable aspects of the decoupling control by using the Model following control can be enumerated as follows.

(1) The torque used to compensate for the coupling force that is called compensation torque can be designed independently. In coupling robot manipulator system, the coupling effect has a great influence on position accuracy of motors. In essence, some interference components caused by the coupling effect are forcibly added to position of motors. In [24] and [28], position of motors are used to construct a semi-closed control loop, as a result, the semi-closed control loop includes some interference components. Therefore, an additional compensation torque has to be designed to eliminate the interference components included in the semi-closed control loop. Ultimately, the design of the compensation torque for the coupling robot manipulator system becomes complex and relies on the design of the semi-closed loop. However, in the MFC, the compensation torque can be designed in feed-forward controller and without using position of motors. Design of compensation torque is independent. Moreover, computational capacity of controller system must be taken into account when a decoupling control is put into practice [29]. In comparison with conventional decoupling control strategies, the decoupling control strategy by using MFC is easier for practical application.

(2) The decoupling control by using MFC is more suitable for general purpose industrial robot manipulators. The already known information of other links is essential for the actual implementation of decoupling control. However, the necessary information of a link is unknown by the other because the general-purpose servo system of each link usually does not have bidirectional communication function. For the decoupling control based on FB control, it is a very serious drawback. In contrast, there is no need to take the bidirectional communication issue into account in the case of the MFC because in feed-forward loop of MFC, information of each link is already known.

However, potential subject arises from the decoupling control by using MFC, such as modeling error problem. If the dynamical model of an industrial robot manipulator is not exact, it would not be able to accomplish the complete decoupling of two links because the designed compensation torques are

designed based on the dynamical model. In other words, the industrial robot manipulator is still a coupling system. For the new subject, observers are employed in FB controllers, to resolve the modeling error issue. With the estimations of observers, compensation torques called disturbance compensation torque are designed. With FB compensations, the robustness of a whole of decoupling control are able to be guaranteed.

General industrial robot manipulators have six or seven links. In this paper, a 2-link manipulator is taken as a decoupling control target because the coupling effect occurs mostly in the case that when two links of the manipulator rotate in the same plane. Among many types of industrial robot manipulators, the coupling effect is especially severe in the type of point to point positioning robots. One of typical examples of the accuracy deterioration due to the coupling phenomenon is in spot welding robots. High-speed positioning of the end effector of the spot welding robots must be realized in very small operating range (most of cases 30mm~50mm), referring to Fig. 3.2. The coupling force between two links adversely affects positioning operation and due to this the welding robots are not able to accomplish a successful straight line welding motion [24], referring to Fig. 3.3. So, in this paper, the decoupling objects are assumed to be a 2-link manipulator of spot welding robots.

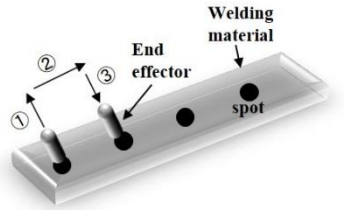

Fig. 3.2 Straight line spot welding

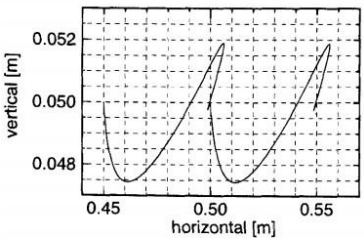

Fig. 3.3 Trajectory of end effector

The proposed decoupling control strategy is presented in detail from section 3.2 to section 3.5. The coupling model of the 2-link manipulator is shown in section 3.2. In section 3.3, fundamental design of torques and design details of compensation torques are presented. The disturbance compensation torques are derived with estimations in section 3.4. Several simulations conducted for verifications are given in section 3.5

3.2 Coupling model of a 2-link manipulator

The derivation of mathematical model is necessary for finding control strategies. In this section, the derivation of the mathematical coupling model of the 2-link manipulator will be prepared in advance for constructing decoupling control strategy.

The dynamics of a 2-link manipulator is derived in subsection 3.2.1 by using Euler-Lagrange equation. In subsection 3.2.2, the dynamics of actuators is covered. With the dynamics shown in

subsection 3.2.1 and subsection 3.2.2, the mathematical coupling model of the 2-link manipulator is obtained and shown in subsection 3.2.3.

3.2.1 Dynamics of a 2-link manipulator

For control design purposes, it is necessary to have a mathematical model that reveals the dynamical behavior of a system. Therefore, in this subsection, the dynamical equations of motion for the 2-link manipulator are derived according to Euler-Lagrange equation of motion.

Before showing the derivation of the dynamics of the 2-link manipulator, the basic derivation of Euler-Lagrange equation will be reviewed for better understanding the later derived dynamics.

Consider a mass m acted upon by force F. Then, the kinetic energy of the mass is

$$K = \frac{1}{2} m\dot{x}^2 . \quad \text{..... (3.1)}$$

The momentum of the mass is

$$p = m\dot{x} , \quad \text{..... (3.2)}$$

where x is function of generalized coordinate

$$x = x(q_1, q_2, ..., q_n;\ t) , \quad \text{..... (3.3)}$$

and each axis is a function of time t

$$q_i = q_i(t) . \quad \text{..... (3.4)}$$

Relation between K and p, p and F are

$$p = \frac{\partial K}{\partial \dot{x}} , \quad \text{..... (3.5)}$$

$$\dot{p} = \frac{d}{dt} p = F . \quad \text{..... (3.6)}$$

It follows that

$$\dot{x} = \frac{d}{dt} x = \sum_{i=1}^{n} \frac{\partial x}{\partial q_i} \dot{q}_i + \frac{\partial x}{\partial t} , \quad \text{..... (3.7)}$$

where $i = 1,2,...,n$. Hence, the differential of $\dot{x}$ with respect to component $\dot{q}_i$ may be written as

$$\frac{\partial \dot{x}}{\partial \dot{q}_i} = \frac{\partial x}{\partial q_i} . \quad \text{..... (3.8)}$$

The momentum of each axis (q_i) of generalized coordinate is

$$p_i = \frac{\partial K}{\partial q_i} = \frac{\partial K}{\partial \dot{x}} \frac{\partial \dot{x}}{\partial \dot{q}_i} = p \frac{\partial \dot{x}}{\partial \dot{q}_i} . \quad \text{..... (3.9)}$$

Then, the differential of p_i is

$$\frac{d}{dt} p_i = \dot{p} \frac{\partial x}{\partial q_i} + p \frac{d}{dt} \left(\frac{\partial x}{\partial q_i} \right) = F \frac{\partial x}{\partial q_i} + \frac{\partial K}{\partial \dot{x}} \frac{\partial \dot{x}}{\partial q_i} = F \frac{\partial x}{\partial q_i} + \frac{\partial K}{\partial q_i} . \quad \text{..... (3.10)}$$

Now, if the force F acting on the mass is conservative, there is

$$F = -\frac{\partial P}{\partial x}, \quad \text{..... (3.11)}$$

where P is the potential energy of the mass. Substituting Eq. 3.11 into Eq. 3.10,

$$\frac{d}{dt} p_i = \frac{\partial (K - P)}{\partial q_i}. \quad \text{..... (3.12)}$$

Now, if the Lagrangian is described as

$$L(q_i, \dot{q}_i, t) = K(q_i, \dot{q}_i, t) - P(q_i), \quad \text{..... (3.13)}$$

Notice that $\frac{\partial P}{\partial \dot{q}_i} = 0$. With Eq. 3.13, Eq. 3.9 can be rewritten as

$$p_i = \frac{\partial L}{\partial \dot{q}_i}. \quad \text{..... (3.14)}$$

Thus, the Lagrange equation can be derived as

$$\frac{d}{dt}\left(\frac{\partial L}{\partial \dot{q}_i}\right) - \frac{\partial L}{\partial q_i} = 0. \quad \text{..... (3.15)}$$

The derived Lagrange equation will be used for deriving the dynamics of the 2-link manipulator.

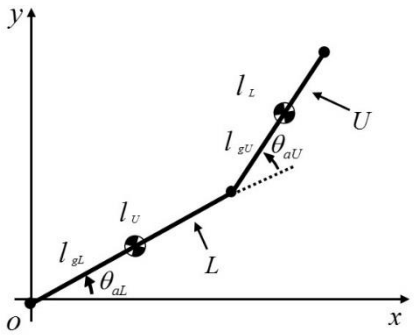

Fig. 3.4 The 2-link manipulator in X-Y coordinate

Table. 3.1 Parameters used for dynamics derivation

Parameters		Unit	Parameters		Unit
l_L, l_U	length of each link	$[m]$	m_L, m_U	mass of each link	$[kg]$
l_{gL}, l_{gU}	length from joint to gravity	$[m]$	θ_{aL}, θ_{aU}	rotation position of each	$[rad]$

Suppose that a 2-link manipulator is positioned in a planar X-Y coordinate, referring to Fig. 3.4. The lower and upper link of the manipulator is denoted by L and U. Parameters used for dynamics

derivation are shown in Table. 3.1.

For link L, the kinetic and potential energies are

$$K_{aL} = \frac{1}{2} m_L l_{gL} \dot{\theta}_{aL}^2 , \text{ ..... (3.16)}$$

$$P_{aL} = m_L g l_{gL} \sin\theta_{gL} . \text{ ..... (3.17)}$$

For link U, there are

$$K_{aU} = \frac{1}{2} m_U [l_L^2 \dot{\theta}_{aL}^2 + l_{gU}^2 (\dot{\theta}_{aL} + \dot{\theta}_{aU})^2 + 2 l_L l_{gU} \dot{\theta}_{aL} (\dot{\theta}_{aL} + \dot{\theta}_{aU}) \cos\theta_{aU}] , \text{ …… (3.18)}$$

$$P_{aU} = m_U g [l_L \sin\theta_{gL} + l_{gU} \sin(\theta_{aL} + \theta_{aU})] . \text{ ..... (3.19)}$$

The Lagrangian for the entire arm is

$$L = K_{aL} + K_{aU} - P_{aL} - P_{aU} . \text{ ..... (3.20)}$$

According to Euler-Lagrange equation, the arm dynamics are given by the two coupled nonlinear differential equations

$$\tau_{aL} = M_{LL} \ddot{\theta}_{aL} + M_{LU} \ddot{\theta}_{aU} + h_{LU} \dot{\theta}_{aU}^2 + 2 h_{LU} \dot{\theta}_{aL} \dot{\theta}_{aU} + G_L , \text{ …..... (3.21)}$$

$$\tau_{aU} = M_{UL} \ddot{\theta}_{aL} + M_{UU} \ddot{\theta}_{aU} + h_{UL} \dot{\theta}_{aL}{}^2 + G_U , \text{ ……..... (3.22)}$$

where τ_{aL} and τ_{aU} are torques supplied by actuators, terms with respect to h_{LU} and h_{UL} are Coriolis and centripetal, G_L and G_U are gravities. In the case of spot welding robots, due to the small distance of two welding spots, the rotation position of each link also changes in a very small range. In other words, θ_{aL} and θ_{aU} are values nearby zeros. Therefore, according to equations of G_L and G_U shown in Eq. 3.23, $\cos\theta_{aL}$ and $\cos(\theta_{aL} + \theta_{aU})$ are approximately equal to one. This means gravity of each link is nearly a constant value.

$$\left.\begin{aligned}
M_{LL} &= m_L l_{gL}^2 + m_U (l_L^2 + l_{gU}^2 + 2 l_L l_{gU} \cos\theta_{aU}) + I_L + I_U \\
M_{LU} &= M_{UL} = m_U (l_{gU}^2 + l_L l_{gU} \cos\theta_{aU}) + I_U \\
M_{UU} &= m_U l_{gU}^2 + I_U \\
h_{LU} &= -m_U l_L l_{gU} (2\dot{\theta}_{aL} + \dot{\theta}_{aU}) \dot{\theta}_{aU} \sin\theta_{aU} \\
h_{UL} &= m_U l_L l_{gU} \dot{\theta}_{aL}^2 \sin\theta_{aU} \\
G_L &= (m_L g l_{gL} + m_U g l_L) \cos\theta_{aL} + m_U g l_{gU} \cos(\theta_{aL} + \theta_{aU}) \\
G_U &= m_U g l_{gU} \cos(\theta_{aL} + \theta_{aU})
\end{aligned}\right\} , \text{ …..... (3.23)}$$

where I_L and I_U are moment of inertia around gravity center. Writing the arm dynamics in vector form yields

$$\begin{bmatrix} \tau_{aL} \\ \tau_{aU} \end{bmatrix} = \begin{bmatrix} M_{LL} & M_{LU} \\ M_{UL} & M_{UU} \end{bmatrix} \begin{bmatrix} \ddot{\theta}_{aL} \\ \ddot{\theta}_{aU} \end{bmatrix} + \begin{bmatrix} d_L \\ d_U \end{bmatrix}, \quad \text{..... (3.24)}$$

where

$$\left.\begin{aligned} d_L &= h_{LU}\dot{\theta}_{aU}^2 + 2h_{LU}\dot{\theta}_{aL}\dot{\theta}_{aU} + G_L \\ d_U &= h_{UL}\dot{\theta}_{aL}{}^2 + G_U \end{aligned}\right\}. \quad \text{..... (3.25)}$$

Inverting Eq. 3.24,

$$\begin{bmatrix} \ddot{\theta}_{aL} \\ \ddot{\theta}_{aU} \end{bmatrix} = \begin{bmatrix} M_{LL} & M_{LU} \\ M_{UL} & M_{UU} \end{bmatrix}^{-1} \begin{bmatrix} \tau_{aL} - d_L \\ \tau_{aU} - d_U \end{bmatrix}. \quad \text{..... (3.26)}$$

Notice that the acceleration of each link is not determined only by the torque supplied by self-actuator and is related to the other.

3.2.2 Modeling for links of a 2-link manipulator

Usually, mechanical structures of the link of industrial manipulators consist of three parts; servomotor, gear transmission and rigid load. Generally, three parts are named actuator, joint and arm. After the discussion of the dynamics of the 2-link manipulator, the dynamics of actuator with joint flexibility need to be derived to obtain a complete dynamical description of the 2-link manipulator. Regarding the gear transmissions as spring systems and converting the inertia of joints into inertia of motors, links of industrial manipulators are modeled as 2-inertia systems. With this understanding, a model of the link without the form of disturbances is shown in Fig. 3.5. The corresponding parameters are reported in Table. 3.2.

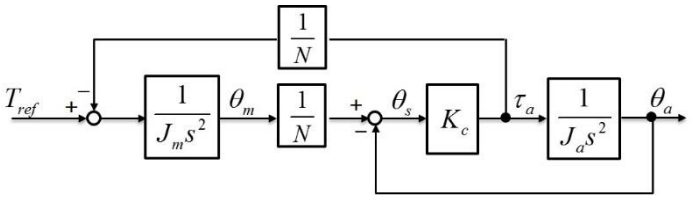

Fig. 3.5 The model of the link (2-inertia system)

Table. 3.2 Parameters used for modelling of the link

Parameters		**Unit**	**Parameters**		**Unit**
J_m	motor inertia	$[kgm^2]$	θ_m	rotation position of motor	$[rad]$
J_a	rigid load inertia	$[kgm^2]$	θ_a	rotation position of rigid load	$[rad]$
N	reduction ratio	$[-]$	θ_s	twist rotation position	$[rad]$
K_c	spring constant	$[Nm/rad]$	T_{ref}	torque reference	$[Nm]$

From the model of the 2-inertial system, mechanical equations of motion can be obtained as

$$\ddot{\theta}_m = -\frac{K_c}{J_m N}\theta_s + \frac{1}{J_m}T_{ref}\ , \quad \text{..... (3.27)}$$

$$\ddot{\theta}_a = \frac{K_c}{J_a}\theta_s\ , \quad \text{..... (3.28)}$$

where

$$\theta_s = \frac{1}{N}\theta_m - \theta_a. \quad \text{..... (3.29)}$$

Up to here, dynamics of motor and rigid load are given in Eq. 3.27 and Eq. 3.28. With the dynamics, a state equation of the coupling model is derived in subsection 3.2.3.

3.2.3 A coupling model

Incorporating two dynamics presented in Eq. 3.27 and Eq. 3.28, the dynamics of the 2-link manipulator is ultimately obtained and expressed as a linear state-equation

$$\dot{\boldsymbol{\theta}} = \mathbf{A}\boldsymbol{\theta} + \mathbf{B}\mathbf{T}_{\mathbf{ref}}\ , \quad \text{..... (3.30)}$$

where $\boldsymbol{\theta}$ is state vector, $\mathbf{A}$ is system matrix, $\mathbf{B}$ is input matrix and $\mathbf{T}_{\mathbf{ref}}$ is torque input vector,

$$\boldsymbol{\theta} = \begin{bmatrix} \theta_{mL} & \dot{\theta}_{mL} & \theta_{aL} & \dot{\theta}_{aL} & \theta_{mU} & \dot{\theta}_{mU} & \theta_{aU} & \dot{\theta}_{aU} \end{bmatrix}^T$$

$$\mathbf{A} = \begin{bmatrix} 0 & 1 & 0 & 0 & 0 & 0 & 0 & 0 \\ a_{21} & 0 & a_{23} & 0 & 0 & 0 & 0 & 0 \\ 0 & 0 & 0 & 1 & 0 & 0 & 0 & 0 \\ a_{41} & 0 & a_{43} & 0 & a_{45} & 0 & a_{47} & 0 \\ 0 & 0 & 0 & 0 & 0 & 1 & 0 & 0 \\ 0 & 0 & 0 & 0 & a_{65} & 0 & a_{67} & 0 \\ 0 & 0 & 0 & 0 & 0 & 0 & 0 & 1 \\ a_{81} & 0 & a_{83} & 0 & a_{85} & 0 & a_{87} & 0 \end{bmatrix}$$

$$\mathbf{B} = \begin{bmatrix} 0 & \frac{1}{J_{mL}} & 0 & 0 & 0 & 0 & 0 & 0 \\ 0 & 0 & 0 & 0 & 0 & \frac{1}{J_{mU}} & 0 & 0 \end{bmatrix}^T$$

$$\mathbf{T}_{\mathbf{ref}} = \begin{bmatrix} T_{refL} & T_{refU} \end{bmatrix}^T$$

$$a_{21}=-\frac{K_{cL}}{J_{mL}N_L{}^2},\quad a_{23}=\frac{K_{cL}}{J_{mL}N_L}$$

$$a_{41}=\frac{K_{cL}}{J_{aL}N_L},\quad a_{43}=-\frac{K_{cL}}{J_{aL}},\quad a_{45}=-\frac{K_{cU}M_{LU}}{J_{aL}M_{UU}N_U},\quad a_{47}=\frac{K_{cU}M_{LU}}{J_{aL}M_{UU}}$$

$$a_{65}=-\frac{K_{cU}}{J_{mU}N_U{}^2},\quad a_{67}=\frac{K_{cU}}{J_{mU}N_U}$$

$$a_{81}=-\frac{K_{cL}M_{UL}}{J_{aU}M_{LL}N_L},\quad a_{83}=\frac{K_{cL}M_{UL}}{J_{aU}M_{LL}},\quad a_{85}=\frac{K_{cU}}{J_{aU}N_U},\quad a_{87}=-\frac{K_{cU}}{J_{aU}}$$

$$J_{aL}=\frac{M_{LL}M_{UU}-M_{LU}M_{UL}}{M_{UU}},\quad J_{aU}=\frac{M_{LL}M_{UU}-M_{LU}M_{UL}}{M_{LL}}.$$

Indeed, the nonlinearities of the items of Coriolis, centripetal and gravities are supposed to exist in Eq. 3.30. These nonlinearities are also supposed to be linearized for constructing a linear control strategy [30]. However, the terms related to the Coriolis and centripetal are neglected in Eq. 3.30 because the Coriolis and centripetal are extremely small in comparison with the coupling force in the case of the spot welding [24]. In this paper, the Coriolis and centripetal are not taken into account in the design of decoupling control because the control object is a spot welding robot. In addition, gravities terms are also omitted in Eq. 3.30 because of a feed-forward compensation which is reported in section 3.3. Therefore, the dynamics of the 2-link manipulator is given by linear Eq. 3.30.

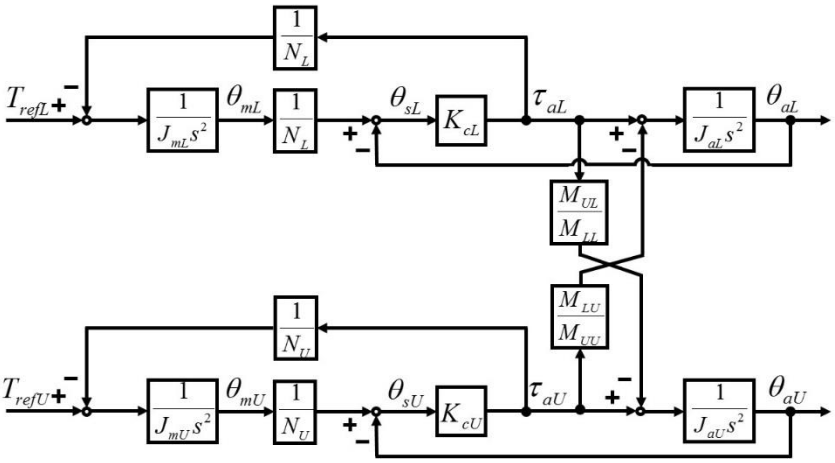

Fig. 3.6 Block diagram of the coupling model of the 2-link manipulator

The coupling effect between two links is reflected in Eq. 3.30. The joint angular acceleration includes interference terms of the other because of the existence of a_{45}, a_{47}, $a_{81}$and a_{83} of system matrix $\mathbf{A}$. The goal of the decoupling control for the 2-link manipulator is to eliminate the elements a_{45}, a_{47}, a_{81} and a_{83}. Based on Eq. 3.30, the block diagram of the coupling model of the 2-link manipulator is given in Fig. 3.6. The coupling effect in an industrial manipulator with flexible joints is different from the DD robot. Two actuators interact through the coupling effect in the case of DD

robots. However, the coupling force are directly applied to rigid loads and inversely act on actuators. Especially, conventional decoupling control strategies that are planned for DD robots are inapplicable to the new decoupling model. Unlike the decoupling control strategy for DD robots, supplies of inverse coupling forces to actuators will no longer work and not completely neglect the coupling effect in the case of the industrial manipulators with flexible joints. So, a derivation of proper supplies of torques for the coupling effect becomes difficult and the corresponding details will be presented in next section.

3.3 Design of feed-forward inputs

Generally it is known that tracking capabilities of feedback control are unavoidably degraded when joint control servos are required to track reference trajectories with higher speed and acceleration. An adoption of feed-forward compensation allows reducing the tracking error. This is just right one of reasons why the proposed decoupling control strategy adopted the MFC. In subsection 3.3.1, a basic design of the decoupling control is given. A mathematical derivation of the compensation torques are based on the basic design and presented in subsection 3.3.2.

3.3.1 Basic design of torques

In this paper, the ultimate torque reference supplied to each link is the incorporation of FF and FB torque input which are defined by

$$T_{refL} = T_{refLFF} + T_{refLFB}, \quad \text{..... (3.31)}$$

$$T_{refU} = T_{refUFF} + T_{refUFB}, \quad \text{..... (3.32)}$$

where T_{refLFF} and T_{refUFF} are feed-forward torque inputs, T_{refLFB} and T_{refUFB} are feedback torque inputs. T_{refLFF} and T_{refUFF} are employed to accomplish two tasks. One is suppression of oscillation of the link due to the low stiffness of the flexible joints. The other is achievement of decoupling of two links of the manipulator. Therefore,

$$T_{refLFF} = T_{refLLFF} + T_{refLCFF}, \quad \text{..... (3.33)}$$

$$T_{refUFF} = T_{refUUFF} + T_{refUCFF}, \quad \text{..... (3.34)}$$

where $T_{refLLFF}$ and $T_{refUUFF}$ are torques designed for suppressing the oscillation of the independent link, $T_{refLCFF}$ and $T_{refUCFF}$ are compensation torques. Here, with regard to the compensations for gravities, it needs to be pointed out emphatically that the compensations for gravities have been taken into account during the design of the compensation torques. In other words, the mathematically derived compensation torques include the compensation components of gravities.

Control strategies for suppressing oscillations of links are different due to different practical

equipment conditions. Sensors that are employed to observe the spatial position of the end effector, or built in links of manipulators to observe rotation acceleration of arm directly influence control strategies. But in usual cases, industrial manipulators are equipped only with sensors that are used to observe rotation position of actuators, not only because cost issues of manufacture of themselves, but also with consideration of that the surrounding environments of industrial manipulators are extremely bad for using sensitive sensors. Without loss of generality, the 2-link manipulator is also assumed to be a manipulator that are not equipped with other sensors in addition to sensors of actuators.

In order to suppress oscillations, torques are generally designed according to the input/output transfer function of an independent link which is given by

$$\theta_a = \frac{\omega_a}{s^2(s^2+\omega_m)} \frac{1}{J_m N} T_{ref} \text{ , } \quad \text{..... (3.35)}$$

where

$$\omega_a = \frac{K_c}{J_a} \text{, } \quad \text{..... (3.36)}$$

$$\omega_m = \frac{K_c}{J_m N^2} + \frac{K_c}{J_a} \text{ . } \quad \text{..... (3.37)}$$

The only observed rotation positions of motors are employed for construction of oscillation suppression in traditional decoupling control [24] and [28]. Due to this, the entire decoupling control systems, as described in introduction, become very complicated. In contrast, the rotation positions of rigid loads are completely available from the mathematical model of the 2-link manipulator in the case of MFC. Therefore, the torques $T_{refLLFF}$ and $T_{refUUFF}$ are designed as follows, which are constructed by state variables that are only related to rigid loads.

$$\begin{aligned} T_{refLLFF} = N_{Ln} J_{LTn} \{ & K_{VLFF} [K_{PLFF} (\theta_{arefL} - \theta_{aLFF}) - \dot{\theta}_{aLFF}] \\ & - K_{a2LFF} \ddot{\theta}_{aLFF} - K_{a3LFF} \dddot{\theta}_{aLFF} \} \end{aligned} \text{ , ……..…….. (3.38)}$$

$$\begin{aligned} T_{refUUFF} = N_{Un} J_{UTn} \{ & K_{VUFF} [K_{PUFF} (\theta_{arefU} - \theta_{aUFF}) - \dot{\theta}_{aUFF}] \\ & - K_{a2UFF} \ddot{\theta}_{aUFF} - K_{a3UFF} \dddot{\theta}_{aUFF} \} \end{aligned} \text{ , ……..… (3.39)}$$

where θ_{arefL} and θ_{arefU} are position references, θ_{aLFF} and θ_{aUFF} denote rotation positions of rigid loads of the mathematical model, J_{LTn} and J_{UTn} are nominal values of total inertia of motors and rigid loads, K_{VLFF} , K_{PLFF} , K_{a2LFF} , K_{a3LFF} and K_{VUFF} , K_{PUFF} , K_{a2UFF} , K_{a3UFF} are control gains of feed-forward loop. Suffix n denotes nominal value.

With the designed $T_{refLLFF}$ and $T_{refUUFF}$, only the compensation torques that are designed for the coupling effect are enough to accomplish the decoupling of two links of the mathematical coupling model. In other words, there is no need to design additional compensations for controllers like what have been done in [24] and [28]. However, special attentions must be paid to components of $\ddot{\theta}_{aiFF}$

and $\dddot{\theta}_{aiFF}$ because $\ddot{\theta}_{aiFF}$ and $\dddot{\theta}_{aiFF}$ are not like θ_{aLFF}, $\dot{\theta}_{aLFF}$ and θ_{aUFF}, $\dot{\theta}_{aUFF}$ that can be directly obtained from the mathematical coupling model. $\ddot{\theta}_{aLFF}$, $\dddot{\theta}_{aLFF}$ and $\ddot{\theta}_{aUFF}$, $\dddot{\theta}_{aUFF}$ need to be derived from the mathematical coupling model and the derivations are given as follows, where suffix i denotes L or U.

$$\begin{aligned}\ddot{\theta}_{aLFF} &= \frac{K_{cLn}}{J_{aLn}}\left\{K_{cLn}\theta_{sLFF} - \frac{M_{LUn}}{M_{UUn}}K_{cUn}\theta_{sUFF}\right\} - \frac{1}{J_{aLn}}G_{LFF} + \frac{M_{LUn}}{J_{aLn}M_{UUn}}G_{UFF} \\ &= \frac{K_{cLn}}{J_{aLn}}\theta_{sLFF} - \frac{K_{cLn}}{J_{aLn}}\frac{M_{LUn}}{M_{UUn}}\theta_{sUFF} - \frac{1}{J_{aLn}}G_{LFF} + \frac{M_{LUn}}{J_{aLn}M_{UUn}}G_{UFF}\end{aligned} \quad , \ldots (3.40)$$

$$\begin{aligned}\ddot{\theta}_{aUFF} &= \frac{K_{cUn}}{J_{aUn}}\left\{K_{cUn}\theta_{sUFF} - \frac{M_{ULn}}{M_{LLn}}K_{cLn}\theta_{sLFF}\right\} - \frac{1}{J_{aUn}}G_{UFF} + \frac{M_{ULn}}{J_{aUn}M_{LLn}}G_{LFF} \\ &= \frac{K_{cUn}}{J_{aUn}}\theta_{sUFF} - \frac{K_{cUn}}{J_{aUn}}\frac{M_{ULn}}{M_{LLn}}\theta_{sUFF} - \frac{1}{J_{aUn}}G_{UFF} + \frac{M_{ULn}}{J_{aUn}M_{LLn}}G_{LFF}\end{aligned} \quad , \ldots (3.41)$$

where G_{LFF} and G_{UFF} denote gravities of the numerical model. Make substitutions as follows:

$$\begin{aligned}\omega_{LLn} &= \frac{K_{cLn}}{J_{aLn}}, \omega_{LUn} = \frac{K_{cUn}}{J_{aLn}}\frac{M_{LUn}}{M_{UUn}}, \\ \omega_{UUn} &= \frac{K_{cUn}}{J_{aUnF}}, \omega_{ULn} = \frac{K_{cLn}}{J_{aUn}}\frac{M_{ULn}}{M_{LLn}}, \\ a_{gLFF} &= \frac{1}{J_{aLn}}G_{LFF} - \frac{M_{LUn}}{J_{aLn}M_{UUn}}G_{UFF}, \\ a_{gUFF} &= \frac{1}{J_{aUn}}G_{UFF} - \frac{M_{ULn}}{J_{aUn}M_{LLn}}G_{LFF}.\end{aligned}$$

$\ddot{\theta}_{aLFF}$ and $\ddot{\theta}_{aUFF}$ are rewritten down as

$$\ddot{\theta}_{aLFF} = \omega_{LLn}\theta_{sLFF} - \omega_{LUn}\theta_{sUFF} - a_{gLFF}, \ldots\ldots\ldots\ldots\ldots\ldots (3.42)$$

$$\ddot{\theta}_{aUFF} = \omega_{UUn}\theta_{sUFF} - \omega_{ULn}\theta_{sLFF} - a_{gUFF}. \ldots\ldots\ldots\ldots\ldots\ldots (3.43)$$

Then,

$$\dddot{\theta}_{aLFF} = \omega_{LLn}\dot{\theta}_{sLFF} - \omega_{LUn}\dot{\theta}_{sUFF} - \dot{a}_{gLFF}, \ldots\ldots\ldots\ldots\ldots\ldots (3.44)$$

$$\dddot{\theta}_{aUFF} = \omega_{UUn}\dot{\theta}_{sUFF} - \omega_{ULn}\dot{\theta}_{sLFF} - \dot{a}_{gUFF}, \ldots\ldots\ldots\ldots\ldots\ldots (3.45)$$

where the backward difference approximations of θ_{sLFF} and θ_{sUFF} are used instead of $\dot{\theta}_{sLFF}$ and $\dot{\theta}_{sUFF}$. For the differential of gravity terms $\dot{a}_{gLFF}$ and $\dot{a}_{gUFF}$, they are approximately seen as zero terms because of the previous explanation that the gravity of each link G_L and G_U is nearly a constant value.

With regard to the determination of gains, many general strategies have been proposed [31]-[34]. The gains of feed-forward loop are determined by comparing with the transfer function of a fourth-

order system. The feed-forward loop input/output transfer function is

$$\frac{\theta_{aiFF}}{\theta_{arefi}} = \frac{\frac{J_{iTn}}{J_{\min}}\omega_{ain}K_{ViFF}K_{PiFF}}{s^4 + \frac{J_{iTn}}{J_{\min}}\omega_{ain}K_{a3iFF}s^3 + \left(\omega_{\min} + \frac{J_{iTn}}{J_{\min}}\omega_{ain}K_{a2iFF}\right)s^2 + \frac{J_{iTn}}{J_{\min}}\omega_{ain}K_{ViFF}s + \frac{J_{iTn}}{J_{\min}}\omega_{ain}K_{ViFF}K_{PiFF}}. \quad \text{……..…… (3.46)}$$

The transfer function of a fourth-order system is

$$G(s) = \frac{\omega_g^4}{s^4 + 4\omega_g s^3 + 6\omega_g^2 s^2 + 4\omega_g^3 s + \omega_g^4}. \quad \text{…… (3.47)}$$

It can be recognized that, with a suitable choice of the gains, it is possible to obtain any value of natural frequency ω_g. Hence, if ω_g is given as design requirements, the following relations can be found:

$$\left.\begin{aligned} K_{PiFF} &= \frac{1}{4}\omega_{gi} \\ K_{ViFF} &= 4\omega_{gi}^3 \frac{J_{\min}}{J_{iTn}\omega_{ain}} \\ K_{a2iFF} &= (6\omega_{gi}^2 - \omega_{\min})\frac{J_{\min}}{J_{iTn}\omega_{ain}} \\ K_{a3iFF} &= 4\omega_{gi}\frac{J_{\min}}{J_{iTn}\omega_{ain}} \end{aligned}\right\}. \quad \text{……..……..…… (3.48)}$$

where $\omega_{gi} = 2\pi f_{giFF}$, f_{giFF} is natural frequency that is used to determine suitable feed-forward loop gains.

3.3.2 Design of compensation torques

After the design of $T_{refLLFF}$ and $T_{refUUFF}$, the mathematical derivation of compensation torques $T_{refLCFF}$ and $T_{refUCFF}$ shall be given in this subsection. At last the compensation torques are added to actuators to suppress the coupling effect between two links of the manipulator. More simply speaking, two connected links become two independent link after decoupling control. Thus, with consideration that each link is modeled as a 2-inetial system, a fourth-order differential equation is supposed to be like

$$\frac{d^4}{dt^4}\theta_a = -a_3\dddot{\theta}_a - a_2\ddot{\theta}_a - a_1\dot{\theta}_a - a_0\theta_a + a_0\theta_{aref} \quad \text{……..…..… (3.49)}$$

where a_0, a_1, a_2 and a_3 are control gains. The differential equation has an obvious characteristic that the differential equation only includes self-state variables. Eq. 3.49 is taken as a standard differential equation and the actual differential equation shall be given to compare with the standard differential equation to reveal what kind of the coupling torque is applied to each link. Prior to the derivation of the compensation torques, some equations that are related to the derivation are

given as follows.

Accelerations of twist rotation positions $\ddot{\theta}_{sLFF}$ and $\ddot{\theta}_{sUFF}$ are derived according to Eq.3.29,

$$\ddot{\theta}_{sLFF} = \frac{1}{N_{Ln}}\ddot{\theta}_{mLFF} - \ddot{\theta}_{aLFF}, \quad \text{(3.50)}$$

$$\ddot{\theta}_{sUFF} = \frac{1}{N_{Un}}\ddot{\theta}_{mUFF} - \ddot{\theta}_{aUFF}. \quad \text{(3.51)}$$

Accelerations of rotation positions of motors are

$$\ddot{\theta}_{mLFF} = \frac{1}{J_{mLn}}\left(T_{refLFF} - \frac{K_{cLn}}{N_{Ln}}\theta_{sLFF}\right), \quad \text{(3.52)}$$

$$\ddot{\theta}_{mUFF} = \frac{1}{J_{mUn}}\left(T_{refUFF} - \frac{K_{cUn}}{N_{Un}}\theta_{sUFF}\right). \quad \text{(3.53)}$$

With Eq. 3.42, Eq. 3.43, Eq. 3.52 and Eq. 3.53, accelerations of twist rotation positions are recalculated and written as

$$\ddot{\theta}_{sLFF} = -(K_{JLn} + \omega_{LLn})\theta_{sLFF} + \frac{1}{J_{mLn}N_{Ln}}T_{refLFF} + \omega_{LUn}\theta_{sUFF} + a_{gLFF}, \quad \text{(3.54)}$$

$$\ddot{\theta}_{sUFF} = -(K_{JUn} + \omega_{UUn})\theta_{sUFF} + \frac{1}{J_{mUn}N_{Un}}T_{refUFF} + \omega_{ULn}\theta_{sLFF} + a_{gUFF}, \quad \text{(3.55)}$$

where

$$K_{JLn} = \frac{K_{cLn}}{J_{mLn}N_{Ln}^2}, \quad K_{JUn} = \frac{K_{cUn}}{J_{mUn}N_{Un}^2}.$$

The differential equation of the coupled links are

$$\frac{d^4}{dt^4}\theta_{aLFF} = \omega_{LLn}\ddot{\theta}_{sLFF} - \omega_{LUn}\ddot{\theta}_{sUFF} - \ddot{a}_{gLFF}, \quad \text{(3.56)}$$

$$\frac{d^4}{dt^4}\theta_{aUFF} = \omega_{UUn}\ddot{\theta}_{sUFF} - \omega_{ULn}\ddot{\theta}_{sLFF} - \ddot{a}_{gUFF}. \quad \text{(3.57)}$$

By using the derived Eq. 3.54 and Eq. 3.55, the results of the recalculation of the differential equations are

$$\begin{aligned}\frac{d^4}{dt^4}\theta_{aLFF} = &-(K_{JLn} + \omega_{LLn})\ddot{\theta}_{aLFF} + K_{JLn}\frac{N_{Ln}}{J_{aLn}}T_{refLFF} \\ &- K_{JLn}\omega_{LUn}\theta_{sUFF} - \omega_{LUn}\ddot{\theta}_{sUFF} - K_{JLn}a_{gLFF} - \ddot{a}_{gLFF}\end{aligned}, \quad \text{(3.58)}$$

$$\begin{aligned}\frac{d^4}{dt^4}\theta_{aUFF} = &-(K_{JUn} + \omega_{UUn})\ddot{\theta}_{aUFF} + K_{JUn}\frac{N_{Un}}{J_{aUn}}T_{refUFF} \\ &- K_{JUn}\omega_{ULn}\theta_{sLFF} - \omega_{ULn}\ddot{\theta}_{sLFF} - K_{JUn}a_{gUFF} - \ddot{a}_{gUFF}\end{aligned}. \quad \text{(3.59)}$$

Notice that, for instance, the differential equation of L Eq. 3.58 includes the interference components of U which are $K_{JLn}\omega_{LUn}\theta_{sUFF}$ and $\omega_{LUn}\ddot{\theta}_{sUFF}$, and the gravities terms. The situation of the differential equation of U Eq. 3.59 is the same with L.

Recalling Eq. 3.33 and Eq. 3.34, the compensation torques designed for eliminating the interference components are given by

$$T_{refLCFF} = \omega_{LC1n}\theta_{sUFF} + \omega_{LC2n}\ddot{\theta}_{sUFF} + a'_{gLFF}\,, \quad \text{..... (3.60)}$$

$$T_{refUCFF} = \omega_{UC1n}\theta_{sLFF} + \omega_{UC2n}\ddot{\theta}_{sLFF} + a'_{gUFF}\,, \quad \text{..... (3.61)}$$

where

$$\omega_{LC1n} = \frac{J_{aLn}}{N_{Ln}}\omega_{LUn},\ \omega_{LC2n} = \frac{1}{K_{JLn}}\frac{J_{aLn}}{N_{Ln}}\omega_{LUn},$$
$$\omega_{UC1n} = \frac{J_{aUn}}{N_{Un}}\omega_{ULn},\ \omega_{UC2n} = \frac{1}{K_{JUn}}\frac{J_{aUn}}{N_{Un}}\omega_{ULn},$$
$$a'_{gLFF} = \frac{\omega_{LC1n}}{\omega_{LUn}}a_{gLFF} + \frac{\omega_{LC2n}}{\omega_{LUn}}\ddot{a}_{gLFF},$$

$$a'_{gUFF} = \frac{\omega_{UC1n}}{\omega_{ULn}}a_{gUFF} + \frac{\omega_{UC2n}}{\omega_{ULn}}\ddot{a}_{gUFF}.$$

Eq. 3.54 and Eq. 3.55 are used again for the substitution of $\ddot{\theta}_{sLFF}$ and $\ddot{\theta}_{sUFF}$ that are included in Eq. 3.60 and Eq. 3.61. The compensation torques of the coupling force and gravities are ultimately obtained and given by

$$T_{refLCFF} = \frac{\omega_{LLn}\omega_{UUn}}{\omega_{LLn}\omega_{UUn} - \omega_{LUn}\omega_{ULn}}(T_{LL} + T_{LU} + T_{Lg})\,, \quad \text{..... (3.62)}$$

$$T_{refUCFF} = \frac{\omega_{LLn}\omega_{UUn}}{\omega_{LLn}\omega_{UUn} - \omega_{LUn}\omega_{ULn}}(T_{UU} + T_{UL} + T_{Ug})\,, \quad \text{..... (3.63)}$$

where T_{Lg} and T_{Ug} are the compensations for gravities,

$$T_{LL} = \left(\omega_{LC2n}\omega_{ULn} - \frac{K_{cLn}\omega_{LUn}\omega_{ULn}}{N_{Ln}\omega_{LLn}\omega_{UUn}} - J_{mLn}N_{Ln}\frac{\omega_{LUn}\omega_{ULn}}{\omega_{UUn}} + \frac{\omega_{LC2n}\omega_{UC1n}}{J_{mUn}N_{Un}}\right)\theta_{sLFF} + \frac{\omega_{LUn}\omega_{ULn}}{\omega_{LLn}\omega_{UUn}}T_{refLLFF}$$

$$T_{LU} = \left(\omega_{LC1n} - (K_{JUn} + \omega_{UUn})\omega_{LC2} + \frac{J_{mLn}N_{Ln}\omega_{LUn}^2\omega_{ULn}}{\omega_{LLn}\omega_{UUn}}\right)\theta_{sUFF} + \frac{\omega_{LC2n}}{J_{mUn}N_{Un}}T_{refUUFF}$$

$$T_{UU} = \left(\omega_{UC2n}\omega_{LUn} - \frac{K_{cUn}\omega_{LUn}\omega_{ULn}}{N_{Un}\omega_{LLn}\omega_{UUn}} - J_{mUn}N_{Un}\frac{\omega_{LUn}\omega_{ULn}}{\omega_{LLn}} + \frac{\omega_{UC2n}\omega_{LC1n}}{J_{mLn}N_{Ln}}\right)\theta_{sUFF} + \frac{\omega_{LUn}\omega_{ULn}}{\omega_{LLn}\omega_{UUn}}T_{refUUFF}$$

$$T_{UL} = \left(\omega_{UC1n} - (K_{JLn} + \omega_{LLn})\omega_{UC2} + \frac{J_{mUn}N_{Un}\omega_{LUn}\omega_{ULn}^2}{\omega_{LLn}\omega_{UUn}}\right)\theta_{sLFF} + \frac{\omega_{UC2n}}{J_{mLn}N_{Ln}}T_{refLLFF}$$

$$T_{Lg} = \frac{\omega_{LC2n}\omega_{UC2n}}{J_{mUn}N_{Un}}a_{gLFF} + a'_{gLFF} + \omega_{LC2n}a_{gUFF} + \frac{\omega_{LC2n}}{J_{mUn}N_{Un}}a'_{gUFF}$$

$$T_{Ug} = \frac{\omega_{UC2n}\omega_{LC2n}}{J_{mLn}N_{Ln}}a_{gUFF} + a'_{gUFF} + \omega_{UC2n}a_{gLFF} + \frac{\omega_{UC2n}}{J_{mLn}N_{Ln}}a'_{gLFF}.$$

3.4 Design of feedback inputs

For the Model Following Control manner, the biggest expectation is a large improvement of control performance. However, the expectation possibly will not come true if the precondition of implementation of the Model Following Control that is accurate modeling of control plant is not satisfied. A modelling error issue directly affects MFC strategy and probably leads to the deterioration of the control performance. Therefore, great importance must be attached to the modelling error issue. In the proposed decoupling strategy, after designing the compensation torques in feed-forward loop, the modelling errors are dealt with in feedback loop.

In this subsection, first of all, modelling errors are discussed to figure out that what kind of errors there are. In this paper, the modelling errors are thought as two types of errors. One is parameter error that is generated during the modelling of the 2-link manipulator. The other is disturbances caused by contact operations. The parameter error of a spring constant is mainly taken into account because in comparison with other parameters of the model of the 2-link manipulator, bigger errors are generated when the gear transmissions are approximately modeled as spring systems. In addition, spring constants are usually derived from the resonant frequencies that are obtained from experimental measurements of links of the 2-link manipulator. In the procedure of experimental measurements of resonant frequencies, some uncertainties such as robot stand vibrations [35] will affects the accuracy of the measurements. Therefore, spring constant error is determined as main parameter error in this paper. For the disturbances, the resistance forces such as friction are generated when the end-effectors of the spot welding robots contact to the welded materials. So, besides parameters errors, friction disturbances are assumed to be main disturbances of the other.

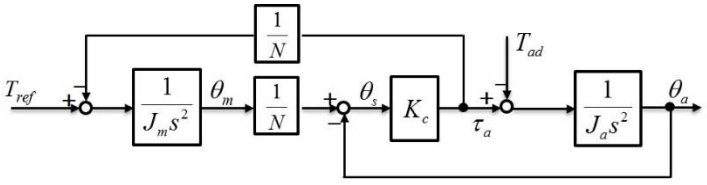

Fig. 3.7 The 2-inertia system with disturbance of rigid load

Since then, the adverse effects of the modelling errors will be discussed. The typical frictional forces caused by contact operations perform in the form of torques and the torques are directly applied to joints of the links. No doubt that the frictional forces ultimately lead to position errors. In addition, the presence of the spring constant errors mean that the designed compensation torques in feed-forward loop are not perfect and the actual coupling torques will not be compensated completely by the designed compensation torques. In other words, the presence of spring constant errors mean the presence of the coupling torques.

At last, the block diagram of a 2-inertia system with the torque disturbance is shown in Fig. 3.7. T_{ad} is a generated torque disturbance due to the modelling errors and it is called a rigid load disturbance in this paper.

3.4.1 A Disturbance estimation

For the rigid load disturbances of a 2-inertia systems, disturbances observers are used to obtain the estimations [36] and the estimations are used in feedback loop to compensate for the rigid load disturbances. A state disturbance observer is used to estimate the torque disturbance of each link as well and it is given by

$$\frac{d}{dt}\begin{bmatrix}\hat{\theta}_m\\ \hat{\dot{\theta}}_m\\ \hat{\theta}_a\\ \hat{\dot{\theta}}_a\\ \hat{u}_d\end{bmatrix}=\begin{bmatrix}0 & 1 & 0 & 0 & 0\\ -\frac{K_{cn}}{J_{mn}N_n^2} & 0 & \frac{K_{cn}}{J_{mn}N_n} & 0 & 0\\ 0 & 0 & 0 & 1 & 0\\ \frac{K_{cn}}{J_{an}N_n} & 0 & -\frac{K_{cn}}{J_{an}} & 0 & 1\\ 0 & 0 & 0 & 0 & 0\end{bmatrix}\begin{bmatrix}\hat{\theta}_m\\ \hat{\dot{\theta}}_m\\ \hat{\theta}_a\\ \hat{\dot{\theta}}_a\\ \hat{u}_d\end{bmatrix}+\begin{bmatrix}0\\1\\0\\0\\0\end{bmatrix}u_{ref}+\begin{bmatrix}l_1\\l_2\\l_3\\l_4\\l_5\end{bmatrix}(\theta_m-\hat{\theta}_m), \quad \text{..... (3.64)}$$

where $\hat{\theta}_m$, $\hat{\dot{\theta}}_m$, $\hat{\theta}_a$ and $\hat{\dot{\theta}}_a$ are estimations of the states of θ_m, $\dot{\theta}_m$, θ_a and $\dot{\theta}_a$. $\hat{u}_d$ is an acceleration estimation of the torque disturbance $\hat{T}_d$, l_1, l_2, l_3, l_4 and l_5 are observer gains

$$u_{ref}=\frac{T_{ref}}{J_{mn}}, \quad \text{..... (3.65)}$$

$$\hat{u}_d=\frac{\hat{T}_d}{J_{an}}. \quad \text{..... (3.66)}$$

The determination strategy of the observer gains is the same with the determination of the control gains of feed-forward loop. The observer gains are determined by comparing the transfer function $u_d(s)/u_{ref}(s)$ with a standard transfer function of fifth order system. Then, the observer gains can be determined as follows.

$$\left.\begin{aligned} l_1&=5\eta\\ l_2&=10\eta^2-\omega_{mn}\\ l_3&=\left(10\eta^3-5\eta\omega_{an}\right)\frac{J_{mn}N_n}{K_{cn}}\\ l_4&=\left[5\eta^4-\left(10\eta^2-\omega_{mn}\right)\omega_{an}\right]\frac{J_{mn}N_n}{K_{cn}}\\ l_5&=\eta^5\frac{J_{mn}N_n}{K_{cn}}\end{aligned}\right\} \quad \text{..... (3.67)}$$

where $\eta=2\pi f_{gOB}$, f_{gOB} is a natural frequency that is used to determine suitable observer gains.

Here, special attention shall be paid to the estimation of the torque disturbance $\hat{T}_d$. $\hat{T}_d$ is the total estimation of all the torque disturbances which are applied to joints of the links. It does not only

includes the rigid load disturbances and also includes the coupling torque components and gravities which have been compensated by the feed-forward compensation torques. The compensated coupling torque components and gravities must be deducted from $\hat{T}_d$. Therefore, the estimations of the rigid load disturbances of the links are obtained by

$$\hat{T}_{adL} = \hat{T}_{dL} - T_{couLFF\_lpf}, \quad \text{(3.68)}$$

$$\hat{T}_{adU} = \hat{T}_{dU} - T_{couUFF\_lpf}, \quad \text{(3.69)}$$

where

$$T_{couLFF} = J_{aLn}(\omega_{LUn}\theta_{sUFF} + a_{gLFF}), \quad \text{(3.70)}$$

$$T_{couUFF} = J_{aUn}(\omega_{ULn}\theta_{sLFF} + a_{gUFF}), \quad \text{(3.71)}$$

$$T_{refLCFF\_lpf} = \left(\frac{1}{1+\tau_{Llpf}s}\right)^5 T_{couLFF}, \quad \text{(3.72)}$$

$$T_{refUCFF\_lpf} = \left(\frac{1}{1+\tau_{Ulpf}s}\right)^5 T_{couUFF}. \quad \text{(3.73)}$$

T_{couLFF} and T_{couUFF} are coupling torques of the numerical model of feed-forward loop, τ_{Llpf} and τ_{Ulpf} are time constants of low pass filters. In order to produce phase lags and to adjust to the phase lags of the disturbance observers, T_{couLFF} and T_{couUFF} are filtered. Therefore, time constants of low pass filters are determined by the natural frequencies which are the same with the natural frequencies of observer gains.

With estimations of rigid load disturbances, the modelling errors will be compensated for in feedback loops. Basic designs of feedback loops are given by

$$T_{refLFB} = T_{refLLFB} + T_{refLDC}, \quad \text{(3.74)}$$

$$T_{refUFB} = T_{refUUFB} + T_{refUDC}. \quad \text{(3.75)}$$

where $T_{refLLFB}$ and $T_{refUUFB}$ are basic feedback loop of the Model Following Control,

$$T_{refLLFB} = J_{LTn}K_{VLFB}[K_{PLFB}(\theta_{mLFF} - \theta_{mL}) + (\dot{\theta}_{mLFF} - \dot{\theta}_{mL})], \quad \text{(3.76)}$$

$$T_{refUUFB} = J_{UTn}K_{VUFB}[K_{PUFB}(\theta_{mUFF} - \theta_{mU}) + (\dot{\theta}_{mUFF} - \dot{\theta}_{mU})], \quad \text{(3.77)}$$

K_{PLFB}, K_{VLFB}, K_{PUFB} and K_{VUFB} are feedback gains and designed as

$$\left.\begin{aligned} K_{VLFB} &= 2\pi f_{gLFB} \\ K_{PLFB} &= \frac{1}{4}K_{VLFB} \end{aligned}\right\}, \quad \text{(3.78)}$$

$$\left.\begin{aligned} K_{VUFB} &= 2\pi f_{gUFB} \\ K_{PUFB} &= \frac{1}{4} K_{VUFB} \end{aligned}\right\} \text{. ..} \quad (3.79)$$

f_{gLFB} and f_{gUFB} are natural frequencies that are used to determine suitable feedback gains. T_{refLDC} and T_{refUDC} are torques designed to compensate for the rigid load disturbances and called disturbance compensation torque. The details of designs of the disturbance compensation torques are presented in subsection 3.4.2.

3.4.2 Compensation designs for disturbances

The most direct impact of the rigid load disturbances is to generate position errors to rotation positions of rigid loads. To avoid this adverse impact, the designs of the disturbance compensation torques are carried out in two steps. The first step is to make a direct compensation for the rigid load disturbances. A differential equation of the rotation position of an independent link is given by

$$\frac{d^4}{dt^4}\theta_a = -\omega_m \dddot{\theta}_a + \frac{\omega_a}{J_m N} T_{ref} - \frac{\omega_a}{J_m N^2} T_{ad} - \frac{1}{J_a} \ddot{T}_{ad} \text{. ..} \quad (3.80)$$

In the differential equation, the third and fourth terms of right side of equal sign are rigid load disturbance components. Recalling Eq. 3.74 and Eq. 3.75, the first of disturbance compensation torque of each link is obtained as

$$T_{refLDC1} = \frac{1}{N_{Ln}} \hat{T}_{adL} + \frac{J_{mLn} N_{Ln}}{K_{cLn}} \ddot{\hat{T}}_{adL} \text{, ..} \quad (3.81)$$

$$T_{refUDC1} = \frac{1}{N_{Un}} \hat{T}_{adU} + \frac{J_{mUn} N_{Un}}{K_{cUn}} \ddot{\hat{T}}_{adU} \text{. ..} \quad (3.82)$$

For the terms of $\ddot{\hat{T}}_{adL}$ and $\ddot{\hat{T}}_{adU}$, they are regarded as zero terms with assumption that the rigid load disturbances do not change suddenly.

The compensation designs in the first step are not enough. As a matter of fact, rotation positions and velocities of motors are also affected by the rigid load disturbances. Due to this, $T_{refLLFB}$ and $T_{refUUFB}$ also include the rigid load disturbance components. The second step is to compensate for the disturbance components that are included in the basic feedback loop.

Rotation acceleration of the rigid load is given by

$$\ddot{\theta}_a = \omega_a \left(\frac{1}{N} \theta_m - \theta_a \right) - \frac{1}{J_a} T_{ad} \text{, ..} \quad (3.83)$$

Then, rotation position and velocity of motor are derived as

$$\theta_m = \frac{1}{\omega_a} \ddot{\theta}_a + N\theta_a + \frac{N}{K_c} T_{ad} \text{, ..} \quad (3.84)$$

$$\dot{\theta}_m = \frac{1}{\omega_a} \dddot{\theta}_a + N\dot{\theta}_a + \frac{N}{K_c} \dot{T}_{ad} \text{. ..} \quad (3.85)$$

Substituting Eq. 3.84 and Eq. 3.85 into Eq. 3.76 and Eq.3.77,

$$T_{refLLFB} = J_{LTn}\Big(K_{VLFB}K_{PLFB}N_{Ln}\theta_{aLFF} + K_{VLFB}N_{Ln}\dot{\theta}_{aLFF} - K_{VLFB}K_{PLFB}N_{Ln}\theta_{aL} - K_{VLFB}N_{Ln}\dot{\theta}_{aL} - K_{VLFB}K_{PLFB}\frac{1}{\omega_{aLn}}\ddot{\theta}_{aL} - K_{VLFB}\frac{1}{\omega_{aLn}}\dddot{\theta}_{aL} - K_{VLFB}K_{PLFB}\frac{N_{Ln}}{K_{cLn}}T_{adL} - K_{VLFB}\frac{N_{Ln}}{K_{cLn}}\dot{T}_{adL}\Big), \quad \text{..... (3.86)}$$

$$T_{refUUFB} = J_{UTn}\Big(K_{VUFB}K_{PUFB}N_{Un}\theta_{aUFF} + K_{VUFB}N_{Un}\dot{\theta}_{aUFF} - K_{VUFB}K_{PUFB}N_{Un}\theta_{aU} - K_{VUFB}N_{Un}\dot{\theta}_{aU} - K_{VUFB}K_{PUFB}\frac{1}{\omega_{aUn}}\ddot{\theta}_{aU} - K_{VUFB}\frac{1}{\omega_{aUn}}\dddot{\theta}_{aU} - K_{VUFB}K_{PUFB}\frac{N_{Un}}{K_{cUn}}T_{adU} - K_{VUFB}\frac{N_{Un}}{K_{cUn}}\dot{T}_{adU}\Big). \quad \text{..... (3.87)}$$

Notice that the basic feedback loop includes the rigid load disturbance components. The second of disturbance compensation torque for each link is employed to eliminate the rigid load disturbance components and derived as

$$T_{refLDC2} = J_{LTn}\frac{N_{Ln}}{K_{cLn}}\left(K_{VLFB}K_{PLFB}\hat{T}_{adL} + K_{VLFB}\dot{\hat{T}}_{adL}\right), \quad \text{..... (3.88)}$$

$$T_{refUDC2} = J_{UTn}\frac{N_{Un}}{K_{cUn}}\left(K_{VUFB}K_{PUFB}\hat{T}_{adU} + K_{VUFB}\dot{\hat{T}}_{adU}\right). \quad \text{..... (3.89)}$$

Finally, the disturbance compensation torques are obtained as follows

$$T_{refLDC} = T_{refLDC1} + T_{refLDC2}, \quad \text{..... (3.90)}$$

$$T_{refUDC} = T_{refUDC1} + T_{refUDC2}. \quad \text{..... (3.91)}$$

3.5 Simulation verifications

In this section, several simulations are conducted to verify the effectiveness of the proposed decoupling control strategy with parameters reported in Table 3.3. The corresponding control gains are shown in Table. 3.4. The resonant frequencies of link L and link U are 10 [Hz] and 19 [Hz].

The first simulation is conducted to verify the effectiveness of the proposed decoupling control strategy in the case of no parameter errors. It would be more accurate to say to demonstrate the validity of the designed compensation torques of feed-forward loop. The simulation results are shown in Fig. 3.8 and Fig. 3.9. Notice that in the case of no compensations for the coupling force (before decoupling control), the resonance suppression of each link is obvious, however, link L and link U of the 2-link manipulator still vibrated around the goal position with large amplitude. Definitely, it is not the generation due to the resonance. In comparison with the position responses of before decoupling

control, link L and link U perform independently when the designed compensation torques are supplied to link L and link U. Hence, it can be said the proposed design strategy of the compensation scheme is valid.

Table. 3.3 Parameters of simulations

Parameter	Value	Unit	Parameter	Value	Unit
m_L	2.34	$[kg]$	m_U	3.00	$[kg]$
l_L	0.25	$[m]$	l_U	0.53	$[m]$
l_{gL}	0.19	$[m]$	l_{gU}	0.30	$[m]$
J_{mL}	2.09×10^{-5}	$[kgm^2]$	J_{mU}	1.95×10^{-5}	$[kgm^2]$
J_{aL}	6.93×10^{-2}	$[kgm^2]$	J_{aU}	8.50×10^{-3}	$[kgm^2]$
K_{cL}	21360	$[Nm/rad]$	K_{cU}	10855	$[Nm/rad]$
N_L	120	$[-]$	N_U	80	$[-]$

Table. 3.4 Simulation Gains

Parameter	Value	Unit
f_{gLFF}	8	$[Hz]$
f_{gUFF}	19	$[Hz]$
f_{gLFB}	6	$[Hz]$
f_{gUFB}	7	$[Hz]$
f_{gLOB}	100	$[Hz]$
f_{gUOB}	100	$[Hz]$

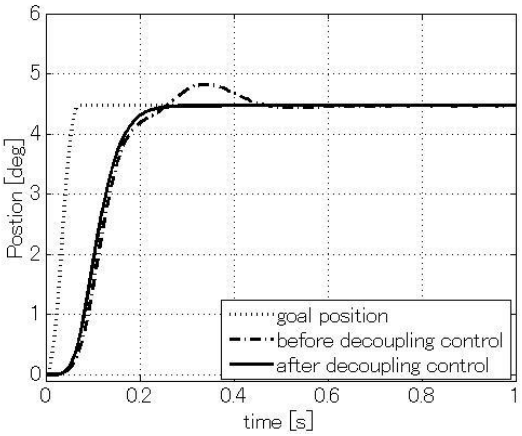

Fig. 3.8 Simulation verification for compensation torque (Link L)

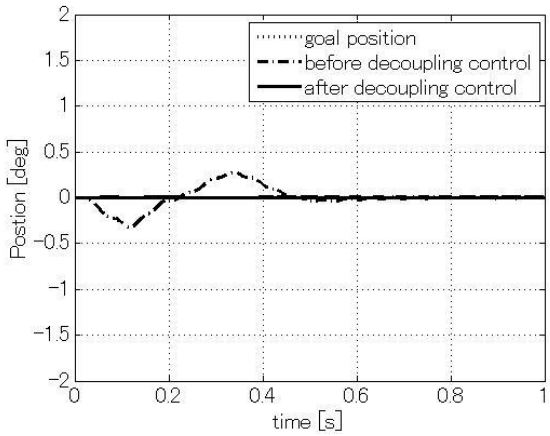

Fig. 3.9 Simulation verification for compensation torque (Link U)

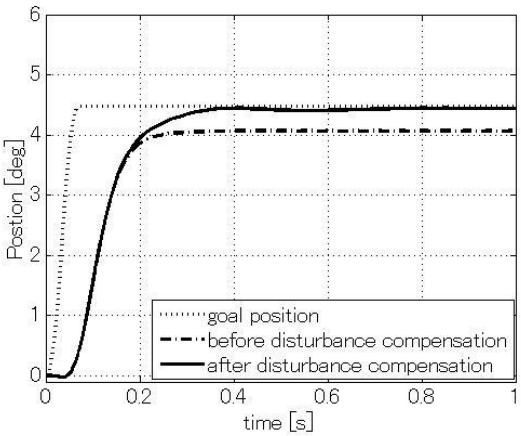

Fig. 3.10 Simulation verification for disturbance compensation (Link L)

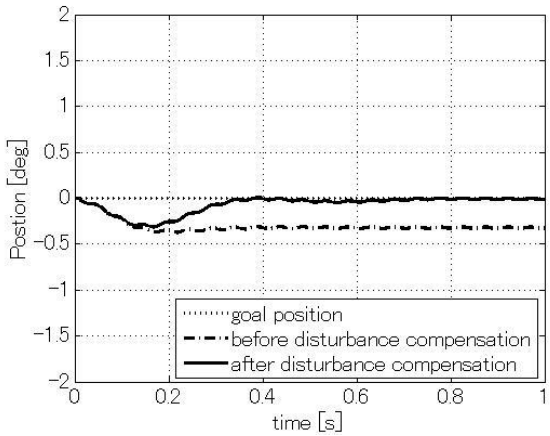

Fig. 3.11 Simulation verification for disturbance compensation (Link U)

The second simulation is conducted to verify the effectiveness of the proposed compensation designs for the rigid load disturbances. The simulation results presented in Fig. 3.12 and Fig. 3.13 are

employed to show the validity of compensation for frictional forces. The frictional forces will be applied to joints when the ends of the spot welding robots contact the surface of welding targets. Due to the small operating range of the end effector of the spot welding robots, rotation angle of rigid loads will not change widely. So the frictional forces applied to the joints of the spot welding robots will not change continuously like sinusoidal signals. The instantaneous frictional forces are more like square wave. Therefore, step disturbances are assumed to be the representation of the frictional forces in this simulations. In the simulation results, the position responses of both link L and link U converge at the goal positions after the step disturbances compensations. There is no doubt that the proposed compensation designs for constant disturbances such as step disturbance are proper.

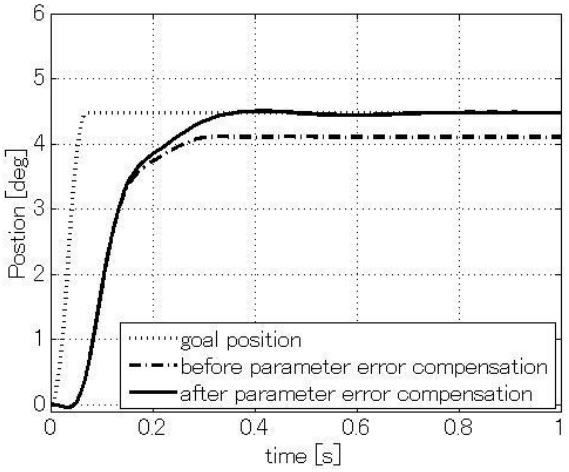

Fig. 3.12 Simulation verification for spring constant error (Link L)

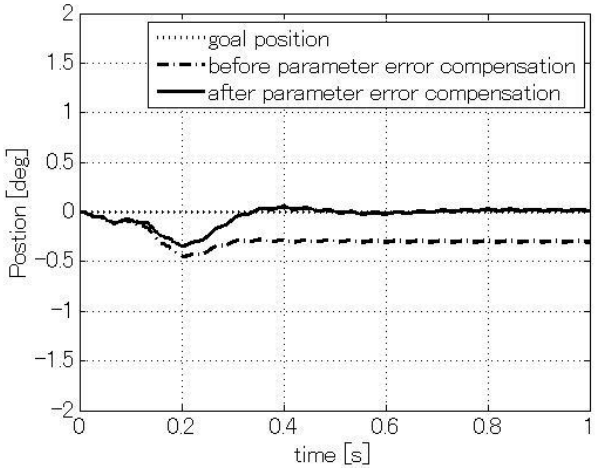

Fig. 3.13 Simulation verification for spring constant error (Link U)

The last simulation is conducted to confirm the robustness of the proposed compensation designs for parameter errors. 20% of the nominal value of spring constant are added to the actual spring constant. Then, the simulation results are shown in Fig. 3.10. In the simulation results, there are not any obviously bad influences of spring constant errors in each response. In other words, with the proposed compensation designs, it is possible to ensure the robustness of the whole control system.

With all above simulation results, it can be finally said that the proposed decoupling control strategy by using Model Following Control is a complete theory and the effectiveness demonstrated by the simulations also indicates that the expectation of the improvement of control performance of spot welding robots is completely possible by using the proposed decoupling control strategy.

However, if the decoupling control objects are not limited to spot welding robots, the proposed decoupling control strategy must be extended for some new issues such as inertia changes of robot arms. As a common-sense question, the inertia of robot arms changes with spatial position of themselves. Generally, inexact identification of the inertia of robot arms causes some inertia errors, which must be taken into account in general control of industrial robot manipulators. In this paper, the inertia errors of robot arms are not considered because in the case of spot welding robots, the inertia of each is almost constant due to the very small change of spatial positions of arms. But, without loss of generality, another simulation is also conducted to make a discussion about the inertia errors of arms.

Table. 3.5 Gains of simulation for inertia errors

Parameter	Value	Unit
f_{gLFF}	7	[Hz]
f_{gUFF}	11	[Hz]
f_{gLFB}	5	[Hz]
f_{gUFB}	15	[Hz]

Control gains are adjusted in order to obtain the best control performance in the case that 5% of inertia error exist between the model and the actual 2-link manipulator. The adjusted gains are shown in Table. 3.5. The simulation results are shown in Fig. 3.14 and Fig. 3.15. With the adjusted gains, stable position responses are obtained. However, in comparison with the simulation results related to spring constant errors, the deterioration is also obvious and it is possibly due to the cause of the inexact estimations of observers. For the very critical inertia issues, the application of observers in the proposed decoupling control need to be discussed further.

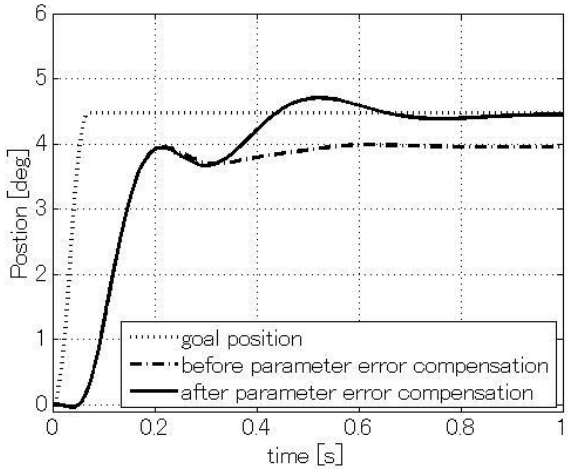

Fig. 3.14 Simulation verification for rigid load inertia error (Link L)

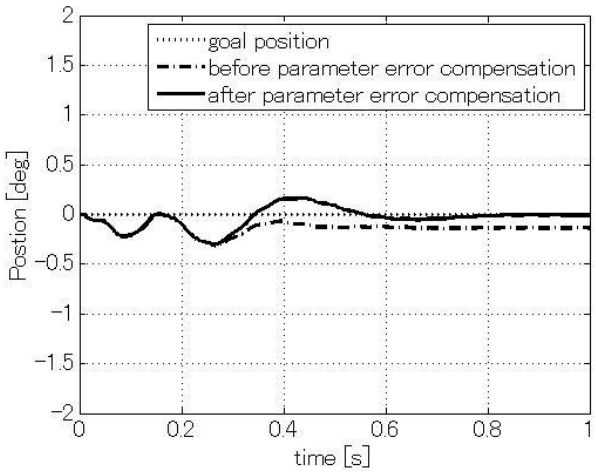

Fig. 3.15 Simulation verification for rigid load inertia error (Link U)

3.6 Conclusions

In this chapter, a new decoupling control strategy by using Model Following Control for the 2-link industrial robot manipulator has been proposed. Several results have been achieved by using the proposed decoupling control strategy.

(1) The compensation torques have been designed in feed-forward loop and the designs become independent and much simpler in comparison with conventional decoupling control methods.

(2) Compensation strategy that using an observer and its estimations has been proposed in feedback loop to cope with the modeling error problems. With the feedback of the estimations, the imperfect compensation torque designed in feed-forward loop have been supplemented.

(3) For practical application, the proposed strategy is a sample of decoupling control strategy, which is probably used for general-purpose servo systems.

Chapter 4

Identification of joint friction

4.1 About friction compensation

Generally, in mechatronics systems, friction is a reaction force between two surfaces in contact, which is opposite to the driving direction. Physically these reaction forces are the results of many different mechanisms and they depend on contact geometry, properties of the bulk, surface materials, displacement and relative velocity of the bodies and presence of lubrication.

Friction is an important aspect of many control systems especially for high precision servo mechanisms. It is a non-linear phenomenon that causes control performance of servo mechanisms to deteriorate. Typical errors caused by friction are steady-state errors in position regulation, besides friction also leads to tracking lags and limit cycles where the controller has integral action. As for the significance of friction, corresponding countermeasures are necessary. Control strategies that attempt to compensate for the effects of friction without resorting to high gain control loops, possibly are considered in two ways. One is to implement friction compensations in a feed-back loop with an estimation by using observer [37] - [39]. The other is to use a suitable friction model to predict and to compensate for the friction [40].

For the former, quality of friction compensations relies on the estimated precision of the effects of friction. However, high precision estimation of nonlinear friction is difficult to realize because observers used for estimation are basically designed based on a linear model. Although nonlinear observers have been proposed for an advanced estimation of nonlinear friction [41], the results are still unsatisfactory because nonlinear observers are originally designed based on a nonlinear friction model, which is ultimately obtained through experimental identifications and influenced by precision of experimental identifications. Be different from the former, the latter is possibly to make a better description of friction phenomena inherently. Therefore, the latter has been developed for years and types of these schemes are named model-based friction compensation techniques [42] - [44].

Several successful applications of model-based friction compensation techniques have been reported recently [45] - [47]. In these literature, linear motion guides were taken as a friction compensation object. Focus has been laid on both sticking and sliding conditions, which generally express relationships between friction and low and high velocities. With interpretation of relationship between friction and low velocity, these literature have also offered a demonstration that it is likely to design better friction compensation based on a suitable friction model, especially for extremely high precision positioning at low velocity.

Taking a view of previous model-based friction compensation literature, a common point is found that equipment of applications of friction model identification and compensation are machines directly driven by DC motors, such as linear motion guides and direct-drive (DD) robots. For the purpose of high torque output of arms of industrial robot manipulators such as handing robot, industrial robot manipulators with gear transmissions are essential and main, and extensively applied to manufactures in current days. In addition, due to the growing requirement of precision and multipurpose usage of industrial robot manipulators, constructions simultaneously become more complicated. Model-based friction compensation techniques become more important, however, have not been applied to types of manipulators with gear transmissions. Therefore, it is necessary to investigate a Model-based friction compensation technique for industrial robot manipulators with gear transmissions. But, before that, priority must be given to modeling and identification of joint friction of industrial robot manipulators. In this chapter, a modeling and identification technique of joint friction has been analyzed for industrial robot manipulators.

In section 4.2, an introduction about classical model and the LuGre model is shown and several properties of the LuGre model are given for the subsequent identifications. The experimental system used for identification is presented in section 4.3 and identification procedure is also shown in the same section. In order to verify the proposed identification strategy, several simulations are employed to compare with the experimental results in section 4.4.

4.2 Friction model

Typical friction models that are classical models and dynamic model are described in this section. Friction that is generally thought as a force in linear systems is considered as a torque in rotating systems in this section.

4.2.1 Classical models

This subsection will give a brief summary of some classical friction models which are also called static models.

Classical friction models are often considered as a function of velocity, see Fig. 4.1. The model shown in Fig. 4.1(a) is a typical Coulomb and viscous friction model. The Coulomb is independent of velocity and is always present. Viscous friction is in proportion to velocity. The behavior in each direction is assumed to be identical and asymmetrical. It is also considered that friction is zero for a velocity equal to zero. The model is given by

$$T_{fr} = \mathrm{sgn}(v)T_C + \sigma_2 v\,, \quad \text{..... (4.1)}$$

where T_{fr} is a friction torque, T_C is the Coulomb friction torque, σ_2 is the viscous coefficient and v is the relative velocity between the two surfaces.

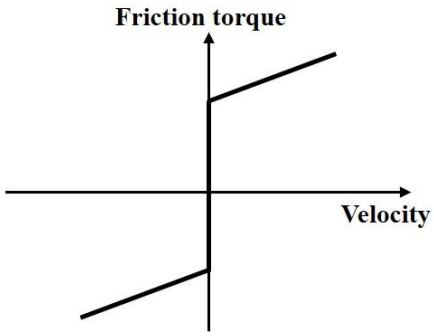

(a)

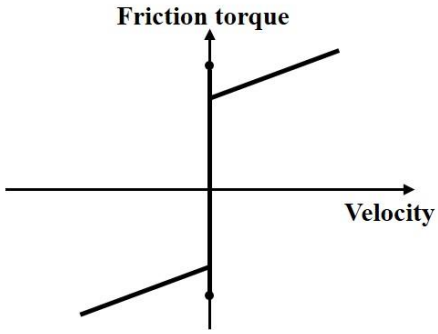

(b)

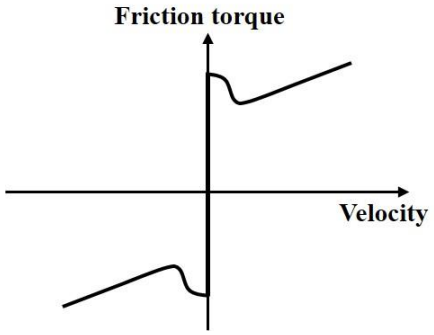

(c)

Fig. 4.1 Classical friction models

However, the Swiss scientist Euler found that a higher and instant force was needed to urge the surfaces to break away the condition of rest. Since that the higher and instant force has been taken into account and was called static friction. The model shown in Fig. 4.1(b) also reveals that friction is not zero when velocity is zero and provided a demonstration that friction is a discontinuous behavior in a transition from zero velocity to nonzero velocity. The model is described as

$$T_{fr} = \begin{cases} T_S & if\ v = 0 \\ \text{sgn}(v)T_C + \sigma_2 v & if\ v \neq 0 \end{cases}, \quad \text{.....} \quad (4.2)$$

where T_S is the static friction torque.

Findings did not stop. Stribeck discovered that the drop from static friction to Coulomb friction does not occur instantly and it is a continuous function of velocity [48]. So, now we have the model shown in Fig. 4.1(c), which is also mostly used for control or for advanced development of friction modeling. Sequentially, a well-known Stribeck effect has been developed by Bo and Pavelescu [49], which gives a significant influence to advanced friction modeling today. The model is given by

$$T_{fr} = T_C \operatorname{sgn}(v) + (T_S - T_C) e^{-(v/v_s)^2} \operatorname{sgn}(v) + \sigma_2 v \ , \quad \text{..... (4.3)}$$

where v_s is the Stribeck velocity.

4.2.2 LuGre models

In 1995, Canudas et al. presented a new dynamic model for friction [41], which captures most of friction characteristics observed experimentally such as the Stribeck effect, hysteresis, spring-like and varying break-away force. The effectiveness for control of this called LuGre model has been demonstrated in literature [41]. As an effective nonlinear friction model, it has been favored by many researchers, who attempted to use the LuGre model to compensate for the friction and to get an improvement of control performances of high precision positioning [44] - [46]. In order to minimize the influences to friction compensation, which are due to changes in external environments, adaptive friction compensation with the LuGre model has also been presented in literature [50] and [51].

As section 4.1 shown, it is necessary to investigate the model-based friction compensation technique for industrial robot manipulators. But, before the friction compensation, an effective and appropriate identification strategy needs to be firstly considered. In this section, I will present a proposed identification strategy for the LuGre model, which has not been implemented in an industrial robot manipulator with transmission up to now.

The basic viewpoint in relation to the LuGre model is that the contact surface between two bodies are very irregular at microscopic level and they are visualized as two rigid bodies that make contact through elastic bristles, referring to Fig. 4.2. A variable z is defined as average deflection.

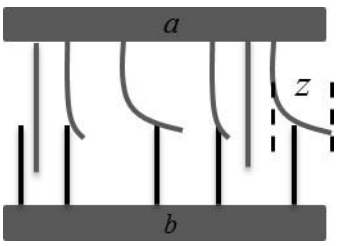

Fig. 4.2 Surface between two bodies in contact

With this average deflection, the LuGre model are described as

$$T_{fr} = \sigma_0 z + \sigma_1 \frac{dz}{dt} + \sigma_2 v, \quad \text{..... (4.4)}$$

$$\frac{dz}{dt} = v - \frac{|v|}{g(v)} z, \quad \text{..... (4.5)}$$

$$g(v) = \frac{1}{\sigma_0}\left[T_C + (T_S + T_C)e^{-(v/v_s)^2}\right], \quad \text{..... (4.6)}$$

where parameter σ_0 is a stiffness and σ_1 is a damping coefficient. Function $g(v)$ is used to describe the Stribeck effect. With function $g(v)$, the average deflection is determined by Eq. 4.5. Then, Eq. 4.4 is proposed to determine the friction torque under condition of knowing the average deflection z.

For better understanding of dynamical behavior of the LuGre model and details of proposed identification strategy shown later, several simulations with the LuGre model are also provided in this subsection. It is assumed that a unit of linear slider is driven by an actuator and friction behaves within the linear slider. Parameters used for simulations are to some extent based on literature [41], which are reported in Table.4.1.

Table. 4.1 Parameters of simulations

Parameter	Value	Unit
J	1	$[kgm^2]$
σ_0	10^5	$[Nm/rad]$
σ_1	$\sqrt{10^5}$	$[Nms/rad]$
σ_2	0.4	$[Nms/rad]$
T_C	1	$[Nm]$
T_S	1.5	$[Nm]$
v_s	0.001	$[rad/s]$

(1) Relationship between the LuGre model and classical models in constant velocity sliding motion

The friction torque of the LuGre model will be a constant in the case of steady-state motion and it can be determined by Eq. 4.7, which is classical model (c). To verify an identical relationship between the LuGre model and classical model (c), the unit of linear slider is assumed to rotate with a constant velocity and subject to friction of the LuGre model. The constant velocity is shown in Fig. 4.3. The identical relationship between the LuGre model and classical model (c) is clearly demonstrated because both the friction torque of static model (c) and the LuGre model are the same value in the simulation result, referring to Fig. 4.4.

$$T_{fr} = T_C \operatorname{sgn}(v) + (T_S - T_C)e^{-(v/v_s)^2} \operatorname{sgn}(v) + \sigma_2 v \ . \quad \text{..... (4.7)}$$

In addition, value of friction torque is 1.4 Nm, which can be derived from Eq. 4.7 with neglect of the exponential item. The exponential item is an extremely small value and can be approximately seen as zero. Thus, a qualitative conclusion can be also drawn that friction torque of the LuGre model will be determined by

$$T_{fr} = T_C \operatorname{sgn}(v) + \sigma_2 v \ , \quad \text{.....(4.8)}$$

if the unit of linear slider is in a sliding motion. In other words, the LuGre model is in fact a classical model (a) in the case of a sliding motion. This conclusion will also be applied for the subsequent identification of T_C and σ_2 which is shown in section 4.3.

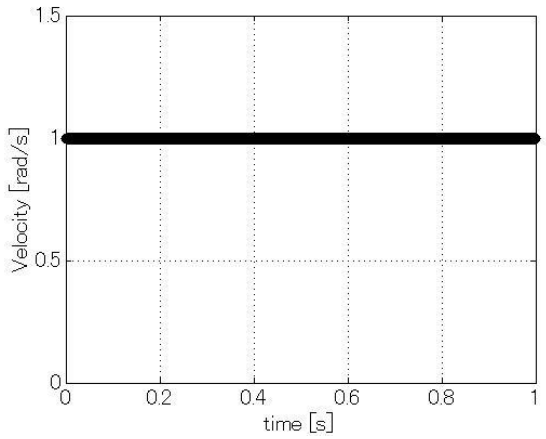

Fig. 4.3 Constant velocity input

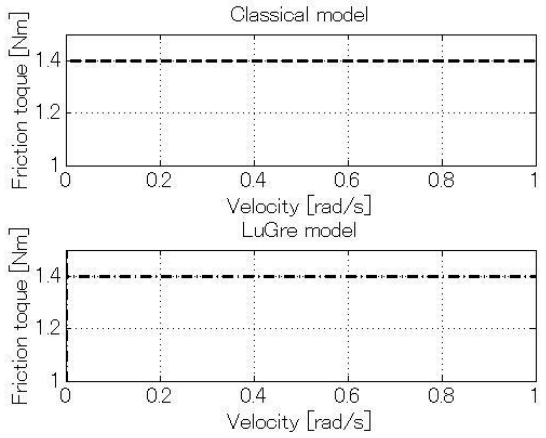

Fig. 4.4 Friction torque

(2) Friction and Microdisplacement in stiction regime

It has also been shown that friction behaves like a spring if the applied force is less than the static force [52]. If a force is applied to two surfaces in contact there will be a displacement. Another simulation was performed to verify that whether the LuGre model can reflect this property.

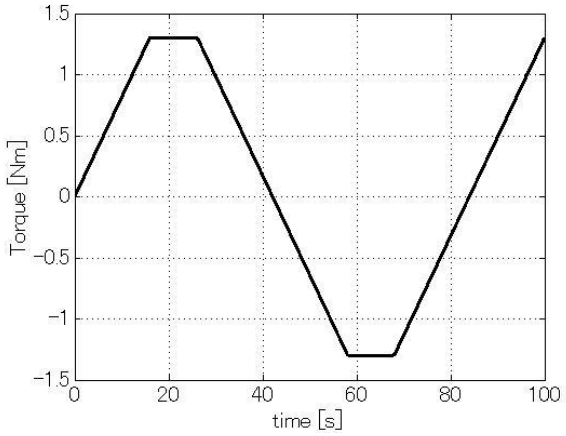

Fig. 4.5 Applied torque

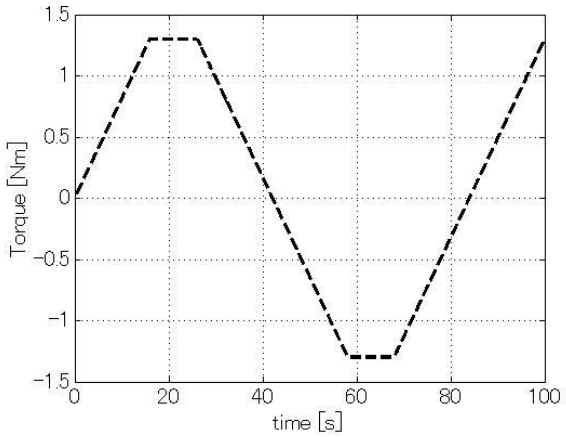

Fig. 4.6 Friction torque

In the simulation, supposed that a torque was applied to the unit of linear slider and maximum value of the torque is 1.3 Nm, less than static friction torque, referring to Fig. 4.5. The unit of linear slider should logically remain the original static regime, not break-away and start to slide due to that on a macro viewpoint, friction torque is identical with the applied torque. From the simulation result, referring to Fig. 4.6, it can be said that the LuGre model is possibly expected to provide a varying friction torque and the varying torque maintains good balance with the applied torque.

Presence of the microdisplacement has also been reflected by the simulation result, see Fig. 4.7. Meantime, notice that friction torque is only a function of displacement and the sign of velocity. It also

implies that the friction torque is only position dependent. This property of the LuGre model fully accords with literature [53] and will be further used for the proposed identification strategy.

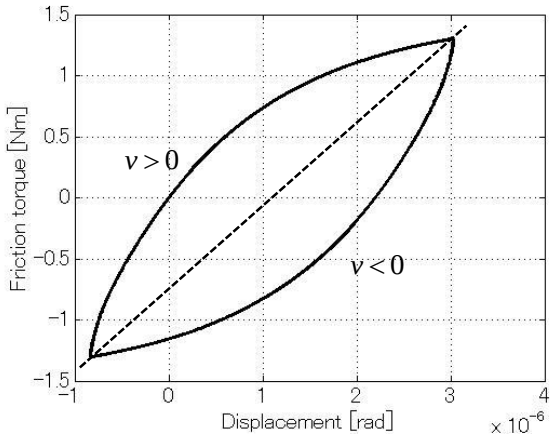

Fig. 4.7 Friction torque and microdisplacement

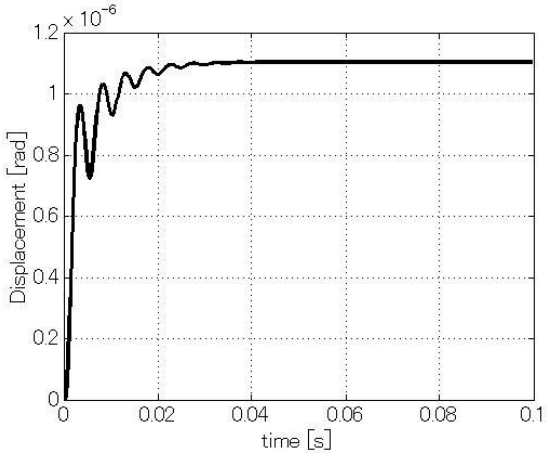

Fig. 4.8 Behavior in stiction regime

(3) Linearization in stiction regime

An investigation of linearization of the LuGre model in stiction regime has been shown in literature [41]. The average deflection z has been totally regarded as displacement and $\dot{z}$ is given by

$$\frac{dz}{dt} = \frac{d\theta}{dt} \quad \text{……..……..…..……} \quad (4.9)$$

Based on Eq. 4.9, the equation of motion is finally given by

$$J\frac{d^2\theta}{dt} + (\sigma_1 + \sigma_2)\frac{d\theta}{dt} + \sigma_0\theta = 0 \quad \text{……} \quad (4.10)$$

where θ is the rotation angle of the unit of linear slider. The motion equation shows that the system behaves like a damped second-order system. A simulation is performed to investigate this property.

Step torque that its maximum value is smaller than the static friction torque, is given to the unit of linear slider. Then, a damped motion just occurs in the simulation result, referring to Fig. 4.8. With this important property of the LuGre model, identification procedure for σ_1 will be proposed in section 4.3.

4.2.3 Modeling of joint friction with LuGre model

In this paper, a definition must be firstly cleared that joint friction of an industrial manipulator does not only mean friction of gear transmissions, it also includes the friction of bearings, which are built in the bodies of motors. The purpose of this chapter is to successfully identify the joint friction.

The friction of bearings of motors and friction of gear transmissions are regarded as one friction in this paper due to next considerations. As presented in chapter 3, gear transmissions are in most cases modeled by spring systems. A spring coefficient is used in model of 2-inertia system to represent the spring system. As an independent mechanical device, the moment of inertia of gear transmissions, of course exist, but it is converted into moment of motors and considered as part of motors. In other words, motor and gear transmission are regarded as "one inertia" of the 2-inertia system. Thus, friction of motors and gear transmissions are naturally supposed to be combined together. Control of 2-inetia system with model-based friction compensation will be simplified and benefit from the combination in the future.

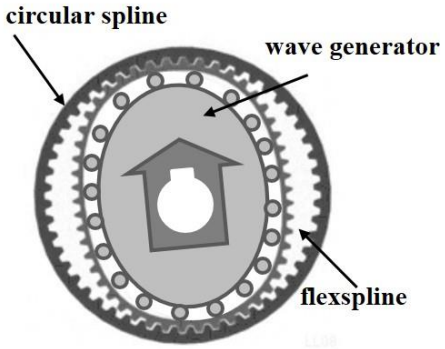

Fig. 4.9 Structure of harmonic drive

In addition, the LuGre model is used for representing the joint friction in this paper because the following reasons. First, the main components in a robot joint are bearings and gears (e.g. harmonic drive, referring to Fig. 4.9), lubricating grease or oil of bearings generates nonlinear friction. The nonlinear friction is the same type with the friction inside ball screw, which is already analyzed and modeled by the LuGre model [44] - [46]. Secondly, friction inside gears is often represented by two lubricated discs in a rolling-sliding contact in tribology. The LuGre model was exactly established based on two lubricated discs. Therefore, friction inside gears can also be represented by the LuGre model. Overall, both friction are types of friction that can be represented by the LuGre model and the

LuGre model was reasonably chosen in this paper.

4.3 Experimental identification for LuGre Model

It was shown that the LuGre model is characterized by six parameters σ_0, σ_1, σ_2, T_C, T_S, v_s in subsection 4.2.2. The proposed identification strategy of these six parameters through experiments will be presented in detail in this section.

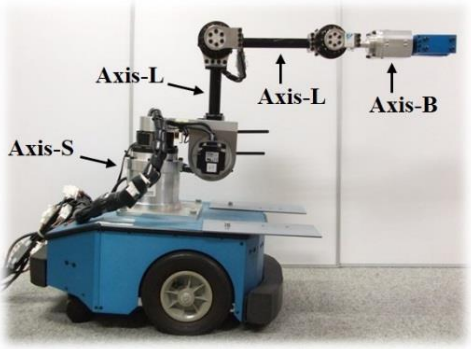

Fig. 4.10 Experimental system

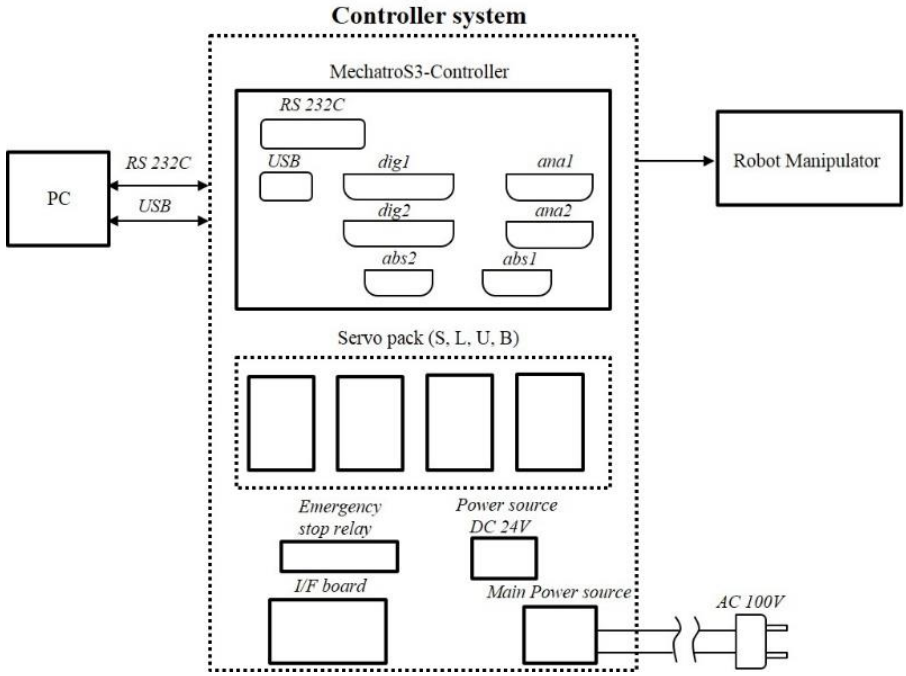

Fig. 4.11 Controller system

4.3.1 Experimental system

The experimental system for the identification of the LuGre model is a 4-degree-of-freedom study model of industrial robot manipulator, referring to Fig.4.10, accompanied with a controller system shown in Fig. 4.11. The study model has one circling axis S and three vertical rotating axes L, U and

B. Links of the study model are driven by AC servo motors provided by Yasukawa Elec. Corp. and each motor is equipped with an absolute position encoder. Gear transmissions that are used for transmitting torques are type of harmonic drive. Specifications of the study model are shown in Table. 4.2. The controller system mainly consists of a motion controller called MechatroS3-Cotroller, four servo packs and I/F board. The MechatroS3-controller houses single-board CPU, Analog Devices A/D and D/A boards, Digital input and output devices, Absolut serial input devices and USB and RS232 communications. More detailed description of the whole experimental system are offered in appendix.

Table. 4.2 Specifications of the study model

Axis	Motion range	Max velocity	Motor capacity	Gear ratio	Load capacity
S	$\pm 160^{\circ}$	$3.66 rad/s$	$200W$	120	$3kg$
L	$+120^{\circ}, -45^{\circ}$	$2.97 rad/s$	$100W$	160	
U	$+180^{\circ}, -20^{\circ}$	$3.93 rad/s$	$50W$	120	
B	$\pm 130^{\circ}$	$5.23 rad/s$	$30W$	80	

4.3.2 Problem of identification in experimental system

For identification of the LuGre model, the first step is to make a measurement of the Stribeck effect through experiments. In a linear screw or a DD robot, constant speed control is implemented to picture curve of the Stribeck effect based on

$$T_{ref} - T_{fr} = J\ddot{\theta} \quad \cdots\cdots\cdots\cdots\cdots\cdots\cdots\cdots\cdots\cdots\cdots\cdots \quad (4.11)$$

where T_{ref} is a torque input for constant speed control.

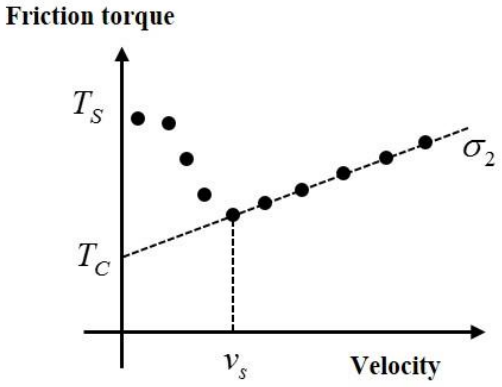

Fig. 4.12 Stribeck effect in positive direction

Realization of constant speed control definitely means that the torque input is equal to friction. Therefore, a curve pictured between torque input and velocities is the curve between friction and velocities. Coulomb friction, viscous friction coefficient, the Stribeck velocity and static friction will

be read from the curve the Stribeck effect, see Fig. 4.12.

In the case of an industrial robot manipulator with gear transmissions, each link is modeled by a 2-inertia system, which is previously shown in chapter 3. Then motion equation of motor is given by

$$T_{ref} - K_C(\theta_m - \theta_a) - T_{fr} = J_m\ddot{\theta}_m . \quad \text{..... (4.12)}$$

The curve of the Stribeck effect between friction and velocities is however, not like in linear screws and DD robots and not able to be pictured through picturing the curve between torque input and velocities due to the unknown twist torque (in fact due to unknown θ_a). Although, estimation techniques such as application of observers can be to some extent applied to estimate twist torque, the issue that whether observers can provide a proper and precise estimation of the twist torque for identifications is still a complicated problem and needed to be carefully considered. So, to resolve the critical problem of the unknown twist torque, which is a significantly unexpected barrier for identifications of parameters of the LuGre model, a new experimental system will be established in next subsection.

4.3.3 Proposed experimental system

The first idea of resolution of the above problem is to remove rigid loads from links. Then, gear transmissions will be directly driven by motors. The twist torque will disappear if the system of combination of motors and gear transmissions is assumed to be a rigid system. However, the above strategy is not reasonable for practical application because the separation of rigid loads from links is not a simple work and disassembly-assembly operations will adversely affect original operation accuracy of industrial robot manipulators. Based on above consideration, another strategy that fixing rigid loads with some kind of mechanical tools or devices to prevent them to rotate comes out. As a consequence, rotation angles of rigid loads will be constant zero and the twist torque become available as a function of only θ_m . With fixed rigid loads, links of industrial robot manipulators are modeled as follows, referring to Fig. 4.13.

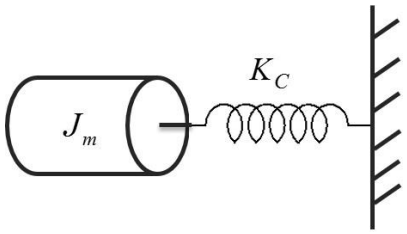

Fig. 4.13 The link with fixed rigid load

Motion equation of the system shown in Fig. 4.13 is given by

$$T_{ref} - K_C\theta_m - T_{fr} = J_m\ddot{\theta}_m . \quad \text{..... (4.13)}$$

In the system, the curve of the Stribeck effect between friction torque and velocities is possibly available. With this system, procedure of the proposed identification strategy will be shown in detail in next subsection.

4.3.4 Friction identification procedure

In this subsection, several experimental tests that are conducted to reveal the LuGre model are described. Prior to the commencement of each series of experimental tests, a brief system warm-up is conducted to circulate and equalize the temperature of the lubricants of the study model of robot manipulator. Besides, the temperature of surrounding environment of experimental system is also paid attention to avoid the temperature influence on the friction identifications. Experimental identification tests of friction are conducted in Axis-B, in both directions, but only samples of single direction of experimental results are shown in this subsection.

(1) Identification of Coulomb, viscous friction and static friction

A completely new experimental test is carefully considered to investigate Coulomb and viscous friction in this paper due to the reason that traditional identification strategy of Coulomb and viscous friction via the curve of the Stribeck effect is not able to be applied in the proposed system. A wide range of velocity desired in traditional strategy means a wide range of rotation displacement of motors at a certain time. Large rotation displacement brings gear transmissions to continuously bear large twist torque, however, the large twist torque does not dissipate because arms are fixed. A sharp increased twist torque is likely to lead to damage to gear transmissions. Therefore, a new experimental test is proposed for identifying Coulomb and viscous friction. Another important thing that must be pointed out here is gravities. Arms are fixed in the proposed system, so there is no need to take gravities into consideration during the identification procedure.

The first step of the proposed experimental test is to determine a proper goal rotation displacement of motors, which must be not too large, and meantime, too small, which brings no motion between motors and gear transmissions. There are no criterions for selection of the goal rotation displacement and the goal rotation displacement in this paper is determined freely according to practical experiences.

The identification of Coulomb and viscous friction is based on an experimental test of position control of motors. Supposed that a typical square wave acceleration is given to motors, referring to Fig. 4.14, the goal rotation displacement is determined by calculating the double integral of acceleration. Rotation displacement of motors are controlled and an example of position response shown in Fig. 4.15 will be read from absolute sensors. A backward difference approximation of position response is regarded as velocity response, referring to Fig. 4.16.

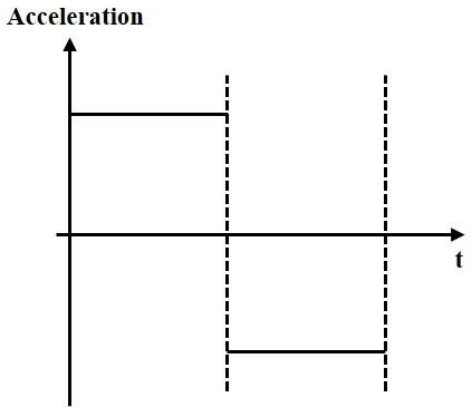

Fig. 4.14 Schematic representation of acceleration input

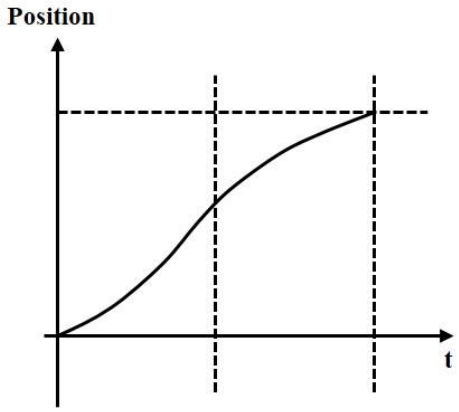

Fig. 4.15 Schematic representation of position response

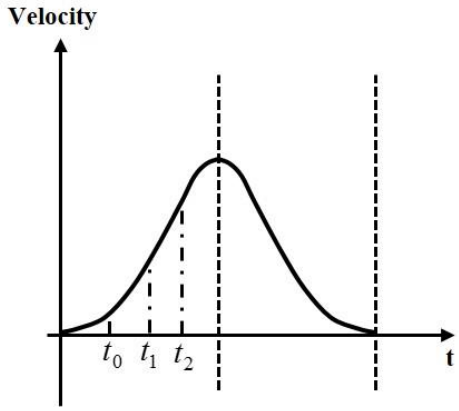

Fig. 4.16 Schematic representation of velocity response

As it is shown in Fig 4.16, three time variables t_0, t_1 and t_2 are defined for identification of Coulomb and viscous friction.

t_0 : start time point of linear motion

t_1 : a certain time point of linear motion

t_2 : another time point of linear motion

With the position and velocity response, Coulomb and viscous friction are derived from Eq. 4.13. The integrals of Eq. 4.13 over time interval $[t_0 \quad t_1]$ $[t_0 \quad t_2]$ are given by

$$\int_{t_0}^{t_1} T_{ref} - K_C \int_{t_0}^{t_1} \theta_m - \int_{t_0}^{t_1} T_{fr} = J_m \int_{t_0}^{t_1} \ddot{\theta}_m \text{ , } \ldots\ldots\ldots\ldots\ldots\ldots\ldots\ldots \text{(4.14)}$$

$$\int_{t_0}^{t_2} T_{ref} - K_C \int_{t_0}^{t_2} \theta_m - \int_{t_0}^{t_2} T_{fr} = J_m \int_{t_0}^{t_2} \ddot{\theta}_m \text{ . } \ldots\ldots\ldots\ldots\ldots\ldots\ldots\ldots \text{(4.15)}$$

Thus,

$$\int_{t_0}^{t_1} T_{ref} - K_C \int_{t_0}^{t_1} \theta_m - J_m(\dot{\theta}_{m1} - \dot{\theta}_{m0}) = \int_{t_0}^{t_1} T_{fr} \text{ , } \ldots\ldots\ldots\ldots\ldots\ldots\ldots \text{(4.16)}$$

$$\int_{t_0}^{t_2} T_{ref} - K_C \int_{t_0}^{t_2} \theta_m - J_m(\dot{\theta}_{m2} - \dot{\theta}_{m0}) = \int_{t_0}^{t_2} T_{fr} \text{ , } \ldots\ldots\ldots\ldots\ldots\ldots\ldots \text{(4.17)}$$

where $\dot{\theta}_{m0}$, $\dot{\theta}_{m1}$ and $\dot{\theta}_{m2}$ are velocities when t is equal to t_0, t_1 and t_2. In section 4.2.2, it has been shown that the LuGre model inherently is classical model (a) in the case of sliding motion and T_{fr} is expressed by

$$T_{fr} = T_C + \sigma_2 \dot{\theta}_m \quad \ldots\ldots\ldots\ldots\ldots\ldots\ldots\ldots\ldots\ldots \text{(4.18)}$$

Inverting Eq. 4.18 into Eq. 4.16 and Eq. 4.17 gives

$$C_1 = T_C(t_1 - t_0) + \sigma_2(\theta_{m1} - \theta_{m0}) \quad \ldots\ldots\ldots\ldots\ldots\ldots\ldots\ldots \text{(4.19)}$$

$$C_2 = T_C(t_2 - t_0) + \sigma_2(\theta_{m2} - \theta_{m0}) \quad \ldots\ldots\ldots\ldots\ldots\ldots\ldots\ldots \text{(4.20)}$$

where

$$C_1 = \int_{t_0}^{t_1} T_{ref} - K_C \int_{t_0}^{t_1} \theta_m - J_m(\dot{\theta}_{m1} - \dot{\theta}_{m0}) \quad \ldots\ldots\ldots\ldots\ldots\ldots\ldots\ldots \text{(4.21)}$$

$$C_2 = \int_{t_0}^{t_2} T_{ref} - K_C \int_{t_0}^{t_2} \theta_m - J_m(\dot{\theta}_{m2} - \dot{\theta}_{m0}) \quad \ldots\ldots\ldots\ldots\ldots\ldots\ldots\ldots \text{(4.22)}$$

Then, two parameters α and β are introduced and

$$\alpha = \frac{\theta_{m2} - \theta_{m0}}{\theta_{m1} - \theta_{m0}} \text{ , } \ldots\ldots\ldots\ldots\ldots\ldots\ldots\ldots\ldots\ldots \text{(4.23)}$$

$$\beta = \frac{t_2 - t_0}{t_1 - t_0} \text{ . } \ldots\ldots\ldots\ldots\ldots\ldots\ldots\ldots\ldots\ldots \text{(4.24)}$$

Finally, T_C and σ_2 are derived from Eq. 4.19 and Eq. 4.20 and given by

$$T_C = \frac{C_2 - \alpha C_1}{t_2 - t_0 - \alpha(t_1 - t_0)} \text{ , } \ldots\ldots\ldots\ldots\ldots\ldots\ldots\ldots\ldots\ldots \text{(4.25)}$$

$$\sigma_2 = \frac{C_2 - \beta C_1}{\theta_{m2} - \theta_{m0} - \beta(\theta_{m1} - \theta_{m0})} \text{ . } \ldots\ldots\ldots\ldots\ldots\ldots\ldots\ldots\ldots\ldots \text{(4.26)}$$

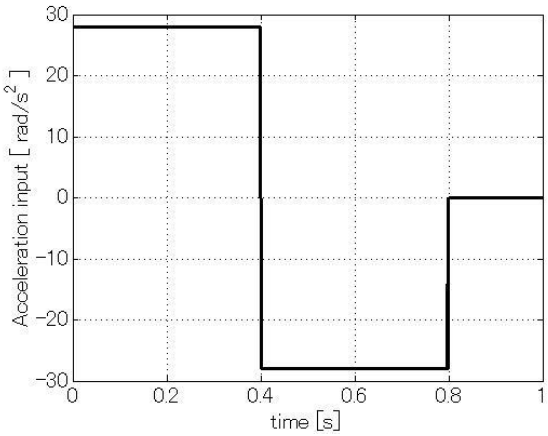

(a) Square-wave acceleration input

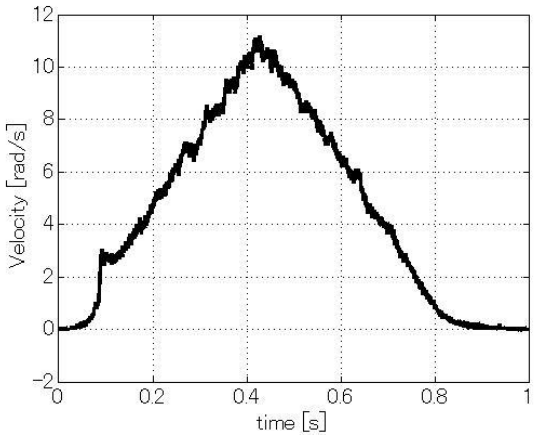

(b) Velocity response

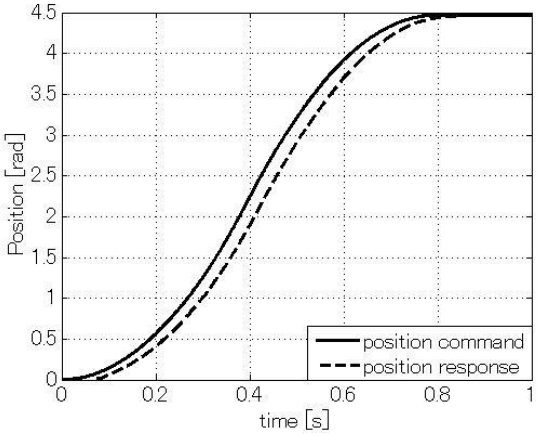

(c) Position response

Fig. 4.17 Experimental results of position control

The used square-wave acceleration input and one of experimental results (position and velocity

response) are shown in Fig. 4.17. In the velocity response, an obvious sudden change phenomena occurs around 0.1 second because motor break-away the static friction. Then, velocity increases monotonically with increasing time till 0.4 second. t_0, t_1 and t_2 are determined within time interval [0.1 0.4]. Naturally, the derivation of T_C and σ_2 is still valid even if t_0, t_1 and t_2 are chosen in monotonic decreasing interval of the velocity response.

The velocity response is also pretreated for improving identification accuracy with filter processing. Obviously, the velocity response is not a perfect ramp and noise that is generated not only by the backward difference approximation of position occur in the velocity response. Two kinds of low-pass filters (called feed-forward and backward low-pass filter) are designed to remove the noise. Firstly, velocity response was filtered by a digital feed-forward low-pass filter

$$v_{fout}(k) = e^{-\frac{T_{samp}}{\tau}} v_{fout}(k-1) + (1 - e^{-\frac{T_{samp}}{\tau}})\dot{\theta}_m(k) \qquad k = 1,2,3... \quad \cdots\cdots\cdots \quad (4.27)$$

where v_{fout} is an output of the feed-forward low-pass filter. Noise is attenuated, however, the signal of v_{fout} is still not able to be used directly for the identification of Coulomb and viscous friction due to the time delay which is generated by the feed-forward low-pass filter.

Then, a backward low-pass filter is applied to velocity response

$$v_{bout}(k) = e^{-\frac{T_{samp}}{\tau}} v_{bout}(k+1) + (1 - e^{-\frac{T_{samp}}{\tau}})\dot{\theta}_m(k) \qquad k = n, n-1, n-2... \quad \cdots\cdots\cdots \quad (4.28)$$

where v_{bout} is an output of the back low-pass filter. With the output of filters, an arithmetical average is calculated

$$v_{fbm}(k) = \frac{v_{fout}(k) + v_{bout}(k)}{2} \qquad k = 1,2,3... \quad \cdots\cdots\cdots\cdots\cdots\cdots \quad (4.29)$$

where v_{fbm} is the arithmetical average.

The filter processing result of the velocity response with $\tau = 0.01[s]$ is shown in Fig. 4.18. In the enlarged view, noise is nearly removed by filtering. The time delay issue of low-pass filter is also resolved. Finally, the arithmetical average is used instead of velocity response for the identification of Coulomb and viscous friction.

Conventional measurement strategy of the static friction that is often adopted is to offer a ramp torque and to observe the sudden change of velocity or position, then, to judge the static friction according to the sudden change time of velocity or position. In this paper, the static friction is read from the input torque, when velocity suddenly changes around 0.1 second. The identification result is shown in Table. 4.3, which is the mean value of ten experimental results.

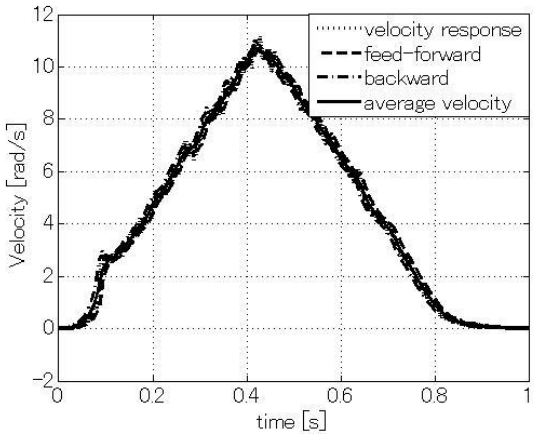

(a) A whole view

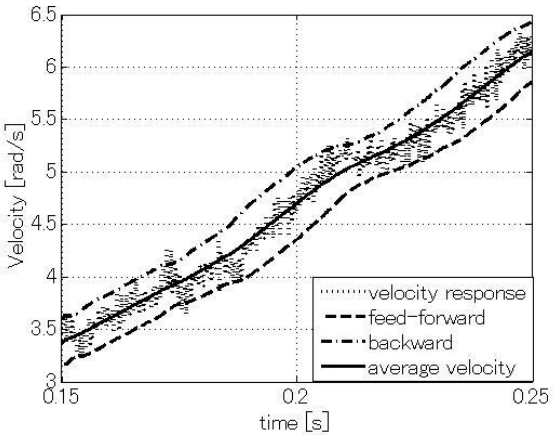

(b) Enlarged view

Fig. 4.18 Filter processing of velocity response

Table. 4.3 Identification result of T_C and σ_2

Parameter	Value	Unit
T_C	1.87×10^{-2}	$[Nm]$
σ_2	3.79×10^{-4}	$[Nm/rad/\sec]$
T_S	2.15×10^{-2}	$[Nm]$

(2) Identification of Stribeck velocity

For the Stribeck velocity, it is known as the representation of the Stribeck effect, which can only be found in the Stribeck effect. However, it is presented that the Stribeck effect is not able to be measured in the proposed system due to the fixed rigid loads. Considering that the Stribeck effect is only related to load, viscosity and velocity, it maybe lead a conclusion that the curve profile of the Stribeck effect is not affected by external force. In other words, the curve profile of the Stribeck effect measured in a

regular link (with rigid load) is the same with the link without rigid load (called no-arm link). An experiment is conducted to prove this conclusion. Velocity control is implemented to the regular link and no-arm link with various velocities to measure the Stribeck effect. The experimental results are reported in Fig. 4.19

In the experimental results, the curve profile of the regular link (expressed with witharm) is almost the same as one of the no-arm link (expressed with noarm). Especially, velocity is the same when the friction becomes the minimum value. The experimental results also lead to a qualitative conclusion that the measurement of the Stribeck velocity is not affected by twist torque. The Stribeck velocity measured in a regular link can be completely taken as the real Stribeck velocity of the proposed system.

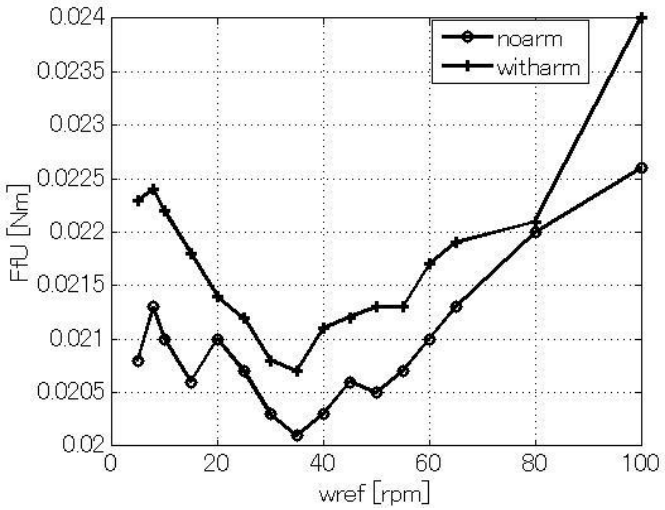

Fig. 4.19 Measurement of the Stribeck effect

From the measured Stribeck effect, the Stribeck velocity is determined in Table. 4.4.

Table. 4.4 Identification result of v_s

Parameter	Value	Unit
v_s	35	$[rpm]$

(3) Identification of stiffness coefficient

The identification of stiffness coefficient is particularly interest and difficult in all parameters identification of the LuGre model. Canudas De Wit and Lischinsky [54] reported that both the stiffness and damping coefficient can be estimated by non-linear numerical optimization methods with prerequisites that the static parameters (static, Coulomb and viscous friction) and system inertia are assumed to be available. The parameters identification by using genetic algorithm was also reported

recently for improvement of identification quality [55]. Improvement of identification are to some extent able to be expected in these optimization algorithms. However, a precise estimation of stiffness coefficient relies on precise estimation of static friction parameters. It is not a direct identification manner to seek the true value and a little complicated to be utilized. Intuitive and simple identification strategy for stiffness coefficient with a suitably designed experiment is proposed in this paper.

As it is presented in subsection 4.2.2, system behaves like a spring (called nonlinear spring behavior) if the applied force is less than the static force. The relation between friction and microdisplacement is developed further to contribute to the identification of stiffness coefficient. An applied torque that varies in the form of a sinusoidal signal is assumed to be given to a system that consists of two contact surfaces.

$$T_{ref} = T_0 \sin(\omega t), \begin{cases} T_0 > T_S \\ T_0 < T_S \\ \omega = 2\pi f \end{cases} \quad \text{……..……..…..} \quad (4.30)$$

where f is an ordinary frequency and is supposed to be determined in low frequency region. Then, Fig. 4.20 shows the relation between the applied force and displacement of the system.

The nonlinear spring behaviors are similar for $T_0 < T_S$, when typical hysteresis motions ($A-A'$, $B-B'$ and $C-C'$) are exhibited. The friction torque is only position dependent and the displacement changes with increasing torque level. For $T_0 > T_S$, a rolling behavior begins and displacement changes obviously ($D-D'$), when the larger input torques exceed the static friction torque.

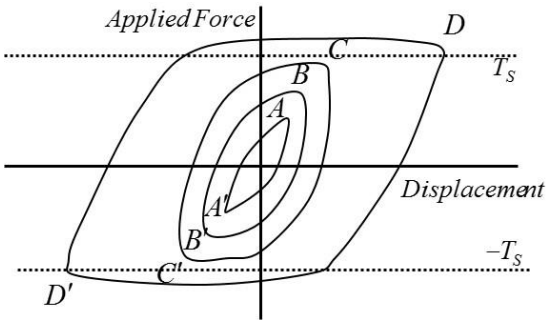

Fig. 4.20 Nonlinear spring behavior and rolling behavior

With the nonlinear spring behavior, the identification of σ_2 is proceeded as follows. During the staticition regime ($T_0 < T_S$), velocity and differential of the average deflection z are extreme small values and need not to be taken into account. Thus, an approximate calculation can be concluded

$$T_{ref} \approx T_{fr} \approx \sigma_0 z \quad \text{……..……..} \quad (4.31)$$

Assuming that the experiment is preformed from initial condition ($z(0) = 0$), then σ_0 can be

explicitly and approximately computed from

$$\sigma_0 \approx \frac{T_{ref}}{z} \approx \frac{T_{ref}}{\theta} \quad \text{..... (4.32)}$$

In Fig. 4.20, σ_0 is considered as the slope of $A-A'$, $B-B'$ and $C-C'$.

Therefore, to obtain σ_0, an experiment that is used to measure the nonlinear spring behavior is necessary. The frequency of the sinusoidal torque chosen for the experiment is 2 Hz. The sinusoidal torque is given to the B link of the study modelof industrial manipulator, referring to Fig. 4.10, to bring a slowly varying hysteresis motion and meanwhile the slowly varying hysteresis motions can be better observed. The experimental tests are conducted for 12 different T_0. Especially, T_0 is chosen for two patterns that are less and larger than the static friction, which are reported in Table. 4.5. In Table. 4.5, T_0 is expressed as the ratio between value of T_0 and rated torque. By the way, approximate ratio between the static friction and rated torque (0.095 Nm) of the B link is 23%.

Table. 4.5 Values of T_0

Pattern	**Value**						**Unit**
$T_0 < T_S$	2	5	8	10	15	20	[%]
$T_0 > T_S$	25	26	27	29	31	32	[%]

Several samples of observed nonlinear spring behavior and rolling behavior are collected from experimental results and shown in Fig. 4.21 and 4.22. The experimental results accords with expectation.

The maximum and minimum displacement are recorded from the hysteresis motions ($T_0 < T_S$). The calculated results of σ_0 from the hysteresis motions ($T_0 < T_S$) are reported in Table. 4.6. Attentively, the data $T_0 = 25\%$ that is close to static friction is also taken into account. Then, notice that σ_0 is not a constant value. This result also accords with the conclusion that are reported in literature [42]. As the same with literature [42], a function shown in Eq. 4.33 is given to determine σ_0.

$$\sigma_0(z) = k_1 + k_2 e^{-\left(\frac{z}{k_3}\right)^2} \quad \text{..... (4.33)}$$

where $k_1 = 2.06$, $k_2 = 4.4$ and $k_3 = 0.004$. The values of the constant coefficient k_1, k_2 and k_3 are determined according to literature [42].

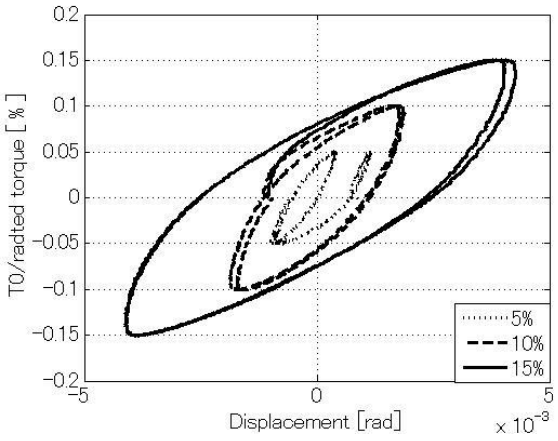

Fig. 4.21 Hysteresis motions $T_0 < T_S$

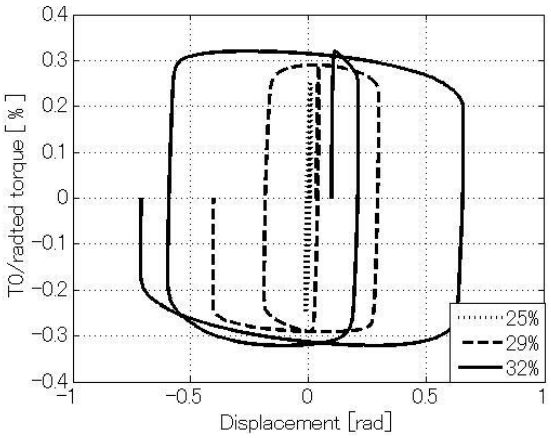

Fig. 4.22 Hysteresis motions $T_0 > T_S$

Table. 4.6 Identification result of σ_0

Parameter	**Value**							**Unit**
T_0	2	5	8	10	15	20	25	[%]
σ_0	9.50	5.93	4.75	5.59	3.65	2.60	2.06	$[Nm/rad]$

(4) Identification of damping coefficient

The damping coefficient is identified by utilizing the linearization property. It has been presented in section 4.2 that the displacement behaves like a damped second-order system. The Laplace transform of Eq. 4.10 is shown in Eq. 4.34 and a typical second-order system is given by Eq. 4.35.

$$J_m s^2\theta_m + (\sigma_1 + \sigma_2)s\theta_m + \sigma_0\theta_m = 0 \quad \text{..... (4.34)}$$

$$s^2\theta_m + 2\zeta\omega s\theta_m + \omega^2\theta_m = \theta_{ref} \quad \text{..... (4.35)}$$

Compared two equations, damping coefficient σ_1 can be explicitly derived from

$$\sigma_1 = J_m 2\zeta\omega - \sigma_2 \quad \text{..... (4.36)}$$

where vicious coefficient σ_2 is an already-known value from subsection 4.3.4.

The experimental test applied a step torque to obtain a displacement of motor. The response of second-order system are fitted to the displacement to determine a suitable value of ζ and ω. Then, damping coefficient σ_1 is computed from Eq. 4.36 with the determined ζ and ω.

One of experimental results and the fitted second-order response are shown in Fig. 4.23. Note that the response of second-order system is not perfectly fitted with the displacement. The response of second-order system is not able to be fitted completely with the displacement due to that the behavior of the displacement is just a likely second-order system. The fitted response of second-order system is determined by trial and error in this paper. With the fitted response, value of the damping coefficient σ_1 is finally determined, which is 0.06 $[Nm/rad/\sec]$.

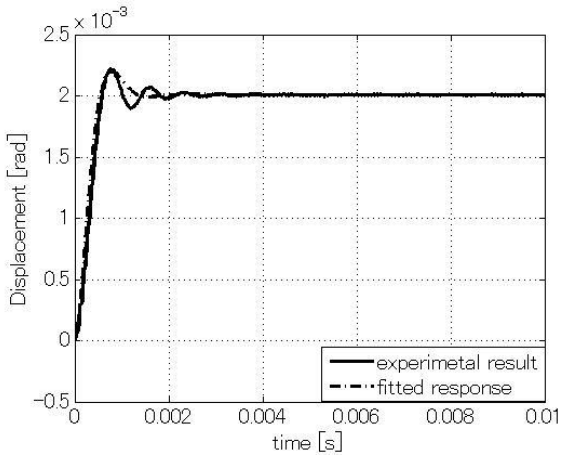

Fig. 4.23 Experimental result and fitted simulation response

4.4 Verifications

The relevance of friction and microdisplacement (shown in subsection 4.2.2) is the most important characteristics for high precision positioning control of industrial robot manipulators. So, with the determined LuGre model, in subsection 4.4.1, the comparison between the simulations and experiments are carried out to verify the relevance of friction and microdisplacement. In subsection 4.4.2, simulation results of square wave torque input are provided to show the behavior in stiction regime. Furthermore, a verification in semi-closed loop is also provided in subsection 4.4.3 to present that the LuGre model is better for model-based friction than classical models. In verifications, both the simulations and experiments are conducted in B link, referring to Fig. 4.10.

4.4.1 Verification for microdisplacement

With a sinusoidal input torque, the simulation results and experimental results are shown in Fig. 4.24, Fig. 4.25 and Fig. 4.26. The maximum values of the sinusoidal input torque T_0 are determined by 10%, 15% and 32% to the rated torque. In the simulations, microdisplacement are produced by the input sinusoidal torque and continuously increase with the increasing torque level. The hysteresis motions also take place in the simulations. Especially, rolling behavior occurs in the simulation when T_0 exceeds the static friction torque, referring to Fig. 4.26.

In addition, the respective maximum displacement of the simulation is $1.7\times10^{-3}\,[rad]$, $3.9\times10^{-3}\,[rad]$ and $6.10\times10^{-1}[rad]$, which is nearly the same with the corresponding experimental results $1.8\times10^{-3}\,[rad]$, $4.4\times10^{-3}\,[rad]$ and $6.18\times10^{-1}\,[rad]$. The same maximum displacement is not only in Fig. 4.24 and Fig. 4.25, where value of T_0 is below the static friction, but also in Fig. 4.26, where maximum value of T_0 is larger than the static friction. With this results, it can be strongly said that the identified σ_0 is proper and exact.

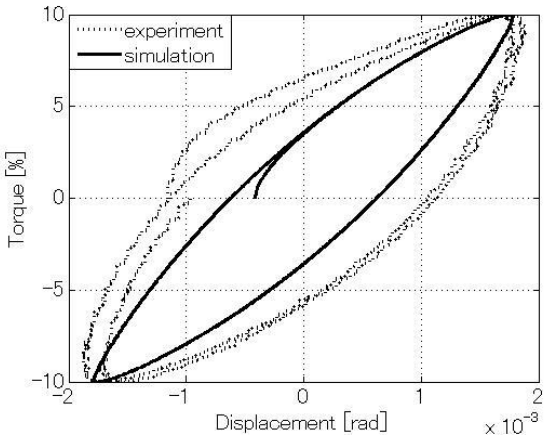

Fig. 4.24 Verification of microdisplacement ($T_0 = 10\%$)

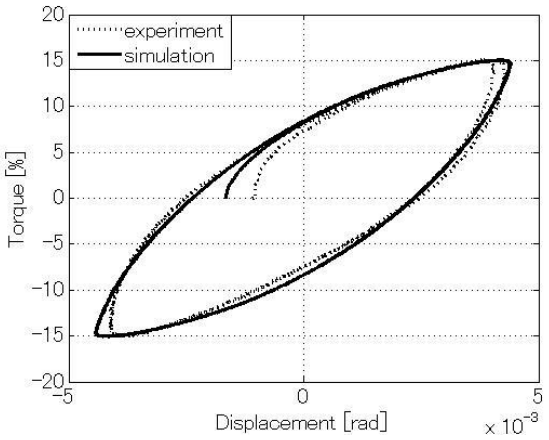

Fig. 4.25 Verification of microdisplacement ($T_0 = 15\%$)

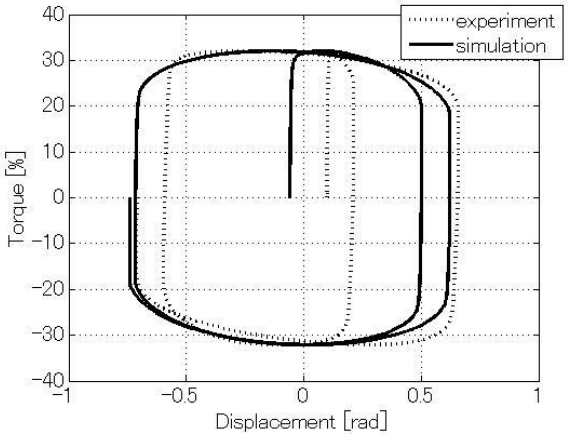

Fig. 4.26 Verification of microdisplacement ($T_0 = 32\%$)

4.4.2 Verification with square wave torque

Experimental tests and simulations with square wave torque are also conducted to mainly discuss the identification of σ_1. The square wave torques are applied to produce vibration of displacement. The maximum values of the square wave torque T_0 are determined by 10%, 15% and 30% to the rated torque, referring Fig. 4.27. Corresponding experiment and simulation results are shown in Fig. 4.28, Fig. 4.29 and Fig. 4.30. The experimental results are shown on left to compare with the simulations that are shown on right.

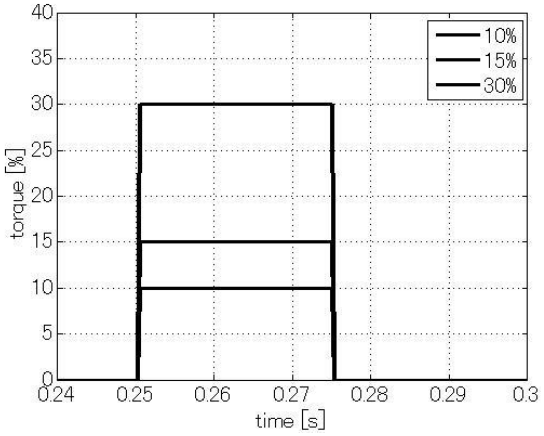

Fig. 4.27 Square wave torque input

In Fig. 4.28, Fig. 4.29 and Fig. 4.30, first, one of the obvious common features is that the maximum displacement of experiments and simulations are almost the same. This feature also demonstrates that parameters of the LuGre model are identified properly. Secondly, as the same with the experimental results, vibration also occurs in the simulations, which means that a similar behavior of second-order

system ($\zeta < 1$) can be reflected by using the identified LuGre model. However, frequency of vibration of the experiments and simulations are not the same. In comparison with the experimental results, the system (B link) behaves like a second-order system with a bigger ζ in the simulations. This is also in accordance with the shown Fig. 4.23, where at the very beginning, a simulated second-order system with bigger ζ is used to identify σ_1.

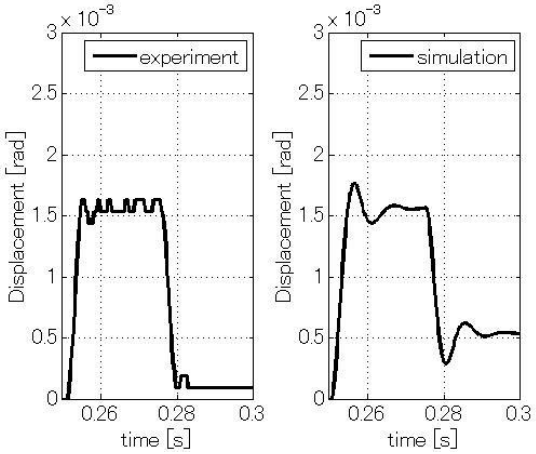

Fig. 4.28 Verification with square wave torque input ($T_0 = 10\%$)

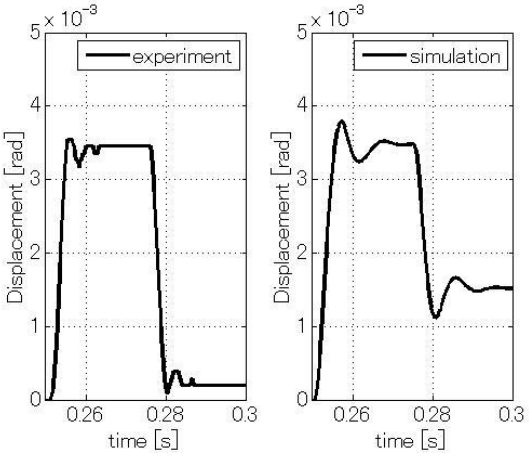

Fig. 4.29 Verification with square wave torque input ($T_0 = 15\%$)

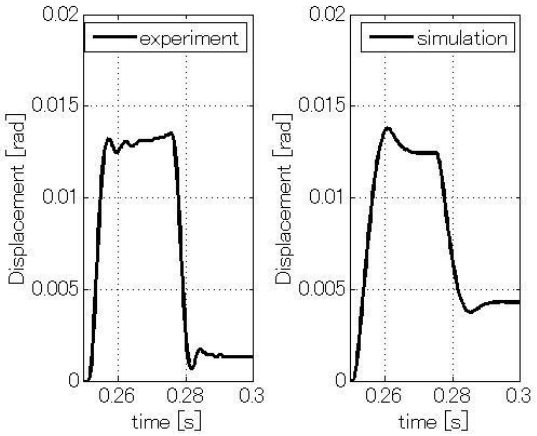

Fig. 4.30 Verification with square wave torque input ($T_0 = 30\%$)

4.4.3 Verification in PD control

In order to truly observe the fricition characteristics of the study model, the experimental tests of subsection 4.4.1 and subsection 4.4.2 are conducted in open loop to avoid the influnce of control. In this part, discusses of effectiveness of the proposed identification strategy and possiblity of friction compensation with the identified LuGre model are based on the experimetal tests that are conducted in closed loop. A PD controller is designed for B link of the study model and the control law is

$$T_{ref} = J_m K_V [K_P(\theta_{ref} - \theta_m) - \dot{\theta}_m] \quad \text{..... (4.37)}$$

where is θ_{ref} the position command, K_V and K_P are control gains and reported in Table. 4.7. Then, the position response and velocity are recorded and meantime, two simulations under the same conditions with the classical friction model and the LuGre model are implemented. The simulated position response and velocity are shown together with the experimetal results in Fig. 4.31 and Fig. 4.32. Fig. 4.31 is postion response and Fig. 4.32 is velocity response.

Table. 4.7 Control gains

Gain	Value	Unit
K_V	160	$[s]$
K_P	40	$[1/s]$

From the position response, the difference between simulations and experimental results appears as the time delay during the transient motion. The final arrival position in the simulation with the LuGre model is nearly the same with the experimental results and also closer to the experimental results than the simulation with the classical model, referring to Fig. 4.31 (b). During the steady-state, the amplitude of vibration of the experimental position response goes decreasingly and finally the system

(B link) stops due to the friction. In the simulation with the LuGre model, a same phenomenon is observed even though the attenuation of the vibration is less than the experimental results. The details of this phenomenon is more obvious in enlarged view of velocity. However, in the simulation with classical model, the position response differs from the experiment which appear as the form of continuous vibration. With above discusses, it can be said that the proposed identification of the LuGre model is effective and in comparison with the classical model, the LuGre model is completely can be used for model-based friction compensation.

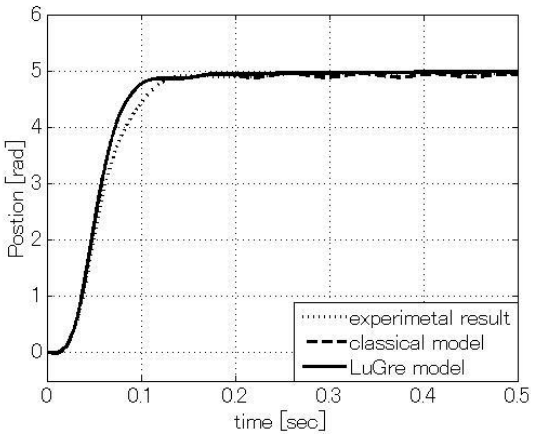

(a) Whole view

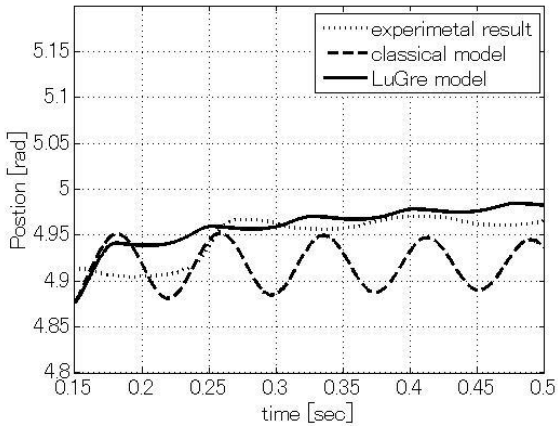

(b) Enlarged view

Fig. 4.31 Verification in PD control (position response)

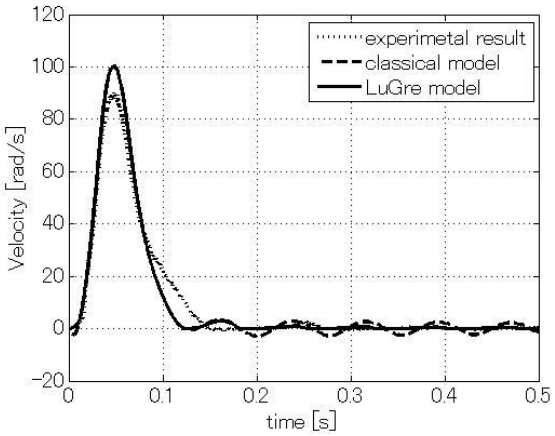

(a) Whole view

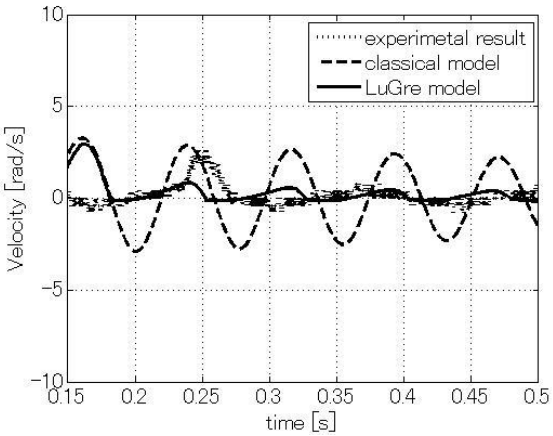

(b) Enlarged view

Fig. 4.32 Verification in PD control (velocity response)

4.5 Conclusions

In this chapter, an identification strategy of joint friction has been proposed and presented for industrial robot manipulators. Several results have been achieved by using proposed identification strategy

(1) The proposed identification strategy has succeed in accurately identifying LuGre model and it is not affected by twist torque when links of industrial robot manipulator are modeled by 2-inertial system.

(2) With the obtained LuGre model, simulations are conducted in both open loop and closed loop to compare with experimental results. The corresponding results of the comparison have further demonstrated that the identified LuGre model is close to the actual friction of joint and it is better than the classical friction model for model-based friction compensation.

Chapter 5

Conclusions

This paper has attempted to improve control performances of industrial robot manipulators and shown three new studies in three aspects. The paper has not only focused on a study of a new control strategy (decoupling control by using Model Following Control), but also studied a new command processing technique (a new interpolation scheme for position) and a new identification technique of friction (identification of joint friction). After making an extensive inquiry concerning high performance control of industrial robot manipulators, it is found that development and progress of high performance control of industrial robot manipulators should not only rely on studies of new control methods, studies should pay more and more attention to input command and mechanical characteristics of the industrial robot manipulator itself because command and mechanical characteristics are very important aspects of the industrial robot manipulator system and they are closely related to high performance control. Therefore, the studies of command processing and identification of mechanical characteristic of industrial robot manipulators are conducted together with the study of control strategy in this paper.

In the study titled a new interpolation methodology for position, the most important achievement is realization of a successive interpolation manner. Due to this, the study has also realized

- High efficiency interpolation of position command
- High accuracy interpolation of position command
- Reduction of computation.

Besides, an application of the new interpolation methodology in perfect tracking control has also been offered and the results demonstrate that use of the studied command processing technique is a very big advantage for high performance control of industrial robot manipulators and moreover, the new interpolation methodology is better than Spline interpolation, which is the most commonly used interpolation technique.

In the study of decoupling control by using Model Following Control, a new decoupling control strategy that is based on Model Following Control has been presented. The emphasis of this work is not only on improvement of control performances but also on practical application issue of the decoupling control theory. In comparison with conventional decoupling control theories, the new decoupling strategy has achieved

- Successful designs of compensation torques in feed forward loop
- Successful designs of compensations for disturbances in feedback loop,

which are also the most difficult potential subjects that arise from the new decoupling strategy. Due to

these, the new decoupling strategy is easy to be used for general purpose industrial robot manipulators and at last, simulation verifications have also shown that the new decoupling strategy is effective for the improvement of control performances.

In the study of identification of joint friction, a completely new identification strategy of joint friction has been proposed and it succeeds in avoiding the effect of twist torque on friction measurement and achieves accurate identification of joint friction. Joint friction has been modeled by LuGre model and six parameters of LuGre model are successfully obtained by using the new identification strategy. With several verifications that are comparisons between simulations and experimental results, it has been demonstrated the obtained LuGre model is proper and effective.

With above three studies, high performance control of industrial robot manipulators has been ultimately realized and this result also provides a very strong demonstration; high performance control of industrial robot manipulators needs to be considered in different perspective and command, control algorithm and mechanical characteristics need to be integrated and studied to improve performances of industrial robot manipulators.

Three aspects of studies have been conducted in this paper and the new interpolation methodology of position command, decoupling control strategy and identification strategy of joint friction will be deeply studies in the future. Moreover, studies of command processing, control strategy and identification of mechanical characteristics are expected to be integrated to contribute to higher performance control of industrial robot manipulators. If an idea needs to be given, three parts of the idea are

- Establishing control strategy according to problems of application of industrial robot manipulators
- Investigating a command processing technique, which is optimal for control strategy
- Clearing mechanical characteristics, which affect control performances.

Processing of command, control and identification of mechanical characteristics should be conducted simultaneously in servo systems. After establishing proper control strategy, command processing technique will be employed for serving control strategy. In other words, the most suitable command for control strategy will be obtained by using command processing technique. Meantime, the already known information of mechanical characteristics obtained by for example, identifying will be notified to control processing to not only clear the adverse mechanical characteristics, but also possibly use some of favorable mechanical characteristics. Study approach of command processing and identification of mechanical characteristic together with a study of control strategy will integrally bring high performance control of industrial robot manipulators to a new level.

Appendix

A.1 Main components of controller system

Main components of controller system are shown in Fig. A.1.

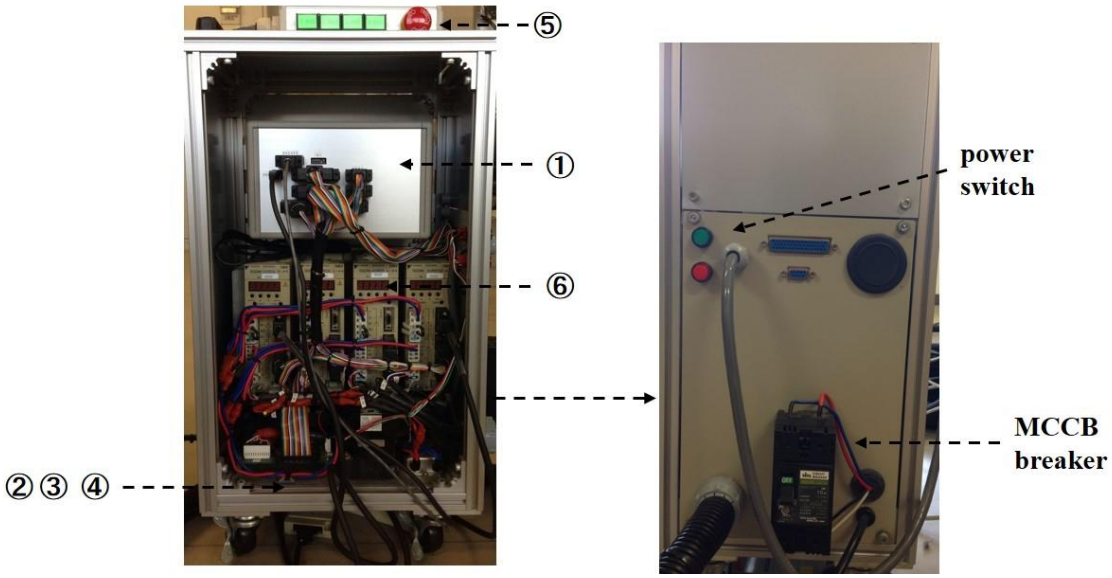

Fig. A.1 External appearance of controller system

① MechatroS3-Controller (MS3-C)

② I/F board

③ DC 24V power supply

④ Main power supply circuit

⑤ Emergency stop relay

⑥ Servo packs

SGDM-02BDA (axis S)

SGDM-01BDA (axis L)

SGDM-A5BDA (axis U)

SGDM-A3BDA (axis B)

⑦ AC servo motors

SGMPH-02B1A6E (axis S)

SGMPH-01B1A6E (axis L)

SGMAH-A5B1A6E (axis U)

SGMAH-A3B1A6E (axis B)

⑥ and ⑦ are products of Yasukawa Corporation and specifications of ⑥ can be known by

referring to *http://www.e-mechatronics.com/product/servo/sgm2/amps/ac/sgdm/index.html*, specifications of ⑦ can be known by referring to *http://www.e-mechatronics.com/product/servo/sgm2/motors/sgmph/index.html*.

A.2 Introduction of MS3-C

The MechatroS3-controller is provided by Yaskawa Elec. Corp. Information Systems Corporation and houses single-board CPU, Analog Devices A/D and D/A boards, Digital input and output devices, Absolut serial input devices and USB and RS232 communications, referring to Fig. A.2. Main specifications of MS3-C are given in Table. A.2

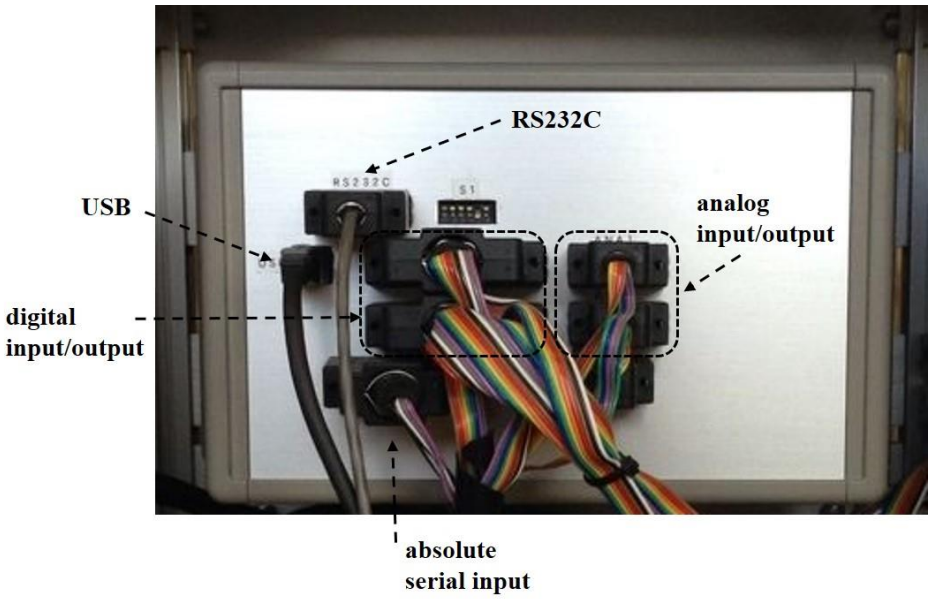

Fig. A.2 MS3-C

Table. A.2 Main specifications of MS3-C

CPU	Manufactured by Hitachi, HD6417750(SH-4) BGA 256 pin Operating frequency 192MHz Maximum bus frequency 96MHz
FlashROM	Manufactured by Toshiba TC58FVT160FT-85 16bit×1Mbit NOR-Flash
Memory	Manufactured by Hitachi SDRAM HM5264165FTD-60×2 (16bit×4Mbit) ×2
SRAM	Manufactured by Toshiba TC55v16256FT-12 16bit×32Kbit

List of References

[1] B. Siciliano and O. Khatib: “Springer Handbook of Robotics”, Springer, 2008.

[2] L. Westerlund: “The Extended Arm of Man – A history of the Industrial Robot”, Informationsförlaget, 2000.

[3] Yaskawa Electric Corporation, Catalog of series of robots, URL: http://www.e-mechatronics.com/product/robot/series/index.html

[4] R. D. Klafter, T. A. Chmielewski and M. Negin: “Robotics Engineering-An Integrated Approach”, Prentice-Hall International, 1989.

[5] H. Asada and J.-J. E. Slotine: “Robot Analysis and Control”, John Wiley and Sons, 1986.

[6] G. M. Mair: “Industrial Robotics”, Prentice-Hall International, 1988.

[7] The Japan Society of Mechanical Engineers: “JMSE Technical Roadmap”, Bulletin of JMSE, Vol.110, No.1067, pp.1-8, 2007.

[8] M. Tomizuka: “Zero Phase Error Tracking Algorithm for Digital Control”, AMSE Journal of Dynamic Systems, Measurement and Control, Vol.109, No.1, pp.65-68, 1987.

[9] I. J. Schoenberg: “Cardinal Spline Interpolation”, CBMS-NSF Regional Conference Series in Applied Mathematics 12, 1973.

[10] http://www.geos.ed.ac.uk/~yliu23/docs/lect_spline.pdf

[11] H. Ozaki, H. Qiu and C. J. Lin: “An Optimization Algorithm by the Complex Method for Trajectory Generation of Manipulators with B-Spline”, Journal of the Robotics Society of Japan, Vol.14, No.4, pp.560-566, 1996.

[12] M. Egerstedt and C. F. Martin: “Optimal trajectory planning and smoothing splines”, Automatica, Vol.37, No.7, pp.1057-1064, 2001.

[13] T. Horsch and B. Jüttler: “Cartesian Spline Interpolation for Industrial robots”, Computer-Aided Design, Vol.30, Issue.3, pp.217-224, 1998.

[14] S. Goto, T. Iwanaga, N. Kyura and M. Nakamura: “High Speed and High Accuracy Control of Industrial Articulated Robot Arms with Jerk Restraint by Spline Interpolated Taught Data”, IEEJ Transactions on Industry Applications, Vol.123, Issue.9, pp.1071-1080, 2004.

[15] M. Müller, G. Erdos and P. Xirouchakis: “High Accuracy Spline Interpolation for 5-axis Machining”, Computer-Aided Design, Vol.36, Issue.13, pp.1379-1393, 2004.

[16] J. S. Ahn, W. J. Chung, and C. D. Jung: “Realization of orientation interpolation of 6-axis articulated robot using quaternion”, Journal of Central South University, Vol.19, Issue. 12, pp.3407-3414, 2012.

[17] E. Fround: “Fast Nonlinear Control with Arbitrary Pole-placement for Industrial Robots and manipulators”, International Journal of Robotics Research, Vol.1, No.1, pp.65-78, 1982.

[18] T. Iwakane and Y. Inoue: “Direct Drive Control of Horizontal Arm with 2 Degree of Freedom”, IEEJ Transactions on Industry Applications, Vol.107, No.1, pp.13-20, 1987.

[19] C. Zhang, G. Z. Zhao and K. J. Tseng: “Robust decoupling control of a three-link robot arm directly driven by permanent magnet synchronous motors”, International Journal of Applied Electromagnetics and Mechanics, Vol.36, No.4, pp.279-293, 2011.

[20] M. Nakao, K. Ohnishi and K. Miyachi: “A Robust Decentralized Joint Control Based on Interference Estimation”, Proceedings of IEEE International Conference on Robotics and Automation, Vol.1, pp.326-331, 1987.

[21] T. Namerikawa, M. Fujita and F. Matsumura: “Robust H_∞ control of a Parallel Link Robot Manipulator”, IEEJ Transactions on Industry Applications, Vol.116, No.2, pp.207-215, 1996.

[22] H. N. Lin, Y. Kuroe and T. Maruhashi: “Decoupling Control of Nonlinear Systems Using Disturbance Observer”, Journal of the Robotics Society of Japan, Vol.13, No.3, pp.420-428, 1995.

[23] I. Akihiro and M. Shiraishi: “Robust Decoupling Control for Articulated Robot”, JMSE International Journal Series C, Vol.40, No.1, pp.89-96, 1997.

[24] R. Nakashima, M. Ojima, R. Oguro and T. Tsuji: “A Decoupling Control Method for Industrial Robots”, IEEJ Transactions on Industry Applications, Vol.120, No.5, pp.673-679, 2000.

[25] L. P. Falb and W. Wolovich: “Decoupling in the Design and Synthesis of Multivariable Control Systems”, IEEE Transactions on Automatic Control, Vol.12, Issue.6, pp.651-659, 1967.

[26] R.V. Monopoli: “Model Following Control of Gas Turbine Engines”, Journal of Dynamic Systems, Measurement, and Control, Vol.103, No.3, pp.285-289, 1981.

[27] A. Balestrino, G. D. Maria and A.S.I. Zinober: “Nonlinear Adaptive Model-Following Control”, Automatica, Vol.20, Issue.5, pp.559-568, 1984.

[28] L. Feng Lan, K. Okabe, R. Oguro and H. Honda: “Decoupling Control of 2-link Manipulator with Model Following Control and Proposed Control Gains Design”, Proceedings of 2012 12th International Conference on Control, Automation and Systems TD09-3, pp.1049-1054, 2012.

[29] C. W. D. Silva: “Recursive Linearizing and Decoupling Control of Robots”, Dynamic and Control, Kluwer Academic Publishers, Vol.2, Issue.4, pp.401-414, 1992.

[30] A. D. Luca: “Decoupling and Feedback Linearization of Robots with Mixed Rigid/Elastic Joints”, International Journal of Robust and Nonlinear Control, Vol.8, Issue.11, pp.965-977, 1998.

[31] K. Yuki, T. Murakami and K. Ohnishi: “Vibration Control of a 2 Mass Resonant System by the Resonance Ratio Control”, IEEJ Transactions on Industry Applications, Vol.113, No.10, pp.1162-1169, 1993.

[32] S. Manabe: “Controller Design of Two-Mass Resonant System by Coefficient Diagram Method”, IEEJ Transactions on Industry Applications, Vol.118, No.1, pp.58-66, 1998.

[33] Y. Hori: “Control Using Resonance Ratio Control and Manabe Polynomials”, IEEJ Transactions on Industry Applications, Vol.114, No.10, pp.1038-1045, 1994.

[34] Y. Hori: “Control of 2-inertia System Only by a PID Controller”, IEEJ Transactions on Industry Applications, Vol.115, No.1, pp.86-87, 1995.

[35] F. Ohkawa, H. Honda, J. Kobayashi, K. Kuboyama and R. Oguro: “Robust Model Following Control of a Feed Drive System Hindered by a Machine Stand Vibration”, Transactions of The Japan Society of Mechanical Engineers, Vol.68, No.668, pp.1127-1132, 2002.

[36] J. Suzuki, T. Murakami and K. Ohnishi: “Vibration Control of Flexible Manipulator Taking Friction-depending Disturbance into Account”, IEEJ Transactions on Industry Applications, Vol.122, No.3, pp.235-240, 2002.

[37] L. L. Tien, A. A. Schaffer, A. D. Luca and G. Hirzinger: “Friction Observer and Compensation for Control of Robots with Joint Torque Measurement”, IEEE/RSJ International Conference on Intelligent Robots and Systems, pp.3789-3795, 2008.

[38] M. Iwasaki, T. Ahibata and N. Masuyi: “Disturbance Observer-Based Nonlinear Friction Compensation and Application to Table Drive System”, IEEJ Transactions on Industry Applications, Vol.118, No.1, pp.51-57, 1998.

[39] Y. Maeda and M. Iwasaki: “Initial Friction Compensation by Disturbance Observer Based on Rolling Friction Model”, IEEJ Transactions on Industry Applications, Vol.130, No.2, pp.228-235, 2010.

[40] S. M. Phillips and K. R. Ballou: “Friction Modeling and Compensation for an Industrial robots”, Journal of Robotics Systems, Vol.10, No.7, pp.947-971, 1993.

[41] C. C. D. Wit, H. Olsson, K. J. Astrom and P. Lischinsky: “A New Model for Control of Systems with Friction”, IEEE Transaction on Automatic Control, Vol.40, No.3, pp.419-425, 1995.

[42] A. H. Brian: “Control of Machines with Friction”, Boston, Kluwer Academic Publishers, 1991.

[43] A. H. Brian, P. Dupont and C. C. D. Wit: “A Survey of Models, Analysis Tools and Compensation methods for the Control of Machines with Friction”, Automatica, Vol.30, Issue.7, pp.1083-1138, 1994.

[44] T. Tanaka, T. Oiwa and J. Otsuka: “Study on Friction Model of Linear Ball Guideway for Precision Positioning”, Precision Engineering, Vol.72, No.4, pp.470-474, 2006.

[45] T. Tanaka, T. Oiwa and J. Otsuka: “Study on Friction Model of Linear Ball Guideway for Precision Positioning-Simulation of Full-closed Loop Control Using Bristle Model”, Precision Engineering, Vol.73, No.4, pp.465-469, 2007.

[46] T. Tanaka, T. Oiwa, J. Otsuka and M. Ikuro: “Study on Friction Model of Linear Ball Guideway for Precision Positioning-Accuracy Improvement by Control Method Using Nonlinear Frictional Model”, Precision Engineering, Vol.74, No.11, pp.1171-1175, 2008.

[47] Y. Maeda and M. Iwasaki: “Analytical Examinations and Compensation Based on Rolling Friction Model for Slow Settling Response in Precise Positioning”, IEEJ Transactions on Industry Applications, Vol.129, No.12, pp.1218-1225, 2009.

[48] R. Stribeck: “Die wesentlichen eigenschaften der gleit-und rollenlager”, Zeitschrift Des Vereines Deutcher Ingenieure, Vol.46, No.38, No.39, pp.1341-1348, 1902.

[49] C. B. Li and D. Pavelescu: “The friction-speed relation and its influence on the critical velocity of the stick-slip motion”, Wear, Vol.82, Issue.3, pp.277-289, 1982.

[50] C. C. D. Wit, P. Noel, A. Aubin and B. Brogliato: “Adaptive Friction Compensation in Robot Manipulators: Low Velocities”, The International Journal of Robotics Research, Vol.10, No.3, pp.189-199, 1991.

[51] K. Sato, K. Tsuruta and A. Shoji: “Adaptive Friction Compensation Control of Linear Slider with Considering a Periodic Reference Signal”, IEEJ Transactions on Industry Applications, Vol.125, No.11, pp.1022-1029, 2006.

[52] J. C. Pratt and E. Eisner: “The effect of a tangential force on the contact of metallic bodies”, Proceedings of the Royal Society, Vol.238, No.1215, pp.529-550, 2005.

[53] R. S. H. Richardson and H. Nolle: “Surface friction under time-dependent loads”, Wear, Vol.37, No.1, pp.87-101, 1976.

[54] C. C. D. Wit and P. Lischinsky: “Adaptive friction compensation with partially known dynamic friction model”, International Journal of adaptive control and signal processing, Vol.11, Issue.1, pp.65-80, 1997.

[55] S. Jer Huang and C. Ming Chiu: “Optimal LuGre friction model identification based on genetic algorithm and sliding mode control of a piezoelectric-actuating table”, Transactions of the Institute of Measurement and Control, Vol.31, No.2, pp.181-203, 2009.